NUMERICAL MODELING OF GROUNDWATER FLOW AT A COAL EXPLORATION SITE IN ESKİŞEHİR - TURKEY

A THESIS SUBMITTED TO
THE GRADUATE SCHOOL OF NATURAL AND APPLIED SCIENCES
OF
MIDDLE EAST TECHNICAL UNIVERSITY

BY

HATİCE KILIÇ

IN PARTIAL FULFILLMENT OF THE REQUIREMENTS
FOR
THE DEGREE OF MASTER OF SCIENCE
IN
GEOLOGICAL ENGINEERING

AUGUST 2016

Approval of the thesis:

NUMERICAL MODELING OF GROUNDWATER FLOW AT A COAL EXPLORATION SITE IN ESKİŞEHİR - TURKEY

submitted by **HATİCE KILIÇ** in partial fulfillment of the requirements for the degree **of Master of Science in Geological Engineering Department, Middle East Technical University** by**,**

Prof. Dr. Gülbin Dural Ünver
Dean, Graduate School of **Natural and Applied Sciences** _____

Prof. Dr. Erdin Bozkurt,
Head of Department, **Geological Engineering** _____

Prof. Dr. Hasan Yazıcıgil,
Supervisor, Geological Engineering Dept., METU _____

Examining Committee Members:

Prof. Dr. Nurkan Karahanoğlu
Geological Engineering Dept., METU _____

Prof. Dr. Hasan Yazıcıgil
Geological Engineering Dept., METU _____

Prof. Dr. Zeki Çamur
Geological Engineering Dept., METU _____

Prof. Dr. M. Lütfi Süzen
Geological Engineering Dept., METU _____

Assist. Prof. Dr. Özlem Yağbasan
Geography Teaching, Gazi University _____

Date: 12/08/2016

I hereby declare that all information in this document has been obtained and presented in accordance with academic rules and ethical conduct. I also declare that, as required by these rules and conduct, I have fully cited and referenced all material and results that are not original to this work.

Name, Last name: HATİCE KILIÇ

Signature :

ABSTRACT

NUMERICAL MODELING OF GROUNDWATER FLOW AT A COAL EXPLORATION SITE IN ESKİŞEHİR - TURKEY

Kılıç, Hatice

M. S., Department of Geological Engineering

Supervisor: Prof. Dr. Hasan Yazıcıgil

August 2016, 131 pages

Numerical groundwater models are useful tools for the evaluation of the complex groundwater systems in the pre-feasibility phase of the mining activities. They can be used to simulate three-dimensional groundwater system and its interaction with these activities. The purpose of this study is to develop conceptual and numerical models of the groundwater flow and evaluate the impact of preliminary dewatering of a coal exploration site in Eskişehir, Turkey.

In this study, conceptual model including calculations of hydrologic-hydrogeological budgets were developed at the first stage. Then, groundwater flow regime was modeled and calibrated under steady state conditions by a three-dimensional finite difference model, namely MODFLOW SURFACT. After conducting sensitivity analyses, calibrated model was used to predict the quantity of inflow to preliminary designs of the underground coal panels. During this process, effect of no flow boundary condition at the northwestern part of the study area on dewatering was also analyzed. For the impact assessment, drawdown maps and the groundwater budgets calculated after

dewatering simulations were evaluated. These simulation results indicate that the average groundwater inflows are about 129.72 L/s and 33.08 L/s to the deeper and shallower panels, respectively. Although most of the pumping wells will not be significantly affected by these simulations, decrease in the amounts of baseflow to Porsuk Stream and discharge from the springs-captages is expected.

Keywords: Numerical groundwater modeling, MODFLOW SURFACT, groundwater inflow, dewatering

ÖZ

KÖMÜR ARAMA SAHASININ (ESKİŞEHİR – TÜRKİYE) SAYISAL YERALTISUYU AKIM MODELLEMESİ

Kılıç, Hatice

Yüksek Lisans, Jeoloji Mühendisliği

Tez Yöneticisi: Prof. Dr. Hasan Yazıcıgil

Ağustos 2016, 131 sayfa

Sayısal yeraltısuyu modelleri, madencilik faaliyetlerinin ön fizibilite evresinde karmaşık yeraltısuyu sistemlerini değerlendirmek için faydalı araçlardır. Bunlar 3 boyutlu yeraltısuyu sistemini ve bu sistemin madencilik faaliyetleriyle etkileşimini simüle etmek için kullanılabilinir. Bu çalışmanın amacı, Eskişehir'de bulunan bir kömür arama sahasının kavramsal ve sayısal yeraltısuyu akım modellerinin geliştirilmesi ve öncül susuzlaştırma planlarının etkisinin değerlendirilmesidir.

Bu çalışmada, ilk aşamada hidrolojik-hidrojeolojik bütçe hesaplamalarını da içeren kavramsal model geliştirilmiştir. Daha sonra, MODFLOW-SURFACT adı verilen 3 boyutlu sonlu farklar modeli yardımıyla yeraltısuyu akım rejimi modellenmiş ve kararlı akım koşulları altında kalibre edilmiştir. Duyarlılık analizleri yapıldıktan sonra, kalibre edilen model öncül yeraltı kömür panelleri tasarımlarına gelen suyun miktarını tahmin etmek için kullanılmıştır. Bu süreçte, ayrıca çalışma alanının kuzeybatı

kısmındaki akımsız sınır koşulunun susuzlaştırma simülasyonları üzerindeki etkisi araştırılmıştır. Etki değerlendirmesi için, yeraltısuyu seviye haritaları, düşüm haritaları ve susuzlaştırma simülasyonları sonrasında hesaplanan yeraltısuyu bütçeleri değerlendirilmiştir. Bu simülasyon sonuçları, ortalama yeraltısuyu akışının derin ve sığ panellerde sırasıyla 129.72 L/s ve 33.08 L/s olarak hesaplanmış olduğunu göstermektedir. Pompaj kuyularının birçoğu susuzlaştırma simülasyonlardan önemli derecede etkilenmeyecekse de, Porsuk Çayı'na baz akımın ve kaynak-kaptaj boşalım miktarlarının azalması beklenmektedir.

Anahtar Kelimeler: Sayısal yeraltısuyu modellemesi, MODFLOW SURFACT, yeraltısuyu girişi, susuzlaştırma

To My Beloved Mother and in Loving Memories of My Father and Sister

ACKNOWLEDGEMENTS

First and foremost, I would like to express my gratitude to my supervisor, Prof. Dr. Hasan Yazıcıgil, for his support, guidance, criticism, insight and encouragement throughout this study. I feel very fortunate and honored to have worked with him at the starting point of my career. I am thankful to him since he trusted me when I despaired during harsh times of the study. I am sure I can solve lots of puzzles in the future with the things that I learned from him.

I am also grateful to Prof. Dr. Zeki Çamur and Assoc. Prof. Dr. Koray K. Yılmaz for their precious supports to the project which provided the basis of this study. It was perfect for me to take answers to my questions from the authorities just like them. Also, I want to express my gratitude to Assoc. Prof. Dr. Kaan Sayıt for his guidance when I become lost within the geological units of the study area. I also would like to thank all members of my defense committee for their time and insightful comments.

I would like to thank Eczacıbaşı Industrial Raw Materials Inc. which has financially supported "Hydrogeological Investigation and Characterization of the Esan-Alpu Coal Mine Exploration Site" project.

My grateful thanks goes to Ayşe Peksezer Sayıt who shares all the burden of my study from the first minute to the last. Without her support and friendship, I can't overcome rough times of the study. I also would like to thank my roommate Çidem Argunhan for her kindness support and understanding. Special thanks goes to Mert Onursal Çatak for his support and gentlemanly behavior during field investigations. He is the best project mate I have ever seen. I would like to express my appreciation to Timur Ersöz who provides free therapy to me just like a professional physiologist. This exhausting period has been enjoyable with him.

It is a pleasure to thank those who made this thesis possible: my family and best friends. Dilge Varlı, Ecenur Kılıç and Kadir Yertutanol are the siblings that God never gave me. Thank you for your cheerful motivations, and for always being there for me. Without you not only writing this thesis but also life is too hard for me. I owe my deepest gratitude to my family, M. Ali Atakan, Zuhal Atakan, Anıl Atakan Çelik and Ali Çelik and my beloved mother, Nursel Kılıç for their love and endless support. Especially my mother took all the agony and replace it with peace and love. I am so lucky to have a mother like her. Finally, the last but not the least, I would like to thank Eren Germeç. I can not ever thank him enough that he never stops believing, loving and encouraging me. Without his support and patience, this could not be achieved.

TABLE OF CONTENTS

LIST OF TABLES

TABLES

LIST OF FIGURES

FIGURES

CHAPTER 1

INTRODUCTION

1.1. Purpose and Scope

Numerical groundwater modeling becomes crucial with the requirements of detailed design of mine water systems. During pre-mining feasibility, water bearing units and their relations should be investigated and conceptual hydrogeological model should be developed. Then, response of the model should be tested by simulating mining activities since encountering groundwater within the excavated area during these processes could cause major hydrogeological problems. At this stage, dewatering designs are necessary to provide dry and safe working conditions for the mining area which is excavated under the water table. An accurate forecast of water inflow to mines which is the basis for these designs is possible with numerical modeling simulations. Additionally, since the dewatering operations modify hydrogeological conditions, the impact of these operations are also understood by using this model.

The primary purpose of this study is to simulate groundwater flow regime of a coal exploration site in Eskişehir province under steady state conditions prior to mining activities and to estimate the dewatering requirements for various panel configurations. The other important purpose is to determine the impact of preliminary dewatering requirement on the surrounding groundwater system. During impact assessment, at the first stage, groundwater inflow to underground coal panels will be predicted. Then, ultimate groundwater level maps, drawdown maps and groundwater budget components will be evaluated to understand the changes in the status of groundwater regime and discharge/recharge mechanism of the study area. It is envisaged that these

studies provide a basis for further real case mine dewatering system design in the study area.

1.2. Location and Extent of the Study Area

The study area is located 14 km east of the city of Eskişehir in the northwestern part of the Central Anatolian Region (Figure 1.1). It covers 95.6 km^2 area between $30^0$41'10''-$30^0$50'46'' E longitudes (UTM 301805-315656) and $39^0$44'21''-$39^0$49'22'' N latitudes (UTM 4401342-4410647) and involves Eczacıbaşı Industrial Raw Materials Inc. license area. The northern part of the study area is bounded by the Porsuk Stream and the southern part forms the watershed divide for the Porsuk Stream. The western and eastern boundaries are surrounded by Sevinç and Karaçay districts, respectively. In the study area, main settlements are Çavlum, Ağapınar and Kireçköy which are administratively within the municipal boundaries of Odunpazarı. The access to the study area is provided by Eskişehir-Alpu road.

1.3. Previous Studies

Coal potential of the region including the study area and its surroundings prompted researchers to conduct geological and hydrogeological investigations. Therefore, a number of studies has been carried out for the study area since 1970s.

The earliest geological study within and around the study area was conducted by Siyako et al. in 1991. This study resulted with a geological report with the name of "Tertiary geology of the Bozüyük-İnönü Eskişehir-Beylikova-Sakarya regions and their coal potential" on behalf of General Directorate of Mineral Research and Exploration (MTA). The purpose of this report was to map the Tertiary age rock units and investigate of their structural and stratigraphic properties with the aim to determine

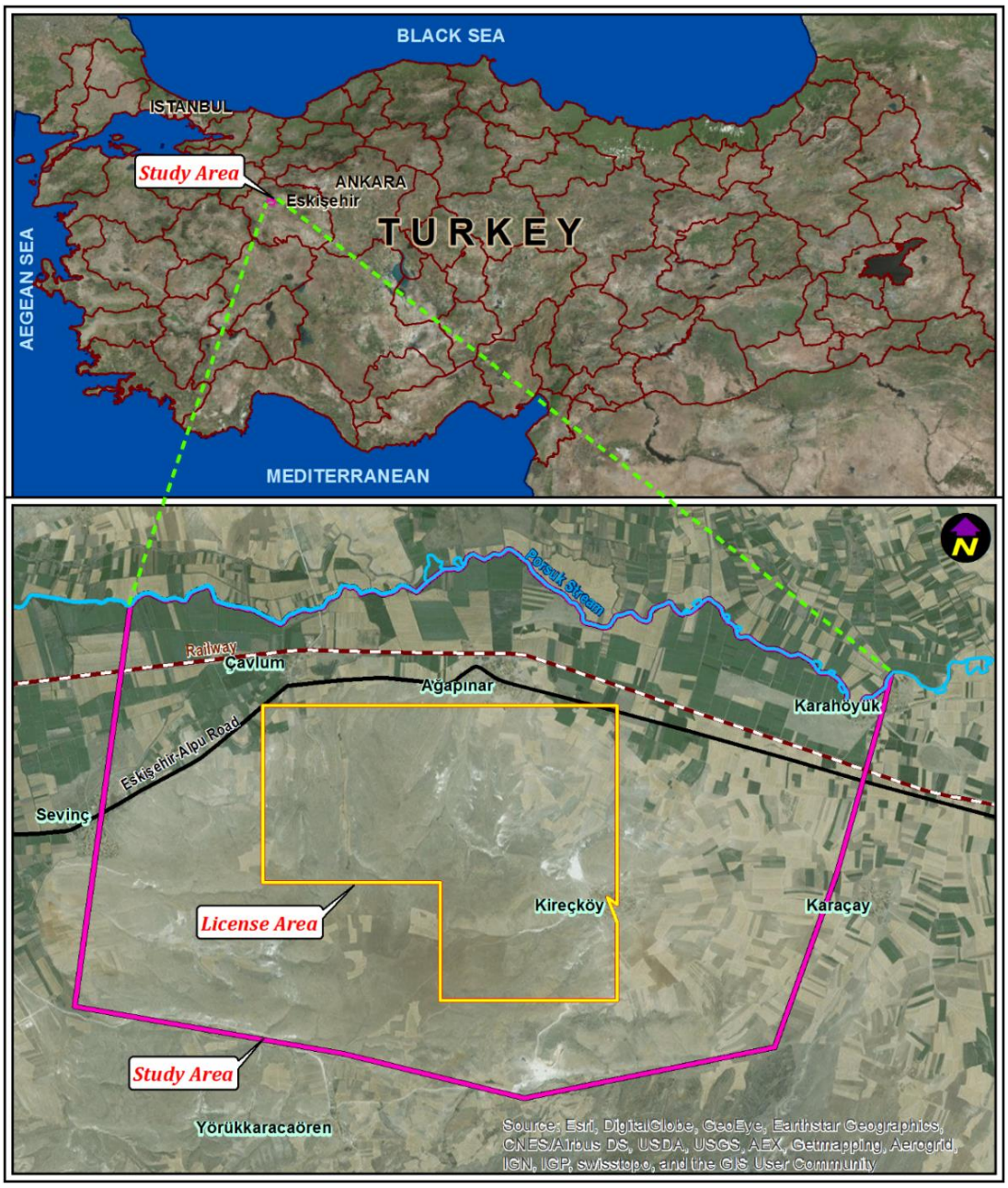

Figure 1.1. Location map of the study area

their coal potential. As a consequence of this study, generalized columnar section of the region and geological maps of scale 1/100.000 for I23, I24, I25, I26 and I27 map

sheets were prepared. Another geological report entitled “Geology of the middle and southern part of the Sakarya Region.” was conducted by Gözler et al. in 1997 for MTA. In this report, as a result of detailed geological studies, generalized columnar section of the region and geological maps of scale 1/100.000 and 1/25.000 for I24, I25, I26 and I27 map sheets were developed. In 2013, a study on “Geology and stratigraphy of Eskişehir–Alpu coal basin” was published (Senguler, 2013). For this study, northern part of the study area was chosen as area of interest and boreholes drilled for coal exploration and reserve improvement by MTA were used for identification of the stratigraphic sequences of the area. In 2015, another study was conducted by Toprak et al. for the same area and it focuses on the effects of faults on the formation of coal basin and petrographical properties and depositional environment of this basin. The recent geological study and estimation of the coal resources in the basin was conducted by Palaris (2016) on behalf of Eczacıbaşı Industrial Raw Materials Inc.

In comparison to geological studies, limited hydrogeological studies have been carried out for the study area and its surrounding. In 1977, General Directorate of State Hydraulic Works (DSI) prepared “Hydrogeological investigation report for Eskişehir–Alpu basin” to determine potential, quantity and quality of the groundwater in this basin and to specify areas suitable for groundwater exploitation. Hydrogeological maps of scale 1/100.000 was also included within this report. In 2010, DSI revised this report to recalculate groundwater reserve in the basin. The latest hydrogeological study was performed by Yazıcıgil et al. in 2016 within the scope of the project “Hydrogeological investigation and characterization of the Esan-Alpu coal mine exploration site”. This study formed the basis for this thesis.

CHAPTER 2

DESCRIPTION OF THE STUDY AREA

2.1. Physiography

The physiography of the study area is characterized by flat alluvium areas around the Porsuk Stream in the north and relatively rugged terrain over Miocene age rock units and metamorphic basin in the southern region. According to digital elevation model of the study area which is created by 5 m interval topographical contours from 1/25.000 scaled maps with 5 m grid size, the altitude of the study area ranges between 760 – 1027 m (Figure 2.1). In the northern part of the study area, alluvium areas around the Porsuk Stream have the lowest ground elevations between 760 – 790 m and in the southern part, Kireç Hill and its surroundings have highest elevations up to 1027 m. Between these lowest and highest elevations, relatively lower hills with 769 – 1012 m elevations are located in the study area dispersedly (Figure 2.1).

2.2. Climate and Meteorology

The study area which is located in the Central Anatolian Region is under the influence of continental climate. As typical characteristic of this climate, summers are hot and dry while winters are cold and snowy.

Turkish State Meteorological Service (MGM) installed four meteorological stations around the study area (Figure 2.2 and Table 2.1).

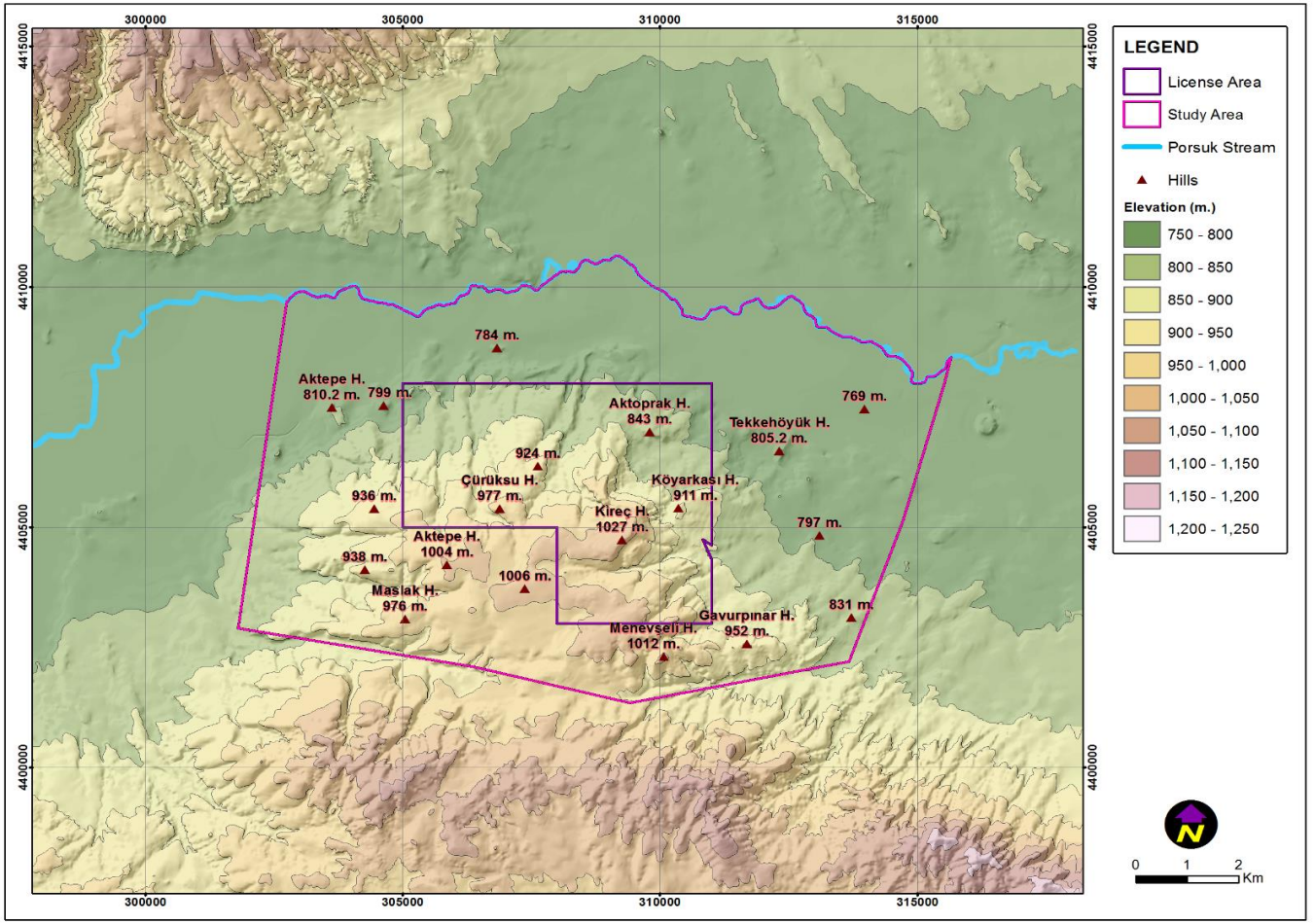

Figure 2.1. Digital elevation model of the study area

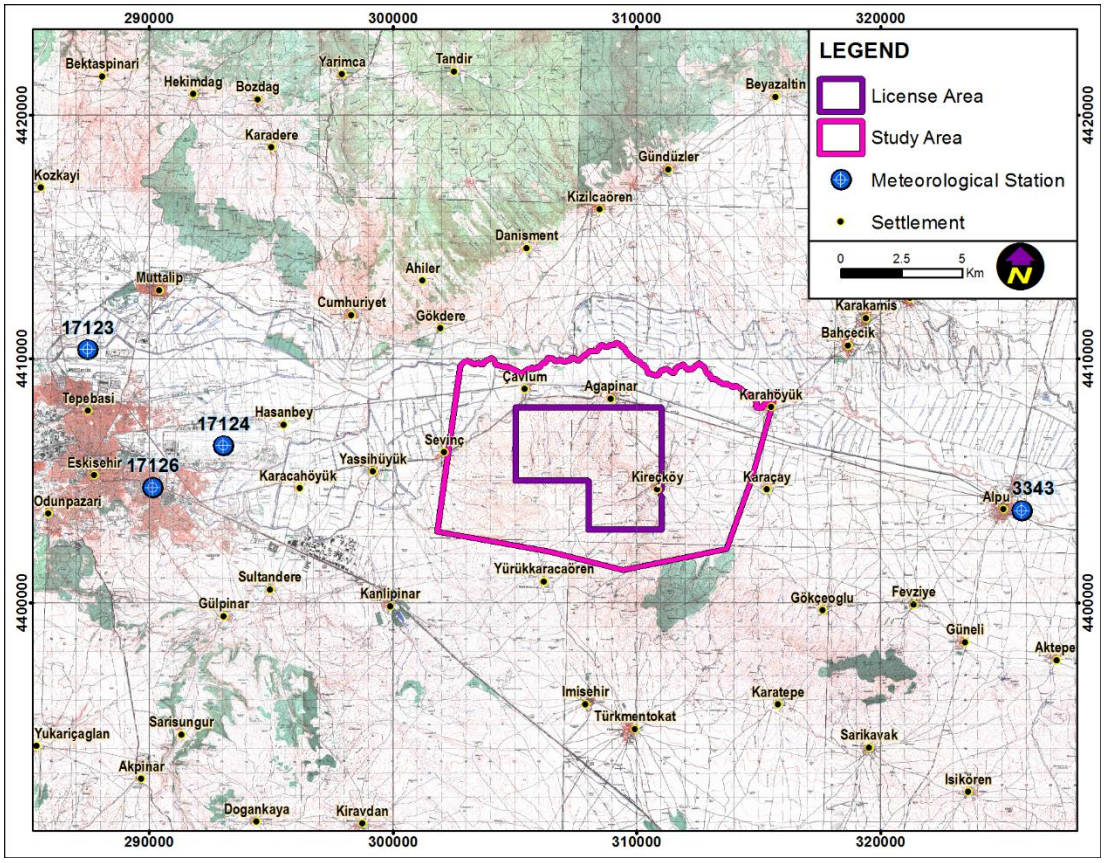

Figure 2.2. Locations of the meteorological stations around the study area

Table 2.1. Detailed information about the meteorological stations

Station No.	Station Name	Coordinates (m)		Elevation (m)	Distance to the Study Area (km)	Data Period
		East	North			
17126	Eskişehir Regional Directorate of Meteorology	290146	4404721	801	12	1929-1978, 1981-1990, 2007-2014
17124	Military Airport	293045	4406434	785	9	1978-1981
17123	Anadolu Civil Airport	287460	4410374	789	14	1990-2012
3343	Alpu	325815	4403788	765	11	1984-2002

Three of them which are named as Eskişehir Regional Directorate of Meteorology (No. 17126), Military Airport (No. 17124) and Anadolu Civil Airport (No. 17123) are located around the Eskişehir city center, approximately 14 km west of the study area

and one of them which is called as Alpu meteorological station (No. 3343) is located in Alpu, approximately 11 km east of the study area. Because the study area is located in between these stations (Figure 2.2), meteorological measurements are expected to be in between the values measured at these stations. Therefore, for this study, Alpu (No. 3343) station with short observation period (1984-2002) and No. 17126 station with long observation period (1929-present) are used. However, although No. 17126 station is still operative since 1929 and has long observation period, it has data loses between the years 1978-1981 and 1990–2006. For these data loses periods, the stations Military Airport (No. 17124) and Anadolu Civil Airport (No. 17123) has been operated. Thus, these stations are also taken into the account for this study to develop a continuous dataset for the Eskişehir city center from 1929 to the present.

2.2.1. Precipitation

Total annual precipitation and cumulative deviation from mean annual precipitation are shown in Figure 2.3 and Figure 2.4 for the 1929-2015 period by obtaining data from No. 17126 station and for the 1985-2001 period by obtaining data from No. 3343 station, respectively. For the 1978-1981 and 1990-2006 years during which the data for station No. 17126 were missing, the data measured in stations 17124 and 17123 were used, respectively. Moreover, precipitation data for meteorological station No. 17126 was deemed inaccurate during 2007-2012 period due to the extremely low precipitation values compared to other stations and other years and hence the precipitation data for the station No. 17123 were used during this period. As shown in Figure 2.3, for the Eskişehir city center, the driest year is 1932 (194 mm) and the wettest year is 1963 (518 mm) while the long term average annual precipitation is 367 mm. Additionally, according to this long term precipitation data, 1929-1937, 1951-1956, 1982-1997 and 2002-2008 years correspond to the dry periods and 1938-1950, 1957-1981 and 2009-2012 years generally correspond to wet periods. If general trend of the graph is examined, 1957-1981 years represent a significantly wet period and 1982-2008 years represent a significantly dry period.

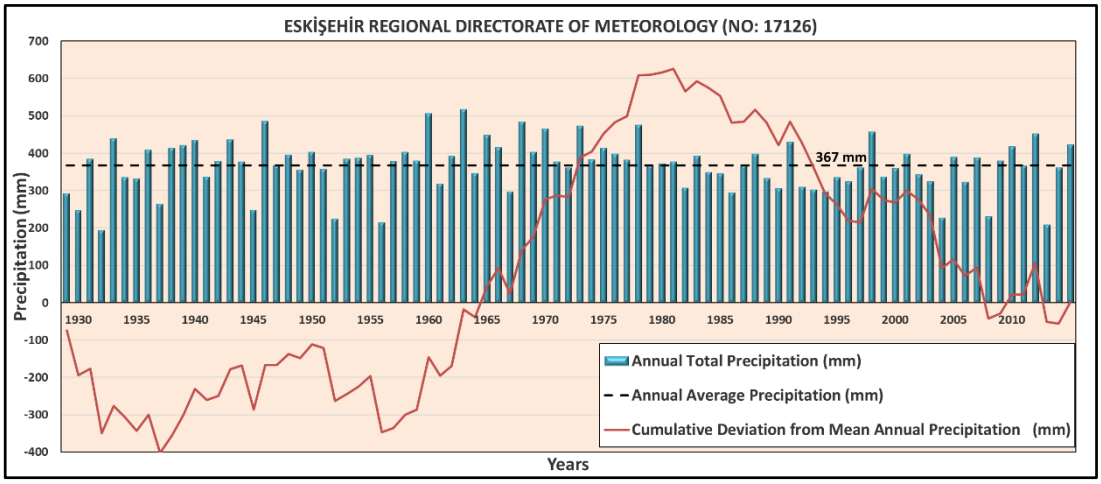

Figure 2.3. Eskişehir Regional Directorate of Meteorology Station total annual precipitation and cumulative deviation from mean annual precipitation graph (1929-2015)

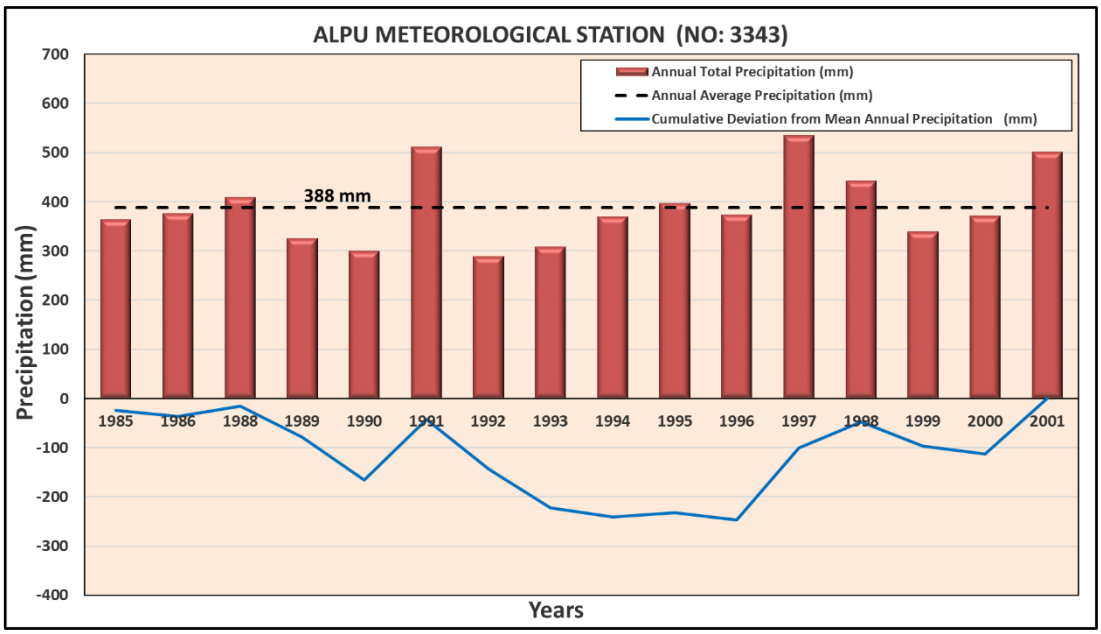

Figure 2.4. Alpu Meteorological Station total annual precipitation and cumulative deviation from mean annual precipitation annual precipitation graph (1985-2001)

According to Figure 2.4, it can be seen that Alpu meteorological station No. 3343 has higher average total annual precipitation (388 mm) in comparison to station in Eskişehir city center. As can be seen from this graph, the driest year is 1992 (288 mm), whereas the wettest year is 1997 (535 mm). Dry and wet periods in this station overlap with station in Eskişehir city center.

Average monthly precipitation data for long term (1929-2015) taken from station No.17126 and short term (1984-2002) taken from station No. 3343 are given in Figure 2.5. According to this figure, December is the wettest month for station No. 17126 (46.4 mm) and No. 3343 (51.8 mm), whereas August (8.3 mm), and September (11.7 mm) are the driest months for station No. 17126 and No. 3343, respectively. If general precipitation trend is examined for these stations, winter and spring seasons (December to May) correspond generally rainy season and July, August and September months have minimum amount of precipitation. However, although they show similar trend, average monthly precipitation is significantly more in Alpu during October, November, December, April and August.

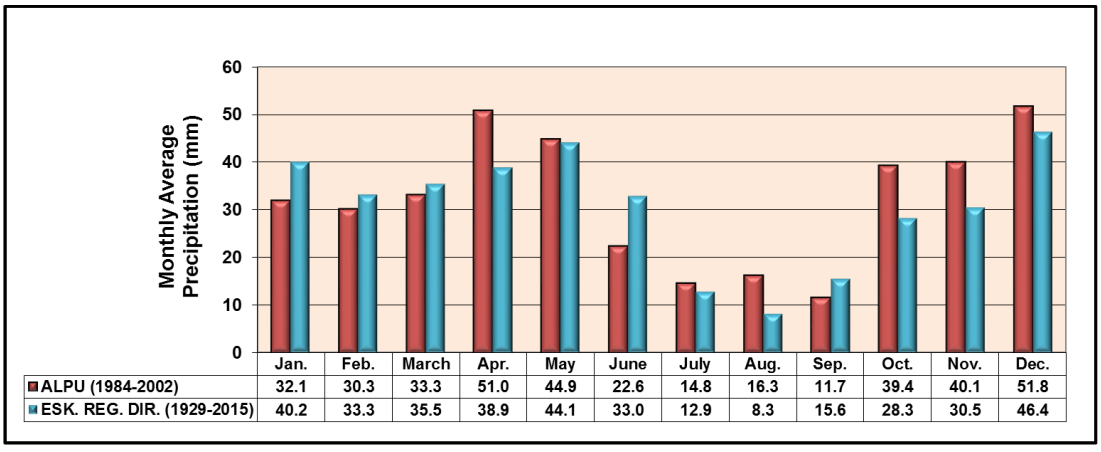

	Jan.	Feb.	March	Apr.	May	June	July	Aug.	Sep.	Oct.	Nov.	Dec.
ALPU (1984-2002)	32.1	30.3	33.3	51.0	44.9	22.6	14.8	16.3	11.7	39.4	40.1	51.8
ESK. REG. DIR. (1929-2015)	40.2	33.3	35.5	38.9	44.1	33.0	12.9	8.3	15.6	28.3	30.5	46.4

Figure 2.5. Average monthly precipitation data for No.17126 (1929-2015) and for No.3343 (1984-2002)

2.2.2. Temperature

Monthly average mean, minimum and maximum temperature values for stations No. 3343 (years 1984-2002) and No. 17126 (years 1929-2015) are represented in Figures 2.6-2.8, respectively. According to Figure 2.6, monthly average temperature values are nearly similar for these two stations. For both of them, average annual temperature is 11 °C and January is the coldest month with average temperature values below zero, while July is the hottest month with average temperature values between 21-22 °C. This similarity shows that nearly same temperature values are expected in the study area. However, for the higher altitudes of the study area, 1-2 °C lower temperature values can be measured.

When the monthly average minimum temperature values are examined in Figure 2.7, except May–September period, temperature values could lie below 0 °C for both stations. Especially in December, January and February, these values reach below - 10 °C.

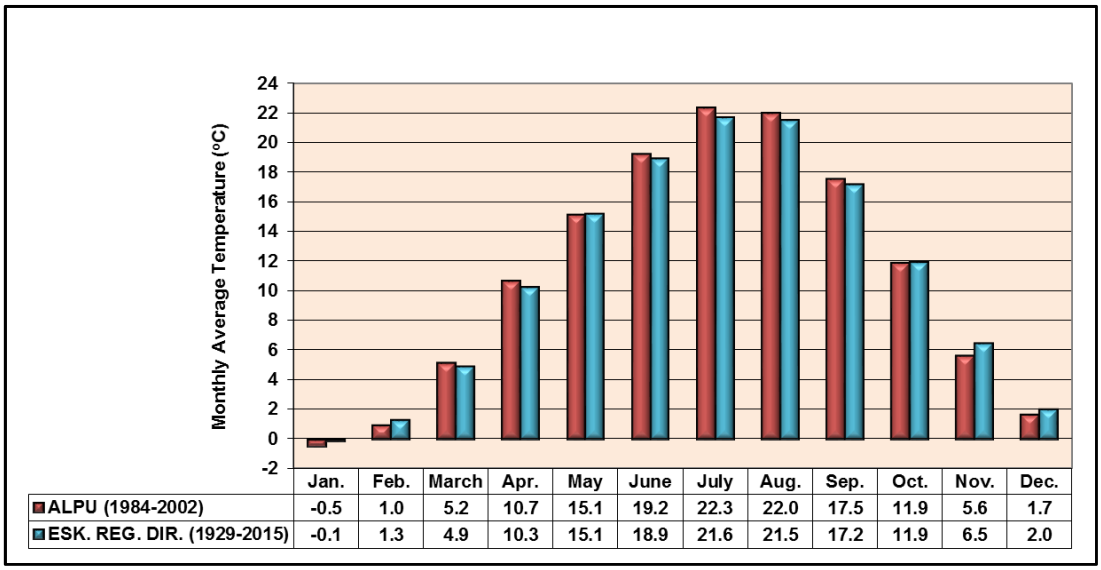

	Jan.	Feb.	March	Apr.	May	June	July	Aug.	Sep.	Oct.	Nov.	Dec.
ALPU (1984-2002)	-0.5	1.0	5.2	10.7	15.1	19.2	22.3	22.0	17.5	11.9	5.6	1.7
ESK. REG. DIR. (1929-2015)	-0.1	1.3	4.9	10.3	15.1	18.9	21.6	21.5	17.2	11.9	6.5	2.0

Figure 2.6. Monthly average temperature of No:3343 and No:17126 meteorological stations

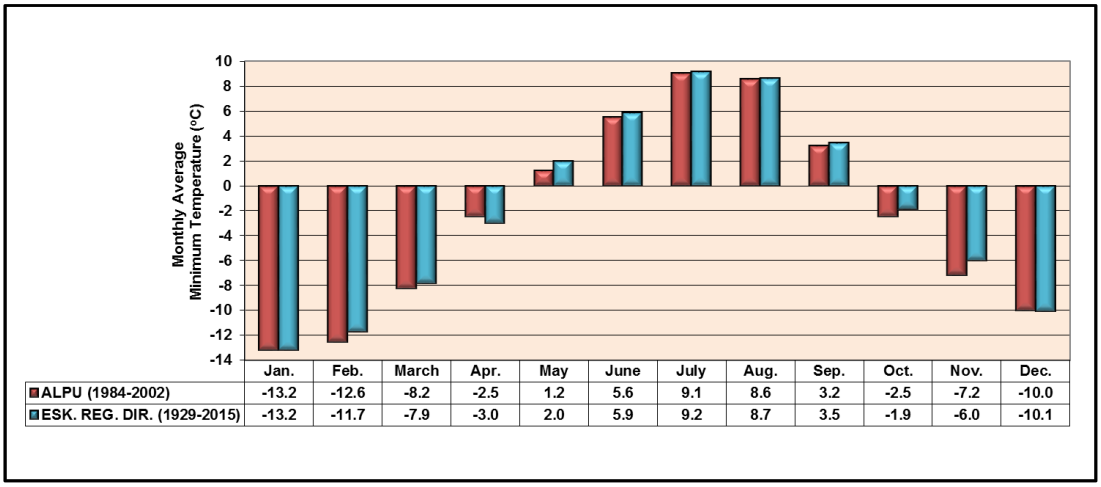

	Jan.	Feb.	March	Apr.	May	June	July	Aug.	Sep.	Oct.	Nov.	Dec.
ALPU (1984-2002)	-13.2	-12.6	-8.2	-2.5	1.2	5.6	9.1	8.6	3.2	-2.5	-7.2	-10.0
ESK. REG. DIR. (1929-2015)	-13.2	-11.7	-7.9	-3.0	2.0	5.9	9.2	8.7	3.5	-1.9	-6.0	-10.1

Figure 2.7. Monthly average minimum temperature of No:3343 and No:17126 meteorological stations

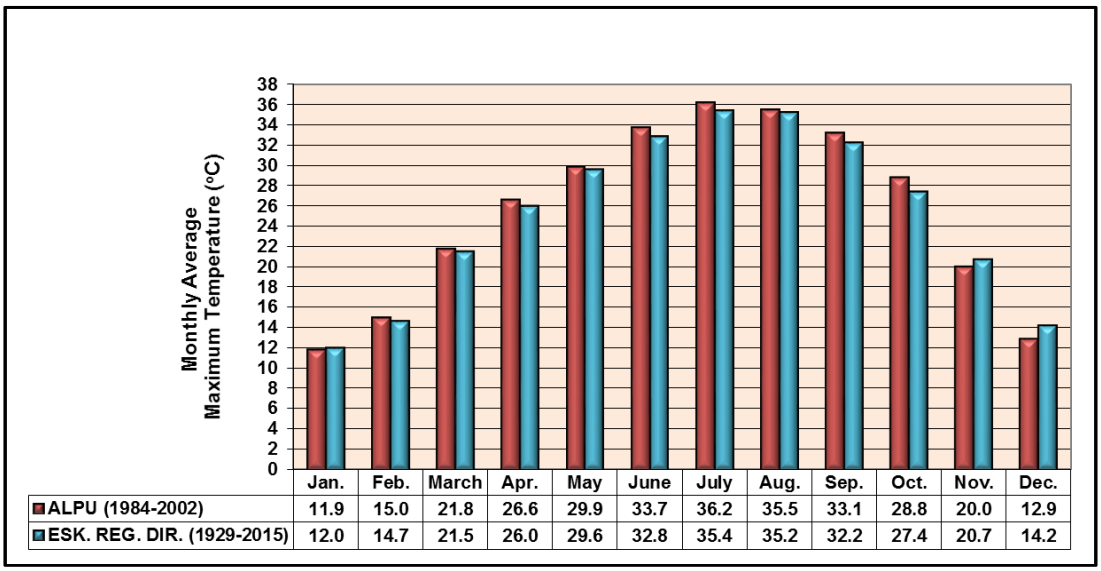

	Jan.	Feb.	March	Apr.	May	June	July	Aug.	Sep.	Oct.	Nov.	Dec.
ALPU (1984-2002)	11.9	15.0	21.8	26.6	29.9	33.7	36.2	35.5	33.1	28.8	20.0	12.9
ESK. REG. DIR. (1929-2015)	12.0	14.7	21.5	26.0	29.6	32.8	35.4	35.2	32.2	27.4	20.7	14.2

Figure 2.8. Monthly average maximum temperature of No:3343 and No:17126 meteorological stations

According to monthly average maximum temperature values (Figure 2.8), July and August are the hottest months with average maximum temperature values ranging between 35-36 °C, whereas in December-February period, monthly average maximum temperature values decreases down to 12-15°C.

2.2.3. Relative Humidity

Monthly average relative humidity values measured in Alpu meteorological station No. 3343 (years 1984-2002) located in Alpu and the Regional Directorate of Eskişehir station No. 17126 (years 1929-2015) located in Eskişehir city center are presented in Figure 2.9. Upon examination of Figure 2.9, the highest monthly average relative humidity values in Eskişehir city center (station No. 17126) are observed in December and January (% 81) and the lowest monthly average relative humidity values are observed in July and August (% 55). Considering the Alpu station, although the distribution of relative humidity values is similar to Eskişehir city center, the actual values are % 2-9 lower.

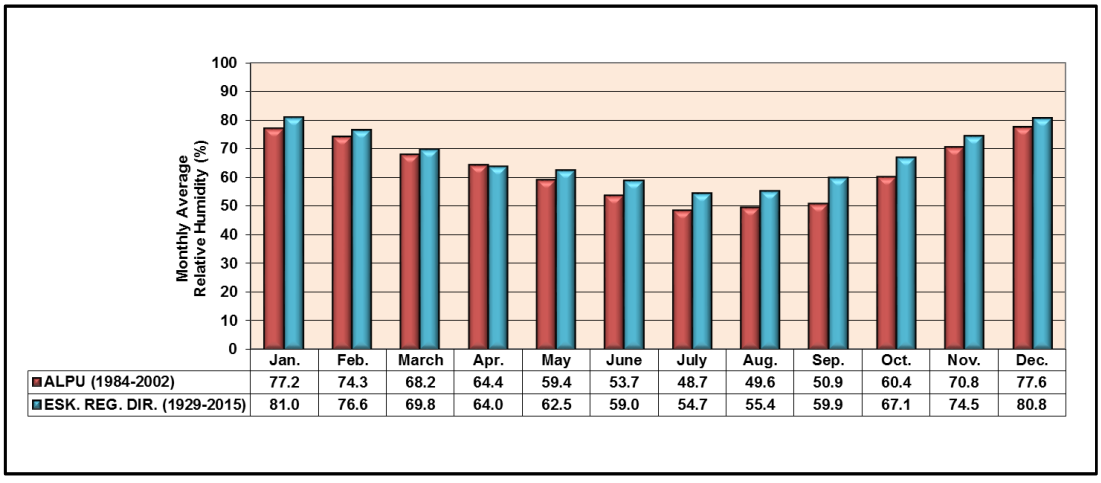

	Jan.	Feb.	March	Apr.	May	June	July	Aug.	Sep.	Oct.	Nov.	Dec.
ALPU (1984-2002)	77.2	74.3	68.2	64.4	59.4	53.7	48.7	49.6	50.9	60.4	70.8	77.6
ESK. REG. DIR. (1929-2015)	81.0	76.6	69.8	64.0	62.5	59.0	54.7	55.4	59.9	67.1	74.5	80.8

Figure 2.9. Monthly average relative humidity values of No:3343 and No:17126 meteorological stations

2.2.4. Evaporation

Monthly total open surface evaporation was measured during April-October period at meteorological stations located in the Eskişehir city center, namely Eskişehir Regional Directorate No. 17126 for years between 1962-1978 and Anadolu Civil Airport Regional Directorate of Meteorology Station No. 17123 for years between 1990-2012 (Figure 2.10). In these stations no evaporation measurements were made during winter months (November-March).

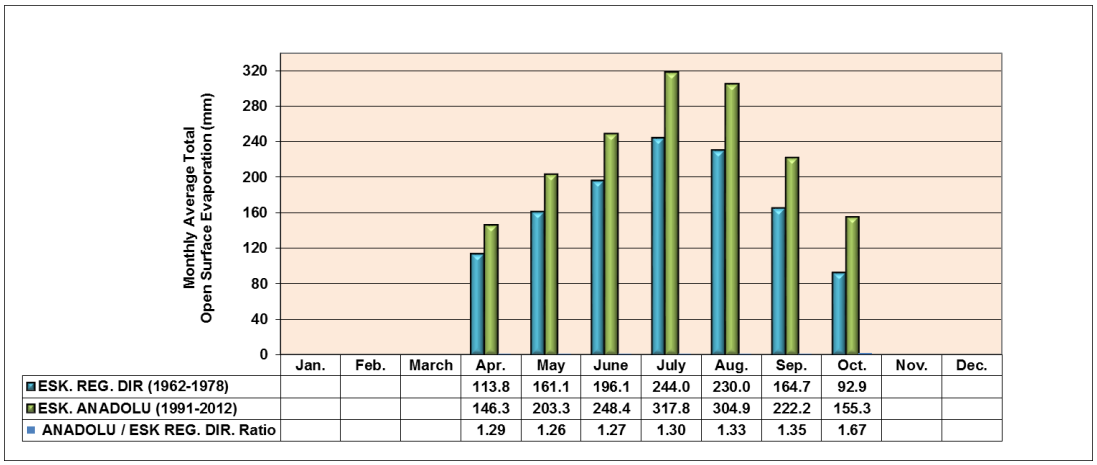

	Jan.	Feb.	March	Apr.	May	June	July	Aug.	Sep.	Oct.	Nov.	Dec.
ESK. REG. DIR (1962-1978)				113.8	161.1	196.1	244.0	230.0	164.7	92.9		
ESK. ANADOLU (1991-2012)				146.3	203.3	248.4	317.8	304.9	222.2	155.3		
ANADOLU / ESK REG. DIR. Ratio				1.29	1.26	1.27	1.30	1.33	1.35	1.67		

Figure 2.10. Monthly total open surface evaporation values of No:17123 (1991-2012) and No:17126 (1962-1978) meteorological stations

As can be seen from Figure 2.10, Anadolu Civil Airport Regional Directorate of Meteorology Station No. 17126, with more current data, measured the values of open surface evaporation about % 30 higher than the values measured in Eskişehir Regional Directorate Station No. 17126. This difference between meteorological stations may be related to the location of the station or urbanization. Taking into account the Anadolu Civil Airport Regional Directorate of Meteorology Station No. 17126 with more recent data, July is the month with the maximum open surface evaporation (317.8

mm) and April is the month with minimum open surface evaporation (146.3 mm) among the months with measurements.

In Figure 2.11, average monthly total precipitation measured by the Eskişehir Regional Directorate Station No. 17126 (years 1929-2015) is shown together with the monthly open surface evaporation calculated by averaging the measurements in this station and station No. 17123. As shown in this figure, in the months with the evaporation measurements evaporation values are significantly higher than the precipitation. In the winter months, where measurements are not taken, evaporation values are expected to be very low and below the precipitation values.

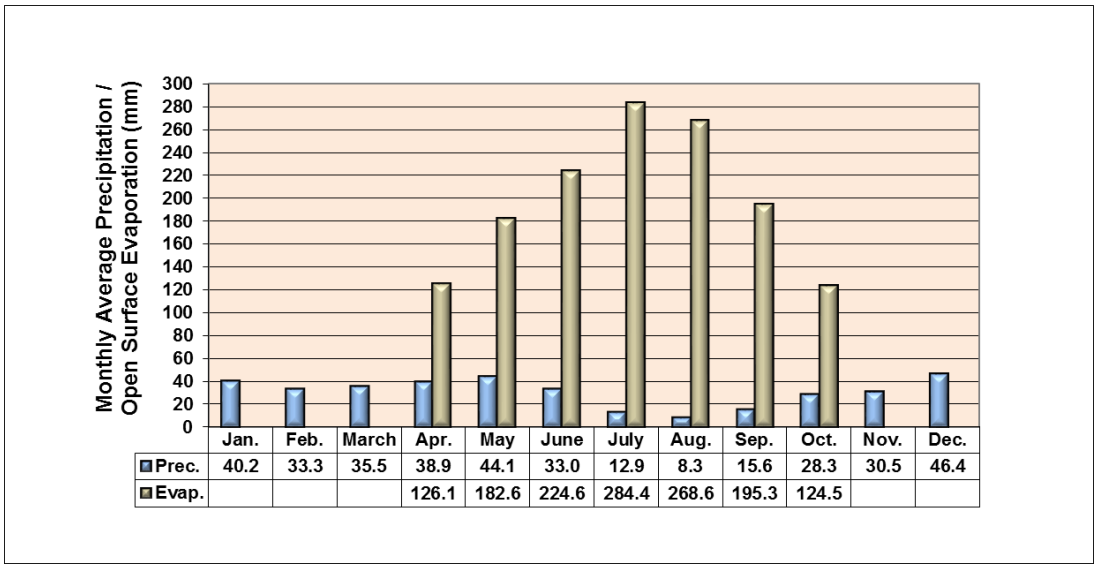

	Jan.	Feb.	March	Apr.	May	June	July	Aug.	Sep.	Oct.	Nov.	Dec.
Prec.	40.2	33.3	35.5	38.9	44.1	33.0	12.9	8.3	15.6	28.3	30.5	46.4
Evap.				126.1	182.6	224.6	284.4	268.6	195.3	124.5		

Figure 2.11. Average monthly total precipitation of Eskişehir Regional Directorate Station No. 17126 (1929-2015)

2.3. Geology

2.3.1. Regional Geology

The study area is located between Sakarya Continent and Anatolide-Tauride Block in the regional scale (Figure 2.12). İzmir-Ankara-Erzincan suture zone which divides these two existing blocks in the area approximately passes from Bozüyük – Eskişehir line. The NW – SE and WNW – ESE trending Eskişehir fault zone which extends from Uludağ at the northwest and to Sultanhanı in the southeast is parallel to this line (Toprak et al., 2015). According to neotectonic and sedimentary data, this fault zone has been active since Pleistocene and it is younger than Upper-Pliocene. The formations of Eskişehir and İnönü basins were strongly influenced by this fault zone. İnönü segment of the Eskişehir fault zone cuts the Lower-Middle Miocene deposits within the Eskişehir Graben located in a restricted area in northern end of the Anatolide Block. The lignite bearing deposits were preserved by Upper Miocene-Lower Pliocene deposits (Senguler, 2013).

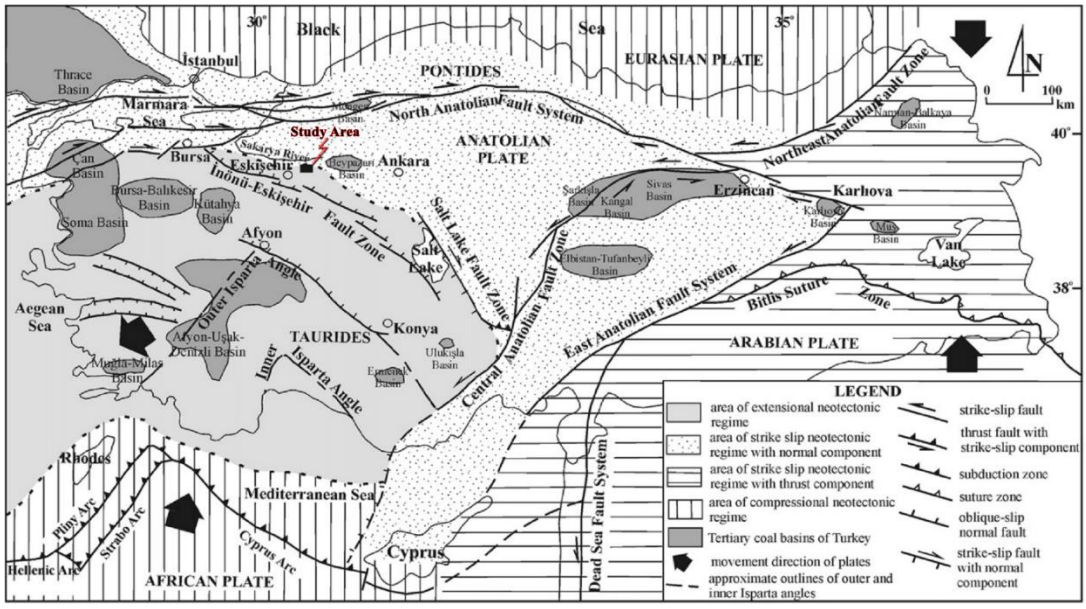

Figure 2.12. Tertiary aged coal basins and the simplified neotectonic sub basin of Turkey and its close vicinity (Toprak, et al., 2015)

2.3.2. Geology and Stratigraphy of the Study Area

The geology and stratigraphy of the study area is summarized from Yazıcıgil et al., (2016). The generalized columnar section and geological map of the study area and its vicinity are given in Figures 2.13 & 2.14, respectively. Within this area, Paleozoic metamorphics and Mesozoic units outcropped in the southeastern and northwestern parts of the study area and tectonically in contact with Paleozoic metamorphics form the basement rocks. This tectonic contact progressed from north to south as an imbricated structure (Gözler et al., 1997). Exact thickness of the metamorphics are not known due to the their folded and jointed structure. However, it can be said that thicknesses of schist and marble are approximately 1000 m and 200 m, respectively (Senguler, 2013). Triassic aged melange (Mja) overlying the metamorphics as nappe and underlying ophiolites as tectonic slices is formed by tectonic relation of the radiolarites, crystalline limestone and marbles, mudstones, diabase, serpentinites, metamorphics, peridotites and gabbro blocks without cementation. Triassic aged ophiolites (ϕ) that are tectonically in contact with the Triassic aged melange comprises of peridotite, serpentinite, pyroxenite, metapyroxenite, hornblende, metahornblende, gabbro, metagabbro, diabase, metadiabase, listwanite as indicator of tectonic zones and eclogite units as the metamorphic equivalence of oceanic crust. Although this unit is seen as nappe structure as usual, they can be observed as tectonic slices (Gözler et al., 1997). Furthermore, these generally mixed structural oceanic crust materials deposited as overturned sequence. Metadetritics (TRkd) overlying ophiolites tectonically include metaconglomerate, metasandstone and phyllites and their metamorphism varies depending on the contact with ophiolites. This unit is overlain by Jurassic-Cretaceous aged limestones discordantly (Jzkçt). These massive formed, dense fractured limestones continue as micritic, thin dolomitic limestones through the upper parts and ended with pinky, cream, variegated colored, thin-medium layered, fossiliferous, cherty layered (1-5 cm) micritic limestones at the top (Gözler et al., 1997). Mesozoic basement rocks are cut by Upper Cretaceous aged granodiorite (G) up to peridotites. This generally porphyritic, locally grained, E-W elongated

granodiorite is highly altered and shows morphological structure concurrent to topography (Figures 2.13 & 2.14).

In the study area, lignite bearing Middle-Upper Miocene deposits (Porsuk Formation) unconformable overlie the basement rocks. At the bottom of these deposits, basal conglomerate comprising pebble stone, sandstone and claystone is located (m1). This multi-layered unit has thick, red, yellowish, greyish colored layers, but it is generally distinguished with reddish-brownish colored. Pebbles of conglomerates mainly consist of schist, marble, radiolarite, chert, gabbro, diabase, serpentinite, granodiorite and limestones.

Basal conglomerate is overlain by a sequence (m2), which is represented by conglomerate, green claystone, lignite seam (C), gray sandstone, bituminous shale, lignite seam (B), bituminous shale, lignite seam (A) and green claystone-sandstone-conglomerate alternation, from the bottom to the top. These sequence has generally green-yellow colors and locally variegated colors. Thickness of the sequence varies from 100 to 500 m in the study area. Within these sequence, tuff, tuffite and marl are also seen. Tuffite and marl especially exist in the eastern part of the study area. In this regions, this m2 unit is laterally and vertically gradational with the upper and lower units and includes limestone.

On the upper part of the m2 unit, the Miocene silicified limestone (m3), which outcrops on the high hills at the southwestern and western part of the study area, is seen (Figures 2.13 & 2.14). This cream, white and grey colored limestone unit contains silica layers and tuffite. Thickness of this unit varies between 5-60 m in the study area.

Miocene aged units are unconformably overlain by Pliocene aged units which are called as Ilıca Formation and outcrop in the eastern and western side of the of the study area.

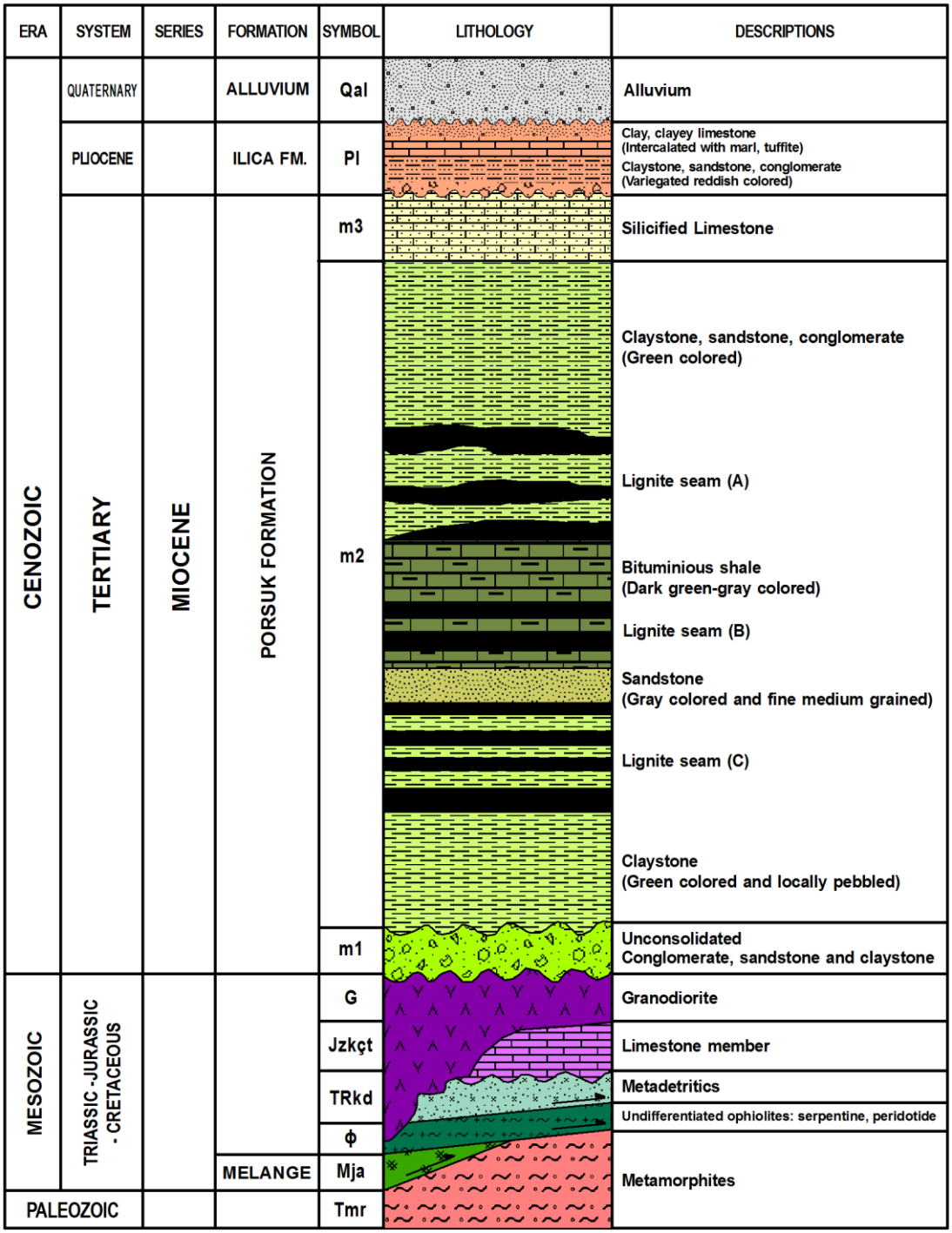

Figure 2.13. Generalized columnar section of the study area and its surroundings (Modified from Gözler et al., 1997, Siyako et al., 1991 and Senguler, 2013)

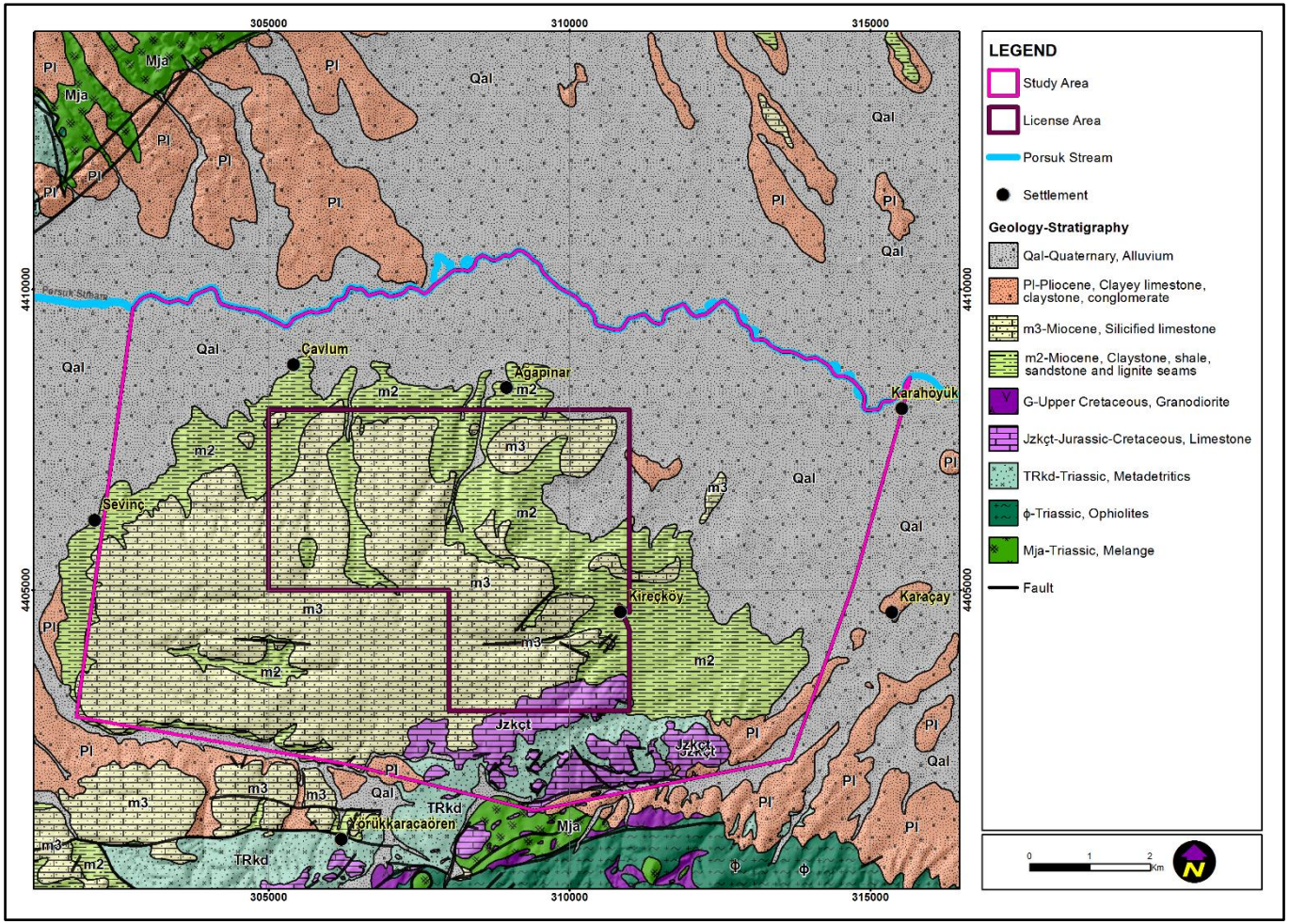

Figure 2.14. Geological map of the study area and its surroundings (Modified from Gözler et al., 1997 and Senguler, 2013)

These units are composed of reddish variegated conglomerate, sandstone, claystone, red colored tuffite intercalated mudstones, variegated colored clayey limestone, marl and light brown to grey colored clays from the bottom to the top (Siyako et al., 1997).

Quaternary alluviums which cover Pliocene units unconformable include silt and clay intercalated sand and gravels. These deposits are seen along the Porsuk Stream and the lowland areas within the study area. Thickness of the alluvium varies between 10-50 m and increases toward the Porsuk Stream. In this study, Pleistocene aged alluvium at the terraces and flat places cannot be distinguished from Holocene aged recent alluvium.

CHAPTER 3

HYDROGEOLOGY

3.1. Water Resources

Water resources provide a basis for the hydrogeological studies. In the study area, they were studied by using topographical maps, a detailed review of previous studies and field investigations. As a result of these, surface water resources, springs, fountains and captages and wells drilled for different purposes were identified within the vicinity of the study area and they will be discussed in detail in the following sections.

3.1.1. Surface Water Resources

The most important perennial surface water body in the vicinity of the study area is the Porsuk Stream which is the longest tributary of the Sakarya River flowing in easterly direction along the northern boundary of the study area (Figure 3.1). It starts drainage from the Murat Mountain which forms the boundary of cities of Kütahya and Uşak at an approximately 125 km distance from the study area, runs through Kütahya Plain and after being collected behind the Porsuk Dam located in 41 km southwest of the study area, passes through Eskişehir Plain and the Eskişehir city center. After that, it passes from the northern boundary of the study area and finally joins the Sakarya River around Yassıhöyük located 100 km east of the study area. Other surface water structures are also seen in the study area.

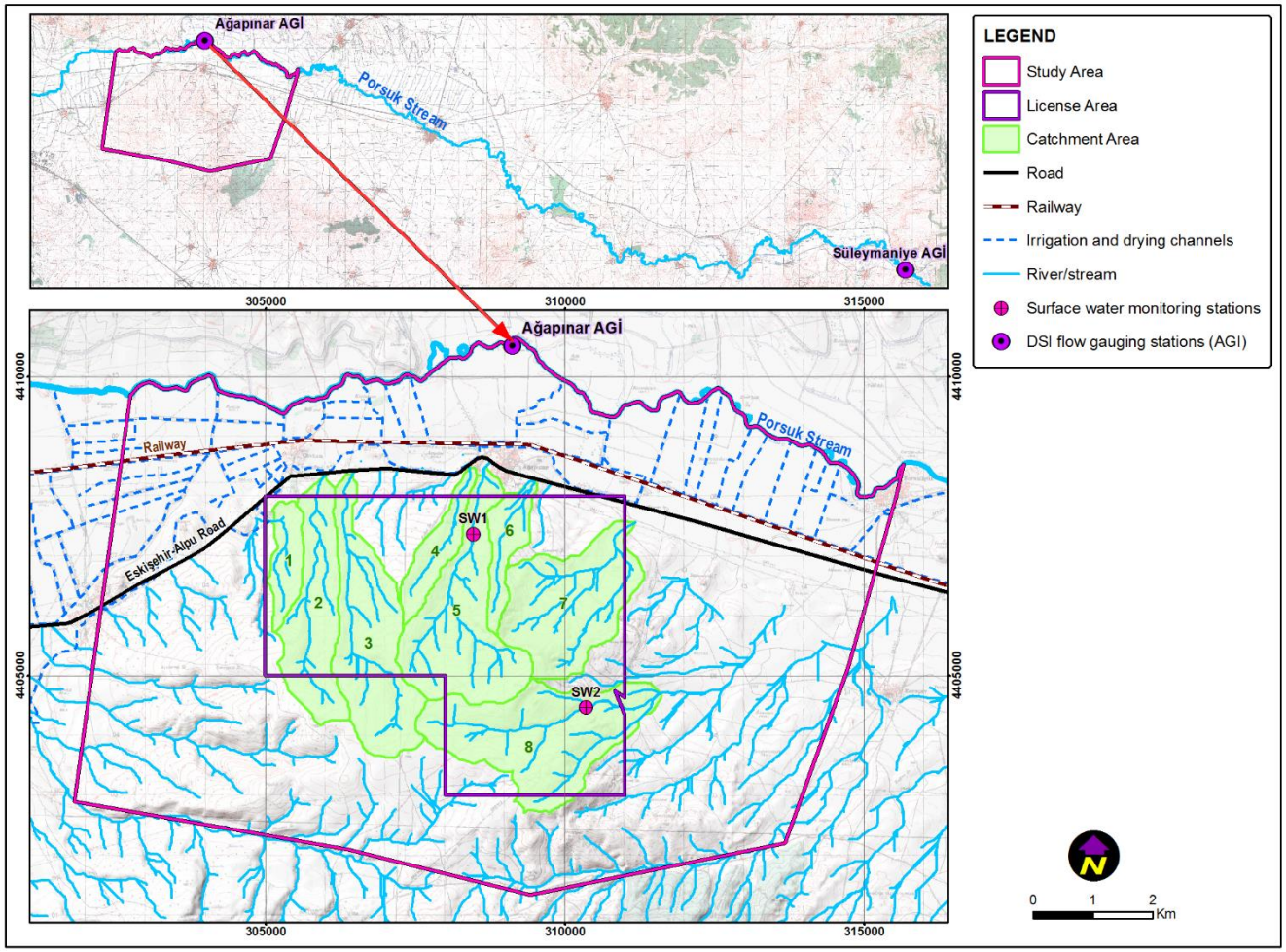

Figure 3.1. Surface water drainage pattern of the study area

These are the right-hand Eskişehir-Alpu irrigation canals starting from Karacaşehir regulator located at the 19 km northwest of the study area and dewatering canals located in the region between the northern part of the Eskişehir-Alpu road and the southern part of the Porsuk Stream.

Apart from the perennial Porsuk Stream, surface drainage is represented by small dry creeks which flow only intermittently as a result of sudden heavy rainfall and snow melt. According to Yazıcıgil et al., (2016), eight creeks drain the study area (Figure 3.1). Their catchment areas are given in Table 3.1. As can be seen from this table, the creeks with the largest catchment area are Pınar Creek (4.90 km^2), Çürüksu Creek (4.16 km^2) and Akpınar Creek (3.95 km^2), respectively. Among these creeks, Pınar Creek drains the southeast part of the license area towards east and leaves the license area after flowing through the Kireçköy whereas the others drain the middle and northern parts of the license area towards north and recharge the plain.

Table 3.1. Catchment areas of the creeks within the study area

Catchment No.	Area (km^2)	Creek Name
1	0.910	
2	2.844	İnönü Creek
3	3.945	Akpınar Creek
4	1.082	
5	4.163	Çürüksu Creek
6	1.017	
7	3.846	
8	4.899	Pınar Creek
SW-1	3.678	Çürüksu Creek
SW-2	2.662	Pınar Creek

During the field investigations, two surface water monitoring stations were identified on the Çürüksu Creek and Pınar Creek as SW-1 and SW-2 by Yazıcıgil et al., (2016) to monitor discharge rates (Figure 3.1). However, both creeks were dry during all

observation period (once in a month from January 28, 2015 to February 7, 2016). It was observed that some of the creeks are fed by fountains and spring located at the upstream locations, however as moving towards low elevations in the north, the surface water infiltrates into the soil and the creek valley becomes dry.

Although discharge rates of the creeks are not measured since they did not show flow pattern during the observation period, monthly discharge measurements were performed at the DSI flow gauging stations (AGI) on the Porsuk Stream between 2007-2009 (DSI, 2010). One of these stations is located around the Ağapınar (Figure 3.1) and the other one is located around the Süleymaniye, approximately 60 km downstream of the Porsuk Stream. In Figure 3.2, monthly discharge rates measured from these stations are given. According to this figure, discharge rates range between 2.42 m^3/s (January, 2009) and 5.64 m^3/s (May, 2007) for Ağapınar flow gauging station at the upstream and 2.57 m^3/s (December, 2009) and 5.86 m^3/s (June, 2007) for Süleymaniye flow gauging station at the downstream. The average discharge rates are 3.56 m^3/s and 3.81 m^3/s for Ağapınar and Süleymaniye stations, respectively.

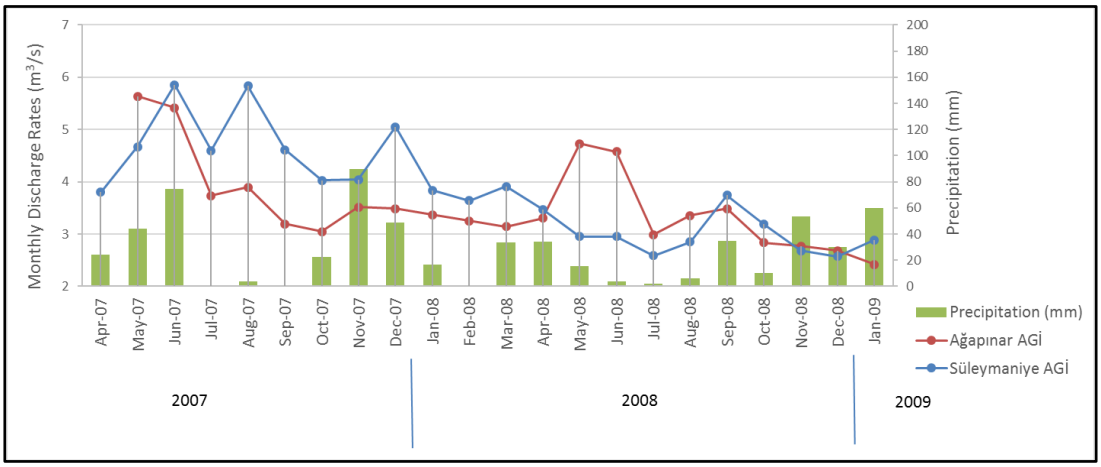

Figure 3.2. Monthly discharge rates at Ağapınar and Süleymaniye gauging stations between 2007-2009 (DSI, 2010)

3.1.2. Springs and Captages

According to Yazıcıgil et al., (2016), five springs and four captages are designated within the study area (Figure 3.3). In Table 3.2, detailed information about these water resources are given. In the study area, springs are generally located in the captages and water captured from them is carried overland by pipe to concreate fountains to provide water for livestock. As can be seen from Figure 3.3, all springs and captages in the study area discharge from the contact of silicified limestone (m3) and lignite intercalated clayey m2 unit. The highly permeable and karstified silicified limestones which outcrop at the higher elevation of the study area are recharged by precipitation and discharge their groundwater at the contact of m2 unit which has lower permeability.

During the nearly one-year period between December, 2014 and February 2016, discharge measurements from the mentioned seven springs were implemented. In Table 3.2, minimum, maximum and average measured discharge rates from these springs are given. In the study area, springs have low discharges which range between 0.04 L/s and 0.39 L/s. The total discharge amount from the springs is equal to 1 L/s.

In Figure 3.4, temporal discharge measurements taken from the springs and their relation with the precipitation are shown. For this analysis, precipitation data from the Eskişehir Regional Directorate of Meteorology (No. 17126) provided until January 01, 2016 was used. As can be seen from Figure 3.4, since the discharge from the springs are related with the precipitation, discharge rates reach maximum values in winter and spring and minimum values in summer and autumn seasons.

Beside lower discharge rates of springs, a significant amount of water discharges from the four captages that supply water to Ağapınar, Çavlum, Kireçköy and Sevinç villages. Since taking discharge measurements was not possible from the captages in the field, total discharge amount is estimated as 14 L/s according to field observations.

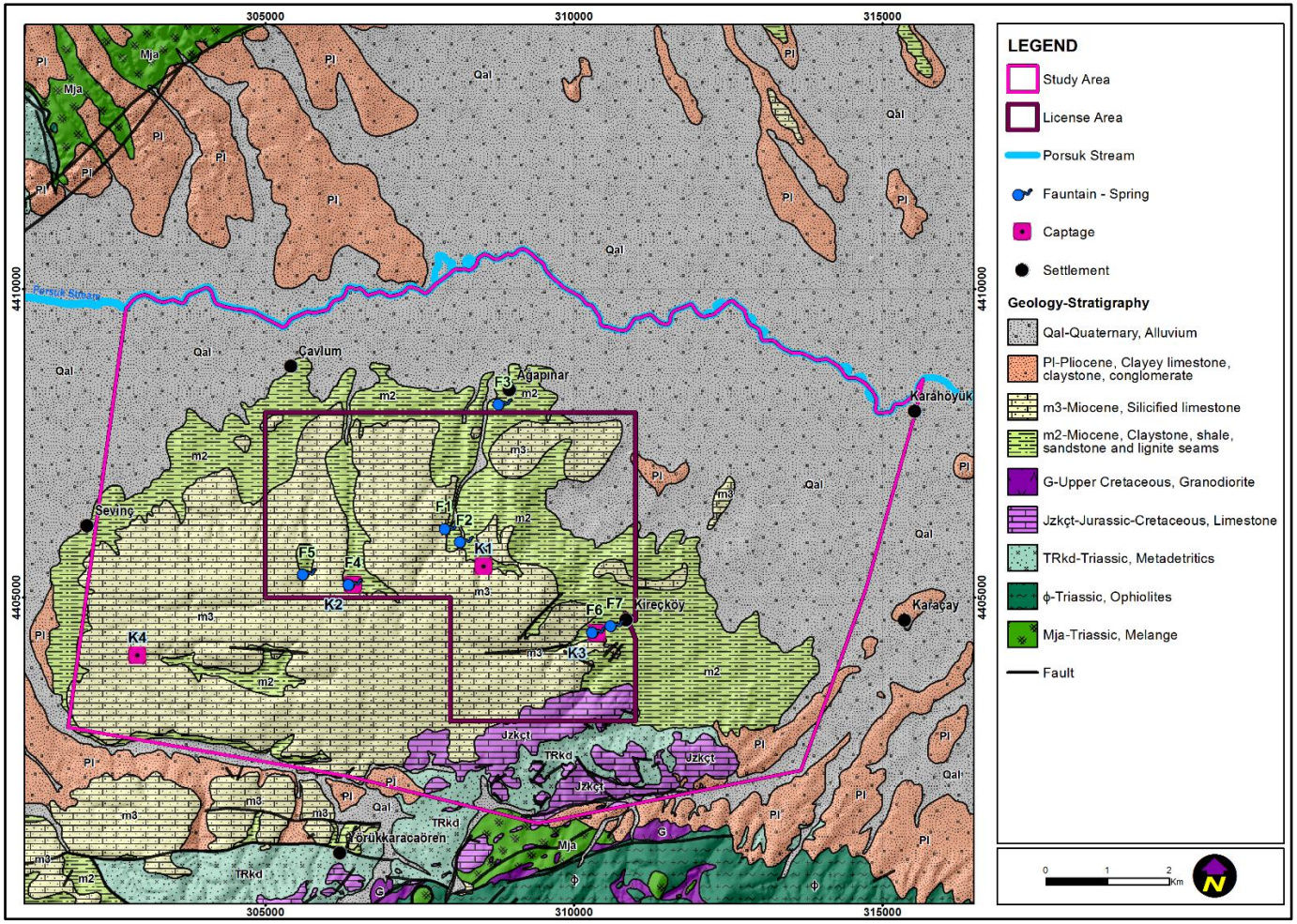

Figure 3.3. Locations of springs and captages within the boundaries of the study area

Table 3.2. Detailed information about spring and captages

No.	Type	Location	Coordinates (m)		Elevation (m)	Discharge rates (L/s)		
			East	North		Minimum	Maximum	Average
F1	Spring - Fountain	Ağapınar	307979	4406132	871	0.03	0.08	0.05
F2			308227	4405919	882	0.05	0.23	0.12
F3			308850	4408153	795	0.04	0.16	0.08
F4		Çavlum	306427	4405230	923	0.02	0.08	0.04
F5			305681	4405393	901	0.01	0.07	0.04
F6		Kireçköy	310369	4404456	880	0.06	0.66	0.24
F7			310666	4404564	863	0.10	1.00	0.39
K1	Captage	Ağapınar	308537	4405511	929	(no measurement)		
K2		Çavlum	306428	4405211	928			
K3		Kireçköy	310375	4404426	884			
K4		Sevinç	302932	4404069	835			

As a result, totally 15 L/s of discharge is occurring from the springs and captages in the study area.

3.1.3. Wells

Water wells can be separated into four main groups, including: DSI wells, village wells, private wells and pumping/observation wells within and the vicinity of the study area. In this section, detailed information for each well group will be given.

DSI Wells

In the study area, seven water wells were completed by DSI and subcontractor firm between the 1988-2012 period with the purposes of investigation, operation and observation (Figure 3.5). Detailed information about these wells are given in Table 3.3. Five of DSI wells (44130, 55322, 55323, 55324 and 55325) located at the eastern part of the study area are used by Kireçköy Irrigational Cooperative to irrigate 189 hectares agricultural estate. The other well in the eastern part numbered as 39005 was installed for the purpose of investigation. These easterly located wells pump water from the Pliocene sandstone, conglomerate and limestone and Quaternary alluvium. In the northern part of the license area, there is another water well installed by DSI

with number of 61357. This 120 m depth well was drilled in 2012 only for monitoring water level changes and it is screened across the marl and sandstones of the Miocene m2 unit.

Village Wells

Village wells W1 and W2 are installed for the drinking and domestic water requirements of the Ağapınar and Kireçköy villages, respectively (Figure 3.5). These wells supply water to these villages' water depots in addition to water obtained from captages. During field investigations, monitoring of W1 well was not possible. W3 is another water well which can be evaluated within this group. This artesian well is located at the eastern part of the license area and enabled monitoring in addition to W2 well.

Private Wells

During field investigations conducted in January-February, 2016, 78 private wells were determined within the boundaries of the study area, generally installed by villagers (Yazıcıgil et al., 2016). These wells are intensely located in the eastern and northeastern part of the license area (Figure 3.5). They generally pump water from Quaternary alluvium and Pliocene units for irrigational purposes. Some of these wells are also used by farmers to supply water for livestock and other purposes. In addition to this information, detailed data cannot be obtained for these wells except their coordinates and altitude.

Pumping and Observation Wells

The final well group was installed within the scope of the project "Hydrogeological Investigation and Characterization of the Esan-Alpu Coal Mine Exploration Site" (Yazıcıgil et al., 2016) between March and July 2015.

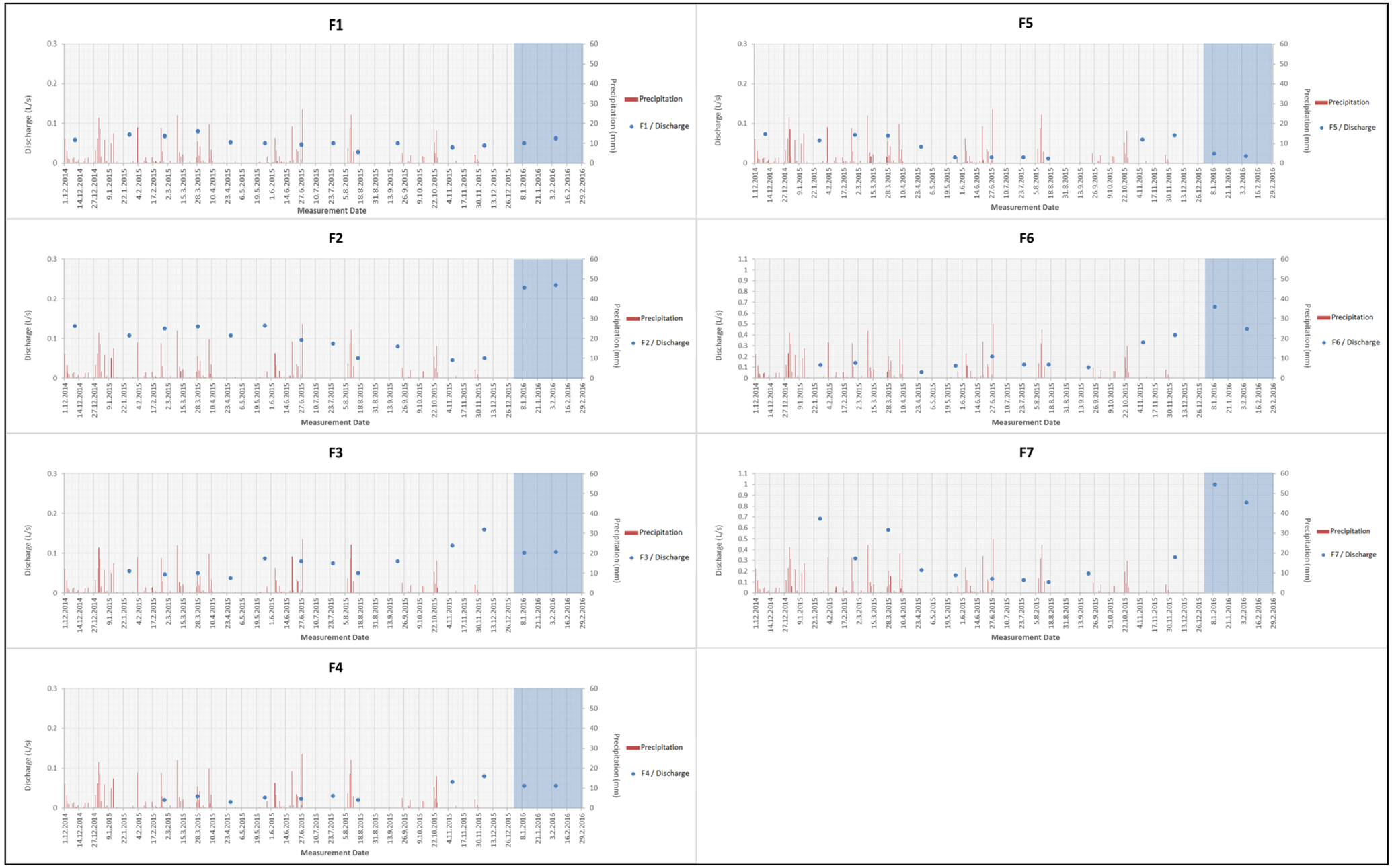

Figure 3.4. Temporal changes in discharge rates measured at the springs (Blue areas show the time interval with no precipitation measurements after 31.12.2015)

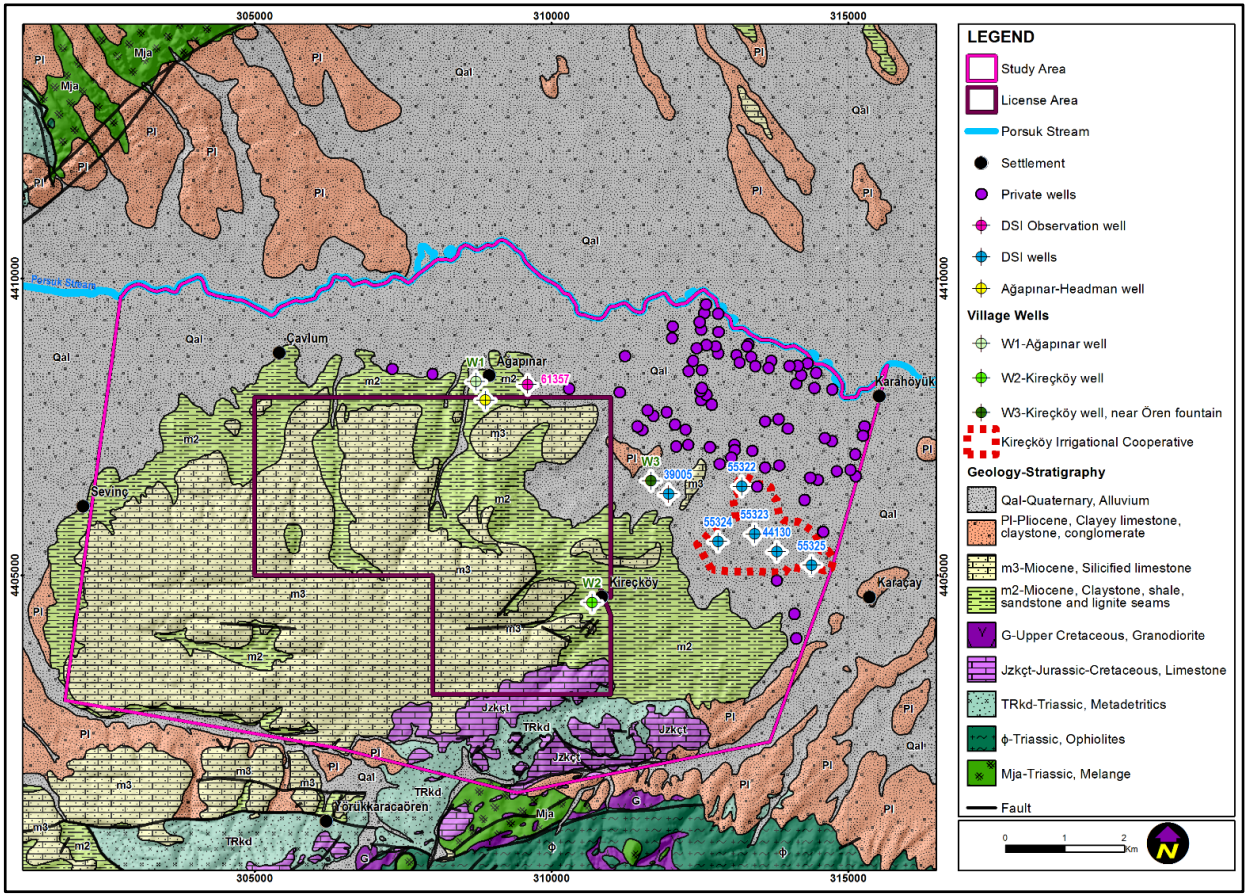

Figure 3.5. Location of wells within the boundaries of the study area

Table 3.3. Detailed information about DSI wells in study area

Well No.	Drilling Contractor	Drilling Purpose	Location	Drilling Year	Coordinates		Elevation (m)	Well Depth (m)	Screen (m)		Total Screen Length (m)	Aquifer Lithology	Formation	Static L. (m)	Dynamic L. (m)	Well Yield (L/s)		Specific Capacity (L/s/m)
					East (m)	North (m)			Top	Bottom						Artesian	Pumping	
39005	DSI	Investigation	Ağapınar	1988	311975	4406375	780	150	24	128	68	Conglomerate, Tuff, Marl	Quaternary-Pliocene	+0.05	54.05	1.00	4.00	0.07
44130	DSI	Investigation	Kireçköy	1993	313800	4405400	787	130	24	120	44	Clay, Limestone, Tuffite, Conglomerate	Quaternary-Pliocene	17.60	50.98		24.97	0.75
55324	G & M	Operating	Kireçköy	2001	312808	4405572	795	70	24	60	24	Limestone, Claystone	Quaternary-Pliocene	28.00	44.68		35.34	2.12
55325	G & M	Operating	Kireçköy	2001	314383	4405170	782	140	32	132	52	Marly Limestone, Claystone, Mudstone	Quaternary-Pliocene	16.00	54.66		36.85	0.95
55322	G & M	Operating	Kireçköy	2001	313207	4406502	766	78	24	64	26	Limestone, Claystone, Marl	Quaternary-Pliocene	11.05	50.27		22.08	0.56
55323	G & M	Operating	Kireçköy	2001	313426	4405702	782	93	28	88	36	Claystone, Marl, Limestone	Quaternary-Pliocene	16.20	48.96		37.23	1.14
61357	DSI	Observation	Ağapınar	2012	309601	4408215	784	120	20	112	40	Marl, Sandstone	Miocene	18.22	91.24		4.00	0.05

This group is composed of five pumping and four observation wells which are clustered in three different locations within the license area to determine the water bearing properties of various hydrogeological units and to estimate their hydraulic parameters and to investigate the hydraulic relations between each other and coal seams (Figure 3.6). A total of 2515 m of drilling was conducted for a total of nine wells with depths ranging between 50 m and 420 m. Detailed information about them is given in Table 3.4.

In the study area, for some pumping wells, pumping and recovery tests were conducted to determine the hydraulic parameters (transmissivity, hydraulic conductivity and storativity) of the water bearing units. In those wells that were not possible to conduct these tests due to low yields, slug tests were performed to determine the hydraulic conductivity of the units.

The first nested wells location is at the northeastern part of the license area close to the AK043 numbered coal exploration well (Figure 3.7). According to lithological logging data of AK043 well, Upper Miocene silicified limestone (m3) outcrops in this location down to 13 m depth. Then, claystone-sandstone-conglomerate intercalation, claystone-lignite seam A, shale-lignite seam B-shale, sandstone-lignite seam C and finally claystone (m2) units are cut from top to bottom, respectively. In this location, 325 m depth pumping well PK-2 and 300 m depth observation well GK-2 were drilled to test all these lignite seams A, B and C and overburden units. The purpose of screening these wells along the all lithological units is to obtain information about the groundwater inflow for the pumping activities during dewatering processes.

The second nested wells group consists of five wells located at the southern part of the license area close to the AK016 numbered coal exploration well (Figure 3.8). This location is chosen in the upland recharge area to examine hydraulic relations of the Miocene silicified limestone (upper lignite unit) and Jurassic-Cretaceous limestone (lower lignite unit) with lignite bearing units.

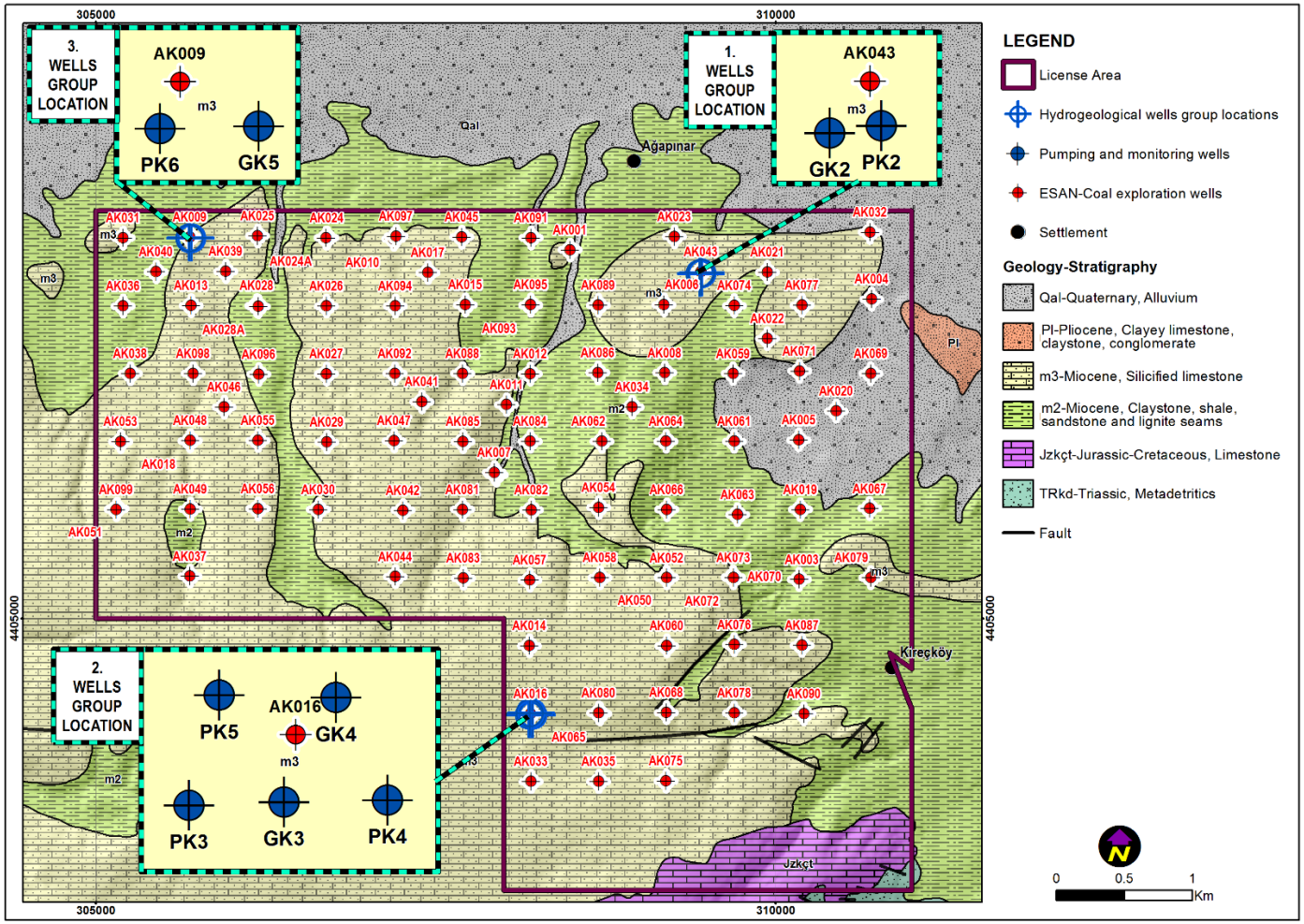

Figure 3.6. Locations of the pumping and observation wells and coal exploration wells within the boundaries of the license area

Table 3.4. Detailed information about the pumping and observation wells

Well Name	Well Type	Coordinates (m)		Elevation (m)	Water Level Measurement Elevation (m)	Depth (m)	Screen Interval (m)	Well Diameter (inch)	Casing Diameter (mm)	Casing Material
		East	North							
PK-2	Pumping	309453	4407541	813	812	325	21-317	17.5	219	Steel
GK-2	Observation	309442	4407539	812	812	300	28-292	12.5	175	PVC
PK-3	Pumping	308187	4404292	995	994	420	352-416	15	219	Steel
GK-3	Observation	308197	4404292	995	995	336	300-330	12.5	140	Steel
PK-4	Pumping	308208	4404293	996	995	60	26-56	12.5	175	PVC
GK-4	Observation	308203	4404303	996	996	50	26-46	12.5	125	PVC
PK-5	Pumping	308190	4404304	996	996	208	136-204	15	200	PVC
PK-6	Pumping	305690	4407800	801	801	420	368-416	17.5	219	Steel
GK-5	Observation	305700	4407800	801	801	396	372-390	12.5	125	Steel

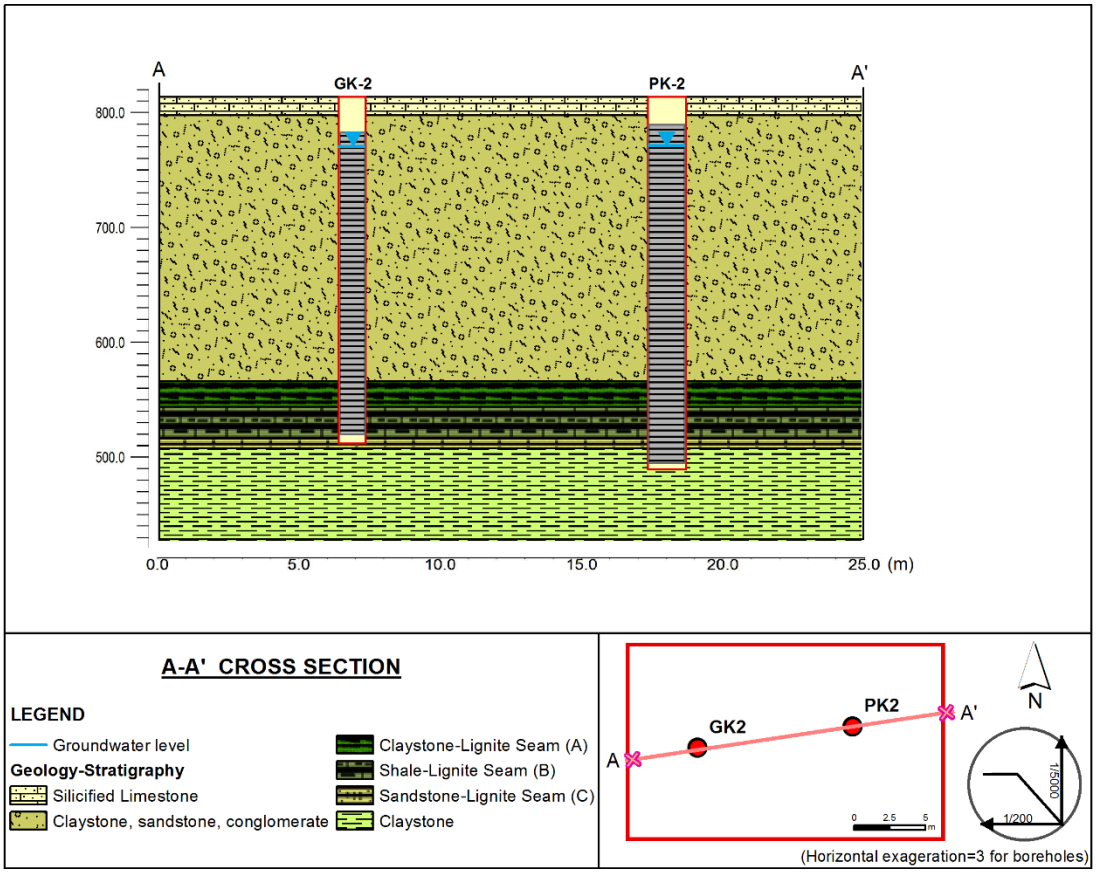

Figure 3.7. Cross section of the first nested wells group

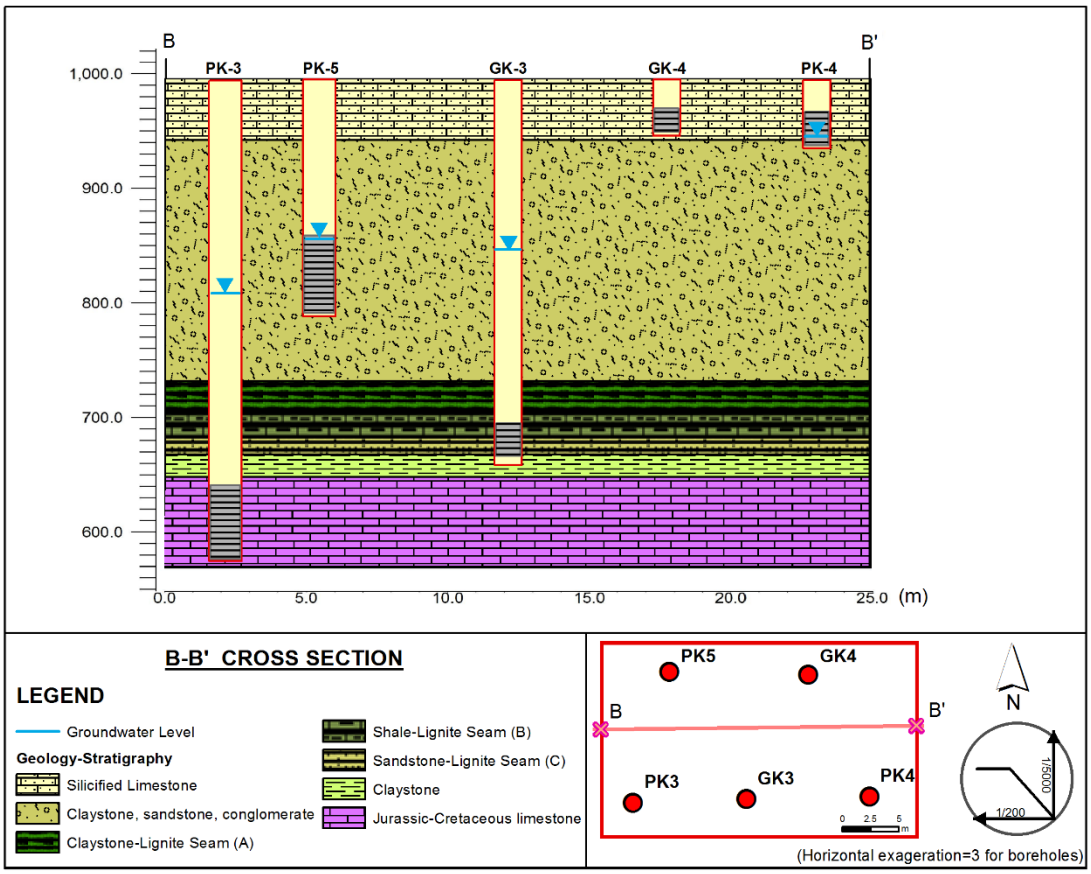

Figure 3.8. Cross section of the second nested wells group

The purpose of drilling 420 m depth PK-3 pumping well is to obtain information for water bearing properties and hydraulic parameters of Jurassic-Cretaceous limestone and hydraulic relations between them with the overlying lignite bearing units. The shallower PK-4 and GK-4 wells with 50-60 m depths, respectively were drilled to determine hydraulic properties of the silicified limestone which are tapped by several captages that supply water to meet the drinking water requirements of the villages in the study area. Furthermore, the information obtained from these wells will shed light to the hydraulic relation between silicified limestones and the underlying lignite bearing units. The pumping well PK-5 and observation well GK-3 were drilled in this location to investigate the hydraulic parameters of the upper Miocene units overlying

the coal seams and lignite bearing units and to determine the hydraulic relation between these units with silicified limestone and Jurassic-Cretaceous limestone.

The third clustered wells location is at the northwestern boundary of the license area (Figure 3.9). In this location, 420 m depth PK-6 pumping well and 396 m depth GK-5 observation well were screened within the lignite seam A and lower units and lignite bearing units, respectively to determine their hydraulic properties and water bearing capacities. Additionally, it is intended to calculate the water pressure of the lower lignite bearing units.

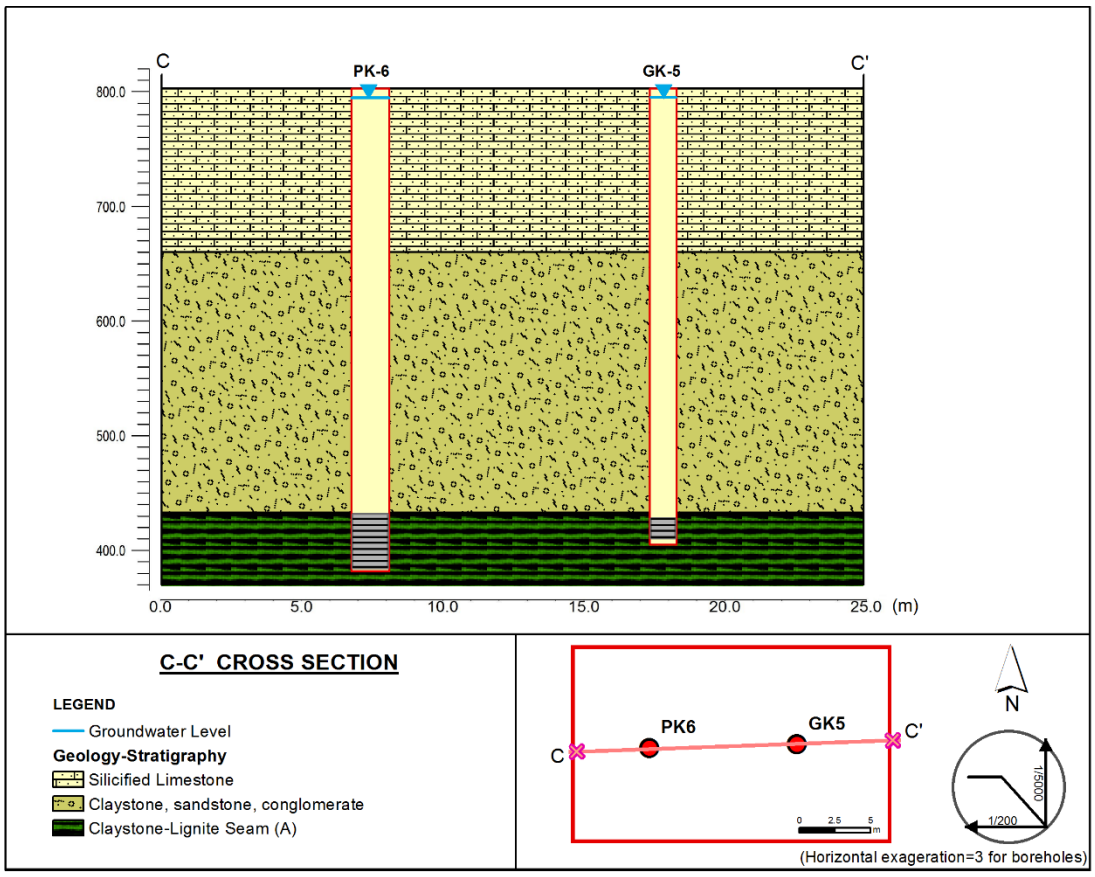

Figure 3.9. Cross section of the third clustered wells

3.2. Hydrogeology of the Study Area

In this section, hydrogeological properties of the geological units within the study area and its near vicinity will be explained from basement to the top. As mentioned in Chapter 2.3, Paleozoic metamorphics, including marble, schist and gneiss, Mesozoic ophiolites, Triassic metaclastic rocks and Jurassic-Cretaceous limestones are the members of the basement unit and they outcrop at the southern part of the study area. These rock units are generally impervious or semi-pervious and they may bear groundwater along their fractures that is probably associated with faulting. Within basement rocks, Jurassic-Cretaceous limestone shows permeable to semi permeable character. However, according to pumping test conducted in this unit, limestones at this locality are relatively impervious with low conductivity ($K=2.35x10^{-8}$ m/s). Additionally, the hydrochemical tests conducted at this unit also showed that it has NaCl facies groundwater which is formed most likely by the effect of slow movement of groundwater that have a long contact time within rock unit (Yazıcıgil et al., 2016). Therefore, additional pumping test, especially in the northwest part of the study area is necessary to understand the water bearing potential and hydraulic parameters of the Jurassic-Cretaceous limestone.

Lignite intercalated Middle-Upper Miocene aged m1 and m2 units are generally represented by claystone, sandstone, conglomerate and bituminous shale. At the bottom of this formation, m1 unit deposited with the conglomerate, sandstone and claystone lithologies. Then, from bottom to top, this unit is overlain by a sequence of conglomerate, green claystone, coal seam (C), gray sandstone, bituminous shale, coal seam (B), bituminous shale, coal seam (A) and green claystone-sandstone-conglomerate alternation (m2 series). According to pumping test results, these series have a low hydraulic conductivity and display unconfined to semi-unconfined behavior.

The Miocene aged m1 and m2 units are overlain by the silicified limestone (m3) which can be seen nearly 34 % of the study area. The field observations, lost circulations in

the drilled pump wells and karstic cavities formed within this unit show that it is permeable with high conductivity values. At the contact zone of this limestone unit and clayey m2 unit, discharges from the springs are observed. This discharged water is used to supply water to Çavlum, Ağapınar, Sevinç and Kireçköy villages.

The Pliocene unit is one of the important water bearing units in the study area. This unit is comprised of reddish variegated colored conglomerate, sandstone, clayey limestone, tuffite bearing red mudstone with variegated colored clayey limestone, marl and gray/light brown clay from bottom to top. Within these lithologies, conglomerates, sandstones and limestones bear groundwater. Therefore, many DSI wells were installed within these deposits for operation and exploration purposes.

The Quaternary alluvium is the main aquifer system in the Alpu Plain and behaves as unconfined to semi-unconfined aquifer. Since this unit includes permeable silt and clay intercalated sands and gravels, most of the private wells and some DSI wells were drilled within this unit. Although alluvium along the Porsuk Stream shows aquifer properties, it is not important water bearing unit along the creeks within the license area due to their limited areal extent and thickness.

3.2.1. Hydraulic Properties of Groundwater Bearing Units

Hydraulic conductivity and storativity are the significant hydraulic parameters due to their effects on groundwater flow. These parameters are obtained by pumping and recovery tests conducted in the field. However, if it was not possible to conduct pumping tests for some units due to low yields, slug tests were conducted to determine the hydraulic conductivity of these units. In addition to low yield wells, slug tests were also performed for some wells such as PK-2, PK-6, GK-2 and GK-5 to compare the hydraulic conductivity obtained from slug tests with those obtained from the pumping and recovery tests. For the study area, all pumping/recovery and slug test results were analyzed by using Aquifer Test Pro 4.2 Software. Ultimate hydraulic parameters

obtained by pumping and recovery tests and slug tests are given in Table 3.5 and 3.6, respectively. According to these two tables, approximately same hydraulic conductivity values were calculated for the same wells from these tests.

The pumping test conducted at PK-3 well is used to determine the hydraulic properties of the basement Jurassic-Cretaceous limestones at this locality. As can be seen from the Table 3.5, geometric mean of the obtained hydraulic conductivities equals to $2.35x10^{-8}$ m/s while the minimum and maximum values of hydraulic conductivities are $9.48x10^{-9}$ and $3.88x10^{-8}$ m/s, respectively. This low hydraulic conductivity value validates the low permeability of this unit. The tests conducted in PK-2 and PK-6 pumping wells and GK-2 and GK-5 observations wells give information about the hydraulic properties of the Miocene aged m2 unit. This unit has low hydraulic conductivity and storativity values that equal to $2.34x10^{-7}$ and $2.3x10^{-2}$ m/s, respectively. The slug tests conducted in PK-4 well completed in silicified limestone (m3) yielded relatively high hydraulic conductivity, $8.37x10^{-7}$ m/s.

In addition to pumping/recovery and slug tests performed in the field, hydraulic properties such as hydraulic conductivity and transmissivity of the Pliocene and Quaternary units are determined from the previous studies conducted by DSI. According to DSI (1977), two pumping tests were conducted in Pliocene unit that resulted in transmissivity values of $2.66x10^{-4}$ and $5.67x10^{-4}$ m^2/s, and hydraulic conductivity of $1.86x10^{-6}$ and $4.1x10^{-6}$ m/s. These results show that, after the Quaternary alluvium, the Pliocene deposits are the most permeable unit within the study area. In addition, 22 pumping tests were conducted in drainage wells to determine the hydraulic parameters of the Quaternary alluvium in this previous study. The test results show that the transmissivity of the alluvium ranges between $2.31x10^{-3}$ and $4.21x10^{-2}$ m^2/s, the geometric mean being equal to $9.11x10^{-3}$ m^2/s. The hydraulic conductivity of the alluvium, on the other hand, varies between $1.29x10^{-4}$ and $2.63x10^{-3}$ m/s, the geometric mean is $5.00x10^{-4}$ m/s. These values show that the alluvium has high transmissivity and hydraulic conductivity.

Table 3.5. Pumping/recovery tests results

Well No.	Filter		Average Groundwater Level (m)	Filtered Level	Geologic Unit	Method	Calculated Hydraulic Conductivity (m/s)	Calculated Storage Coefficient	Average Hydraulic Conductivity (m/s)	
	Top (m)	Bottom (m)							Arithmetic Mean	Geometric Mean
PK-2	21	317	38.28	Above Coal, Coal, Below Coal	Claystone - sandstone - conglomerate, Claystone - Lignite seam (A), Shale - Lignite Seam (B), Sandstone - Lignite Seam (C), Claystone	Neuman	$6.34x10^{-8}$	-	$6.57x10^{-8}$	$6.56x10^{-8}$
						Boulton	$6.56x10^{-8}$			
						Theis-Jacob Correction	$7.12x10^{-8}$			
						Theis Recovery	$6.26x10^{-8}$			
PK-3	352	416	184.82	Above Coal	Limestone	Cooper & Jacob	$3.51x10^{-8}$	-	$2.78x10^{-8}$	$2.35x10^{-8}$
						Theis	$3.88x10^{-8}$			
						Theis Recovery	$9.48x10^{-9}$			
PK-6	368	416	7.37	Coal	Claystone-Lignite seam (A)	Cooper & Jacob	$2.63x10^{-7}$	-	$2.32x10^{-7}$	$2.20x10^{-7}$
						Theis	$1.39x10^{-7}$			
						Theis Recovery	$2.94x10^{-7}$			
GK-2	28	292	39.07	Above Coal, Coal	Claystone - sandstone - conglomerate, Claystone - Lignite seam (A), Shale - Lignite Seam (B), Sandstone - Lignite Seam (C)	Neuman	$6.88x10^{-7}$	$8.55x10^{-2}$	$6.32x10^{-7}$	$6.23x10^{-7}$
						Boulton	$6.49x10^{-7}$	$8.05x10^{-3}$		
						Theis-Jacob Correction	$7.23x10^{-7}$	$7.82x10^{-3}$		
						Theis Recovery	$4.67x10^{-7}$	-		
GK-5	372	390	5.6	Coal	Claystone-Lignite seam (A)	Cooper & Jacob	$3.40x10^{-7}$	$6.94x10^{-3}$	$3.67x10^{-7}$	$3.66x10^{-7}$
						Theis	$3.58x10^{-7}$	$8.24x10^{-3}$		
						Theis Recovery	$4.04x10^{-7}$	-		

Table 3.6. Slug tests results

Well No.	Filter		Average Groundwater Level (m)	Filtered Level	Geologic Unit	Test Type		Method	Calculated Hydraulic Conductivity (m/s)	Average Hydraulic Conductivity (m/s)	
	Top (m)	Bottom (m)								Arithmetic Mean	Geometric Mean
PK-2	21	317	38.28	Above Coal, Coal, Below Coal	Claystone - sandstone - conglomerate, Claystone - Lignite seam (A), Shale - Lignite Seam (B), Sandstone - Lignite Seam (C), Claystone	Slug Test	Falling Phase	Hvorslev	$1.69x10^{-7}$	$1.61x10^{-7}$	$1.58x10^{-7}$
								Bouwer & Rice	$1.22x10^{-7}$		
							Rising Phase	Hvorslev	$2.08x10^{-7}$		
								Bouwer & Rice	$1.45x10^{-7}$		
PK-4	26	56	48.05	Above Coal	Silicified limestone, claystone - sandstone - conglomerate	Slug Test	Falling Phase	Hvorslev	$1.06x10^{-6}$	$8.59x10^{-7}$	$8.37x10^{-7}$
								Bouwer & Rice	$6.87x10^{-7}$		
							Rising Phase	Hvorslev	$1.04x10^{-6}$		
								Bouwer & Rice	$6.47x10^{-7}$		
PK-5	136	204	144.98	Above Coal	Claystone - sandstone - conglomerate	Slug Test	Falling Phase	Hvorslev	$3.20x10^{-7}$	$3.40x10^{-7}$	$3.27x10^{-7}$
								Bouwer & Rice	$2.10x10^{-7}$		
							Rising Phase	Hvorslev	$4.31x10^{-7}$		
								Bouwer & Rice	$3.97x10^{-7}$		
PK-6	368	416	7.37	Coal	Claystone-Lignite seam (A)	Slug Test	Falling Phase	Hvorslev	$3.91x10^{-7}$	$2.51x10^{-7}$	$2.31x10^{-7}$
								Bouwer & Rice	$3.00x10^{-7}$		
							Rising Phase	Hvorslev	$1.72x10^{-7}$		
								Bouwer & Rice	$1.40x10^{-7}$		
GK-2	28	292	39.07	Above Coal, Coal	Claystone - sandstone - conglomerate, Claystone - Lignite seam (A), Shale - Lignite Seam (B), Sandstone - Lignite Seam (C)	Slug Test	Falling Phase	Hvorslev	$1.52x10^{-7}$	$1.36x10^{-7}$	$1.35x10^{-7}$
								Bouwer & Rice	$1.16x10^{-7}$		
							Rising Phase	Hvorslev	$1.50x10^{-7}$		
								Bouwer & Rice	$1.25x10^{-7}$		
GK-3	300	330	146.58	Coal	Shale - Lignite seam (B), Sandstone - Lignite seam (C), Claystone	Slug Test	Falling Phase	Hvorslev	$1.59x10^{-7}$	$1.37x10^{-7}$	$1.36x10^{-7}$
								Bouwer & Rice	$1.19x10^{-7}$		
							Rising Phase	Hvorslev	$1.48x10^{-7}$		
								Bouwer & Rice	$1.21x10^{-7}$		
GK-5	372	390	5.6	Coal	Claystone-Lignite seam (A)	Slug Test	Falling Phase	Hvorslev	$1.26x10^{-7}$	$1.61x10^{-7}$	$1.54x10^{-7}$
								Bouwer & Rice	$1.09x10^{-7}$		
							Rising Phase	Hvorslev	$2.30x10^{-7}$		
								Bouwer & Rice	$1.77x10^{-7}$		

The test results show that the storativity of the alluvium ranges between $3.00x10^{-3}$ and $2.00x10^{-1}$, indicating that the alluvium behaves as unconfined to semi-unconfined aquifer. Above mentioned hydraulic conductivity and storativity values of the various lithologic units outcropped within the boundaries of study area are summarized in Table 3.7.

Table 3.7. Hydraulic parameters of the geological units within the study area

Geologic Units	Hydraulic conductivity (m/s)			Storage Coefficient	
	Min	Max	Geo.Mean	Min	Max
Alluvium (sand, conglomerate)	$1.29x10^{-4}$	$2.63x10^{-3}$	$5.00x10^{-4}$	$3x10^{-3}$	$2x10^{-1}$
Pliocene (clayey limestone, claystone, conglomerate)	$1.86x10^{-6}$	$4.10x10^{-6}$	$2.76X10^{-6}$		
Silicified limestone (m3)	$6.47x10^{-7}$	$1.06x10^{-6}$	$8.37x10^{-7}$		
Claystone, sandstone, shale and coal seams (m2)	$6.26x10^{-8}$	$7.23x10^{-7}$	$2.34x10^{-7}$	$6.94x10^{-3}$	$8.55x10^{-2}$
Jurassic-Cretaceous limestone	$9.48x10^{-9}$	$3.88x10^{-8}$	$2.35x10^{-8}$		

3.2.2. Areal Distribution of Groundwater Levels

In this study, a groundwater table map was drawn by using static water levels measured from pumping/observation wells, DSI wells and some private wells and the discharge elevations of the springs and captages to determine the groundwater flow directions and hydraulic gradients (Figure 3.10).

The groundwater flow in the study area, in general, is from the upland areas in the south to the Porsuk Stream in the north. Moreover, there are also groundwater flow in western, northwestern and northeastern directions. The groundwater levels vary from 940-950 m at the upland in the south to 760-770 m close to the Porsuk Stream in the north. Thus, the lowland in the south forms the recharge area for the groundwater system. The vertical downward gradient observed in wells drilled in the second nested wells location in the southern part of the license area (Figure 3.8).

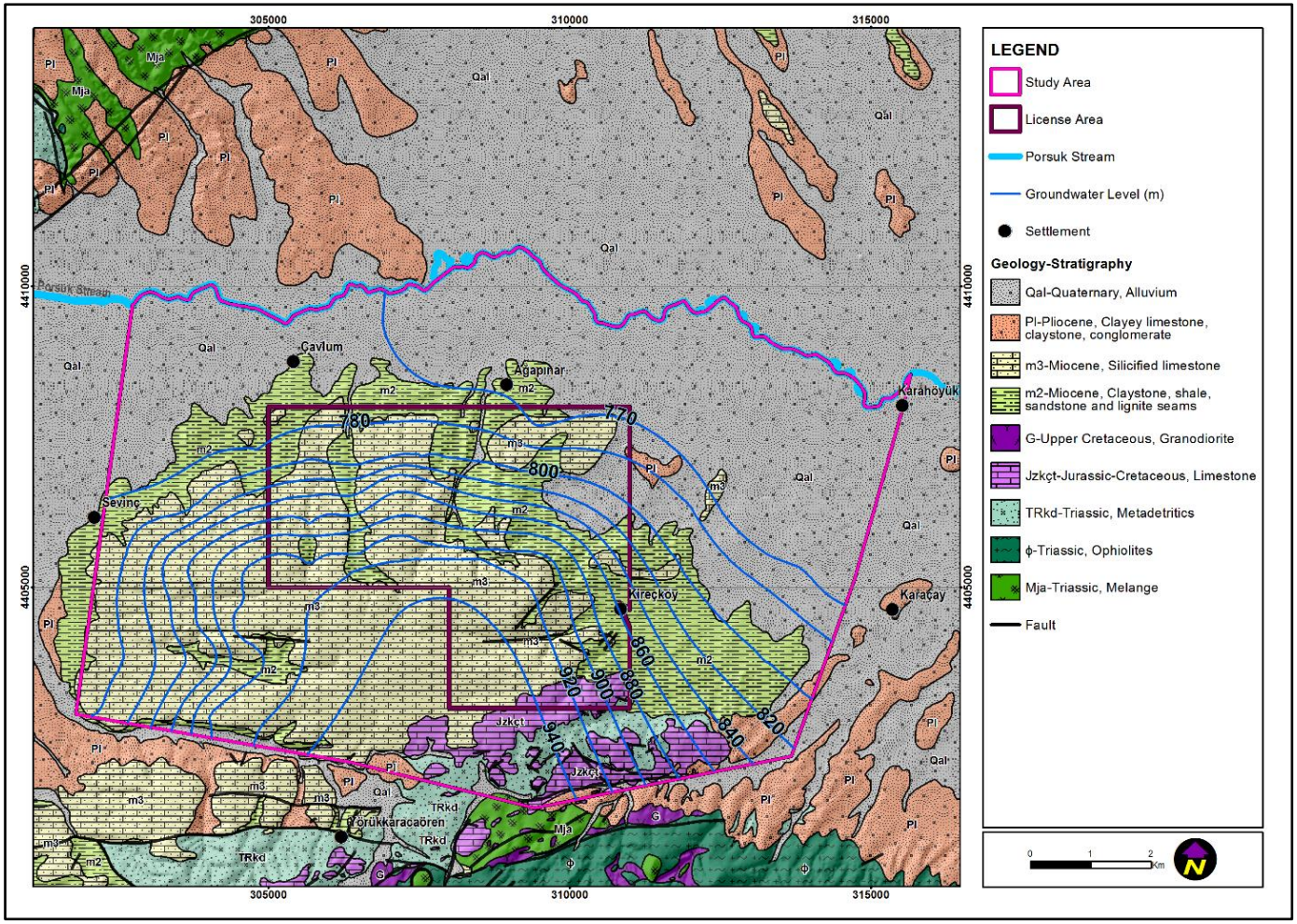

Figure 3.10. Aerial distribution of groundwater levels on geological map of the study area

Although the Porsuk Stream generally forms the discharge area for the groundwater system, there is also subsurface outflow along the western boundary between the south of the study area and the Sevinç village. The hydraulic gradient increases from a value of 0.02 in the south to 0.07 toward north in the middle of the license area and afterwards decreases to 0.004 in the alluvium area of the Porsuk Stream. The rapid decrease in hydraulic gradient in the vicinity of the Porsuk Stream is mainly due to the high transmissivity of the alluvium and underlying Pliocene system.

3.2.3. Temporal Changes in Groundwater Levels

In the study area, groundwater levels were measured on a monthly basis following the completion of pumping and observation wells within the scope of the project "Hydrogeological Investigation and Characterization of the Esan-Alpu Coal Mine Exploration Site". Measured static groundwater levels are given in Table 3.8. As can be seen from this table, GK-4 observation well is practically dry since the water level decreased continuously from July, 2015 and it finally dropped below the bottom of the filtered level of the well.

In Figure 3.11, groundwater level hydrographs are given for the pumping and observation wells until March, 2016 to examine the temporal variations of groundwater. In these hydrographs, precipitation data (until January, 2016) of the Eskişehir Regional Directorate of Meteorology Station (No. 17126) is also used to understand relation between precipitation and these groundwater level changes. Although groundwater levels did not vary with respect to precipitation in some wells such as in PK-4 and PK-5, groundwater levels increased from a minimum of 0.3 m to a maximum of 6.2 m in other wells.

The variations in groundwater levels observed in PK-2 and GK-2 wells drilled in the northeastern part of the license area are similar to each other (Figure 3.11).

Table 3.8. Static groundwater levels

Well No.	Static Water Level (m)													
	20.06.2015	22.06.2015	01.07.2015	11.07.2015	14.07.2015	23.07.2015	27.07.2015	16.08.2015	20.09.2015	07.11.2015	05.12.2015	09.01.2016	06.02.2016	10.03.2016
PK-2	x	x	x	x	38.66	38.62	38.65	41.26	41.05	40.99	40.58	39.97	39.94	39.87
GK-2	x	x	x	x	x	39.42	39.44	41.06	40.87	40.88	40.21	-	-	40.00
PK-3	x	x	x	185.22	185.19	185.14	185.10	186.21	185.78	186.71	186.24	181.82	180.52	180.74
GK-3	x	x	x	146.92	146.89	146.85	146.82	146.79	146.47	146.52	146.17	146.30	146.23	146.28
PK-4	x	x	x	48.69	48.56	48.68	48.65	48.71	48.55	49.01	48.83	49.03	49.02	49.08
GK-4	x	x	x	45.96	45.99	DRY	DRY	DRY	DRY	DRY	DRY	DRY	DRY	DRY
PK-5	x	x	x	141.16	141.14	140.40	140.53	140.20	139.83	140.02	139.88	140.20	140.18	140.29
PK-6	7.89	7.88	8.10	7.72	7.71	7.68	7.66	5.26	5.23	5.17	4.99	4.76	4.62	4.67
GK-5	6.98	6.14	6.40	5.92	5.91	5.86	5.85	5.02	5.01	4.98	4.77	3.95	3.82	3.92

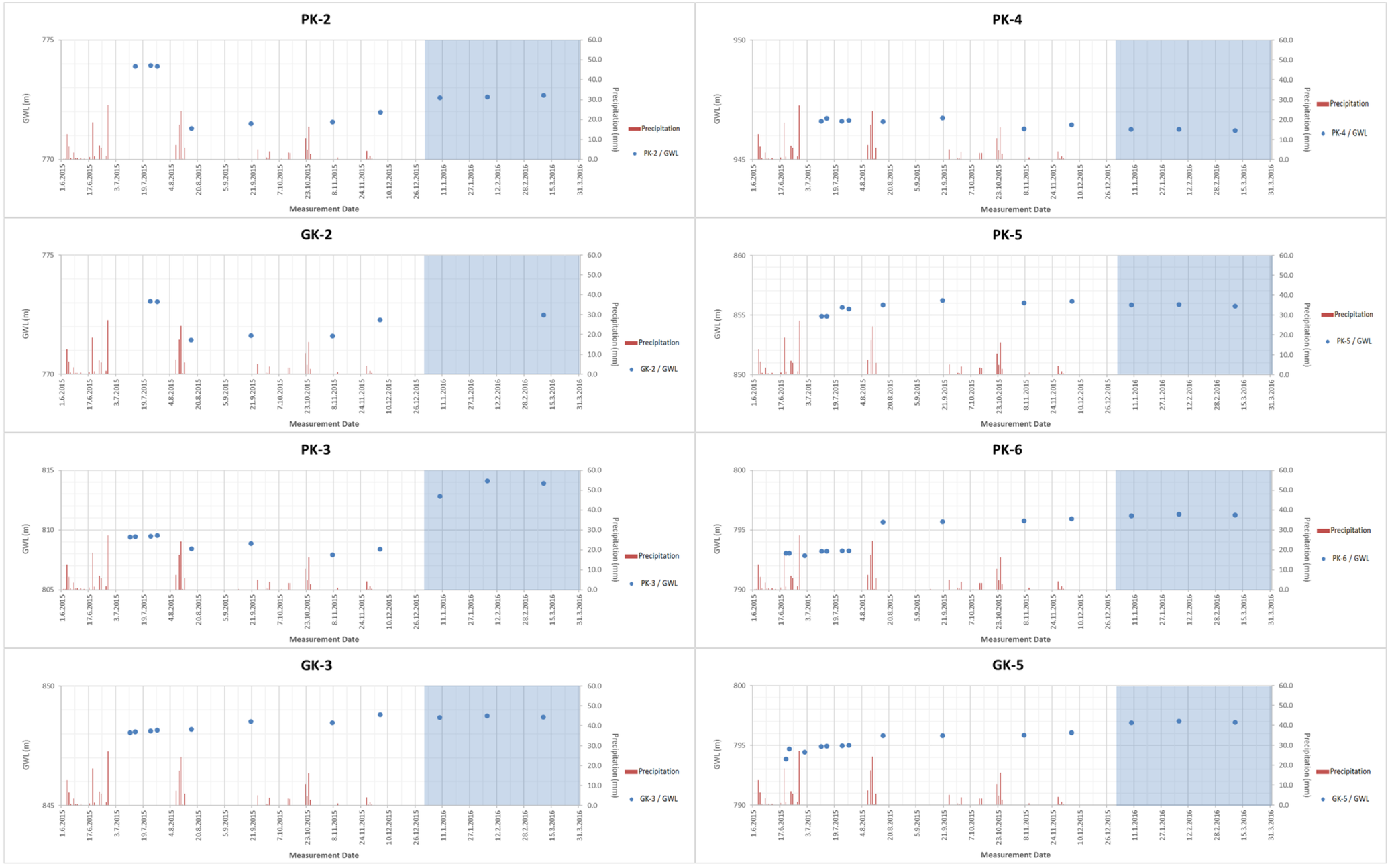

Figure 3.11. Temporal changes in groundwater levels measured at pumping and observation wells (Blue areas show the time interval with no measurements after 31.12.2015)

While groundwater levels increased 1.18 m in PK-2 well during September 2015-March 2016 period, they increased 0.87 m in GK-2 well over the same period.

In PK-4 and PK-5 wells that were respectively completed in silicified limestones and above the lignite seams in the southern part of the area, temporal variations are not observed in groundwater levels. In the same locality, groundwater levels increased only 0.3 m during November 2015-February 2016 period in GK-3 observation well screened within the coal seams whereas, they increased 6.2 m over the same period in PK-3 pumping well completed below the lignite seams (Figure 3.11). The excessive rise in groundwater levels observed in PK-3 well shows that the limestones are recharged through the outcrop zones in the south. On the other hand, no response to precipitation in observed groundwater levels in PK-4 well completed in silicified limestones can be attributed to the karstified nature of these limestones. The cavities that developed as result of karstification become avenues for the rapid circulation and discharge of groundwater through springs and captages; thereby, eliminating the storage of the water within the system. In addition, the small saturated thickness (10-11 m) and relatively deeper groundwater levels seem to support the effect of karstification explained above.

The variations in groundwater levels observed in PK-6 and GK-5 wells screened within the A-coal seams in the northwestern part of the license area are similar to each other. While groundwater levels increased 0.61 m in PK-6 well during September 2015-February 2016 period, they increased 1.19 m in GK-5 well over the same period (Figure 3.11).

To investigate the hydraulic relations among lithological units within and below the coal seams, groundwater level hydrographs in nested wells PK-2 & GK-2, PK-3-GK-3-PK-4-PK-5 and PK-6 & GK-5 are given in the same graph (Figure 3.12). Since PK-2 & GK-2 and PK-6 & GK-5 wells are screened in the same unit separately, they show very similar pattern to each other.

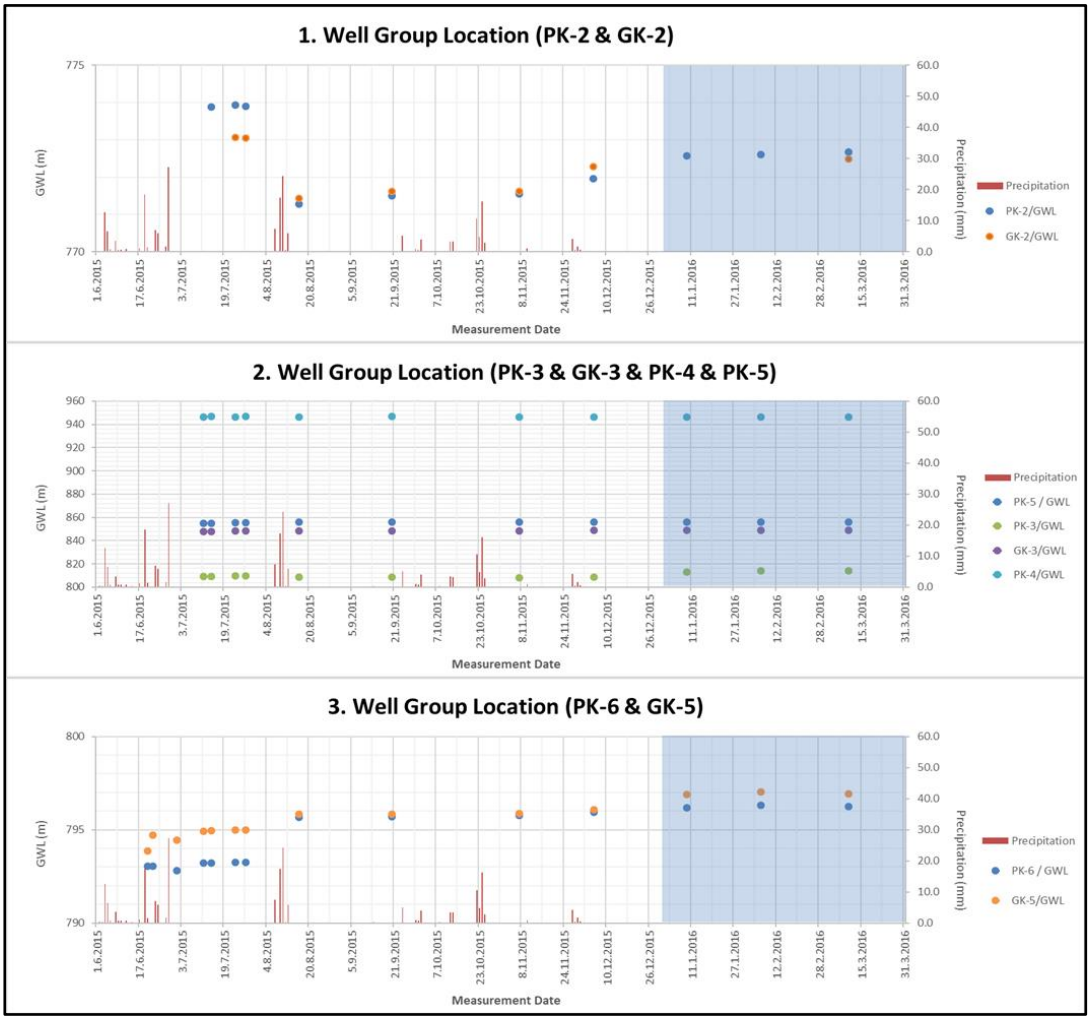

Figure 3.12. Temporal changes in groundwater levels measured at the clustered wells groups (Blue areas show the time interval with no measurements after 31.12.2015)

On the contrary, the groundwater levels in nested wells located in the south are significantly different from each other because they are screened in different geological units. The groundwater level has the highest elevation in PK-4 completed in silicified limestones in this location. While groundwater level in PK-5 screened above the coal seams are slightly greater than the groundwater levels in GK-3 screened within the coal seams, they are close to each other. The lowest groundwater levels are observed in PK-3 well completed below the coal seams within the Jurassic limestones.

Thus, it can be stated that there is a vertical hydraulic gradient in downward direction, producing flow from the silicified limestones to coal seams at the lower elevations and to Jurassic-Cretaceous limestones at the bottom. This phenomenon which is seen in the recharge zones proves the presence of a recharge area in the south.

3.3. Conceptual Budget of the Study Area

3.3.1. Conceptual Hydrologic Budget

Precipitation in an area is transformed into runoff, infiltration and evapotranspiration components. In water budget calculations, the ratio of these components to precipitation is calculated. The hydrologic water budget components of the study area were computed for each month by using long term average data. The Thornthwaite method is used to calculate potential evapotranspiration and the Curve Number (CN) method is used for surface runoff estimations. The remaining portion of the precipitation is assumed to be equal to infiltration into groundwater.

To calculate the conceptual water budget using the Thornthwaite method, the monthly total precipitation and monthly total potential evapotranspiration values for the study area is required. Potential evapotranspiration values are calculated using the mean monthly temperature and latitude values of the study area (Yazıcıgil et al., 2016).

The long-term monthly total precipitation values representing the study area were estimated using the meteorological stations No.17123 (14 km northwest of the study area), No. 17126 (12 km west of the study area) and Alpu station No. 3343 (11 km east of the study area). The meteorological station in Alpu is deemed to represent the study area compared to other stations. However, since the Alpu station is only operated for 1984-2002 period, the long-term measurements made at the Eskişehir city center were corrected to represent the meteorological station in Alpu. Due to the fact that the meteorological stations in Eskişehir city center were operated periodically (non-overlapping), Alpu meteorological station data for 1984-2002 were compared with

Eskişehir Regional Directorate station data during 1984-1990 period and Civil Airport meteorological station data during 1990-2002 period. Monthly total precipitation values for Alpu meteorological station (3343) were compared with Eskişehir Regional Directorate (17126) and Civil Airport (17123) meteorological stations during the overlapping time period, 1984-2002, using scatterplots (Figure 3.13).

The diagonal orange colored line in these graphs is the 1:1 line and represents equal precipitation for horizontal and vertical axis. Blue dashed line, on the other hand, is the linear fit line used to calculate the correlation coefficient (R^2) for each graph. The statistical comparisons in this study include, in addition to the correlation coefficient, % BIAS and % absolute BIAS (% |BIAS|) (Table 3.9). These statistics are calculated by the following equations:

$$\%\text{BIAS} = \frac{\text{y}-\text{x}}{\text{x}}.100 \tag{3.1}$$

$$\%|BIAS| = \frac{|y-x|}{|x|}.100 \tag{3.2}$$

In these equations, y is the monthly total precipitation (mm/month) in Alpu Meteorological station, x is the monthly total precipitation (mm/month) in Eskişehir Regional Directorate and Civil Airport meteorological stations.

The best statistics are achieved when correlation coefficient is 1, % BIAS and % absolute BIAS are zero. % BIAS values that are less than zero indicate that Alpu meteorological station receives less precipitation on average compared to Eskişehir meteorological stations.

As can be seen from Table 3.9, correlation coefficient values between monthly precipitation in Eskişehir and Alpu meteorological stations range between 0.33 and 0.86 in winter, spring and fall seasons which are significantly higher compared to the correlation coefficient values in summer months (between 0.06 and 0.52).

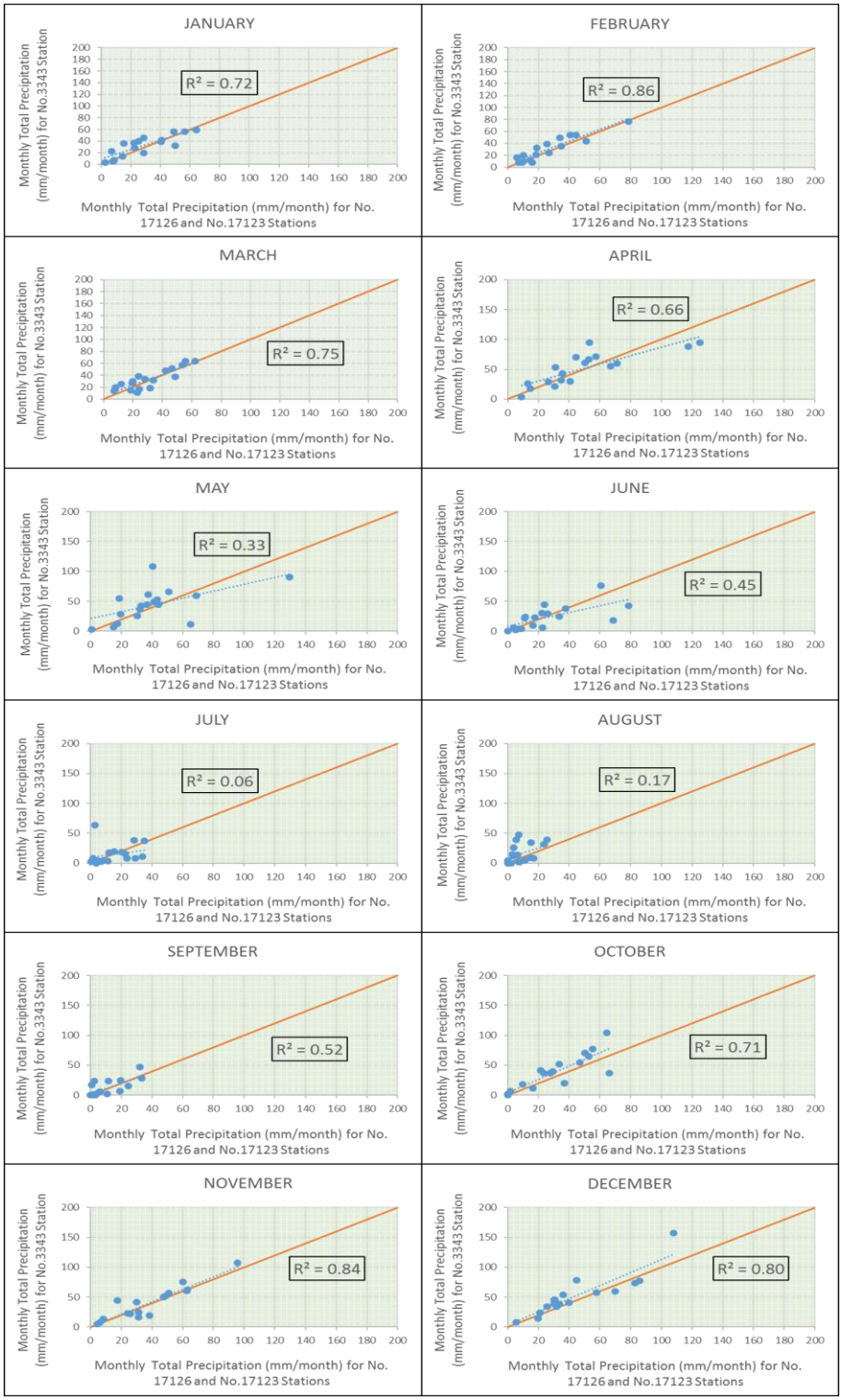

Figure 3.13. Scatterplots of monthly total precipitation of No.3343 meteorological station and No.17126 and No.17123 meteorological stations between 1984 and 2002

Table 3.9. Statistical values of the calculation of Alpu meteorological station and Eskişehir Reg. Dir. and Civil Meydan meteorological stations between 1984 and 2002

	Jan.	Feb.	Mar.	Apr.	May	Jun.	July	Aug.	Sept.	Oct.	Nov.	Dec.
R^2	0.72	0.86	0.75	0.66	0.33	0.45	0.06	0.17	0.52	0.71	0.84	0.80
% ERROR	12.34	15.00	7.51	4.90	9.86	-10.91	1.76	78.08	-7.32	24.70	5.67	16.80
% |ERROR|	27.96	25.47	25.87	30.32	43.10	45.41	70.32	126.20	43.50	44.20	20.81	25.94

The low correlation coefficient values in summer months are possibly due to the local convective precipitation systems. Upon investigation of the statistics listed in Table 3.9, the % BIAS values that are generally higher than zero indicate that Alpu station generally have higher precipitation compared to Eskişehir stations. % BIAS values in December-February period is around %15 on average, whereas % BIAS values in June-August period range between -10.91 and 78.08. Marginal changes in % BIAS values in summer months could be due to low precipitation values and convective precipitation character in this season. In conclusion, average monthly total precipitation values obtained from meteorological stations located in Eskişehir city center were corrected using the % BIAS values in Table 3.9 to represent Alpu meteorological station (Table 3.10).

Table 3.10. Average total precipitation of Alpu meteorological station after the correction procedure

	Jan.	Feb.	Mar.	Apr.	May	Jun.	July	Aug.	Sept.	Oct.	Nov.	Dec.
Eskişehir (mm/month)	40.16	33.25	35.48	38.88	44.13	33.01	12.95	8.34	15.64	28.34	30.51	46.43
% ERROR	12.34	15.00	7.51	4.90	9.86	-10.91	1.76	78.08	-7.32	24.70	5.67	16.80
Corrected (mm/month)	45.10	38.20	38.10	40.80	48.50	29.40	13.20	14.90	14.50	35.30	32.20	54.20

In Eskişehir meteorological stations annual average precipitation value prior to the correction is 367 mm, whereas it is 404 mm after correction. These corrected

precipitation values were used in the conceptual water budget model. This correction procedure has been checked with the precipitation-elevation relationship. Figure 3.14 shows the relationship between elevation and average annual precipitation measured in meteorological stations around the study area (DSI, 2010).

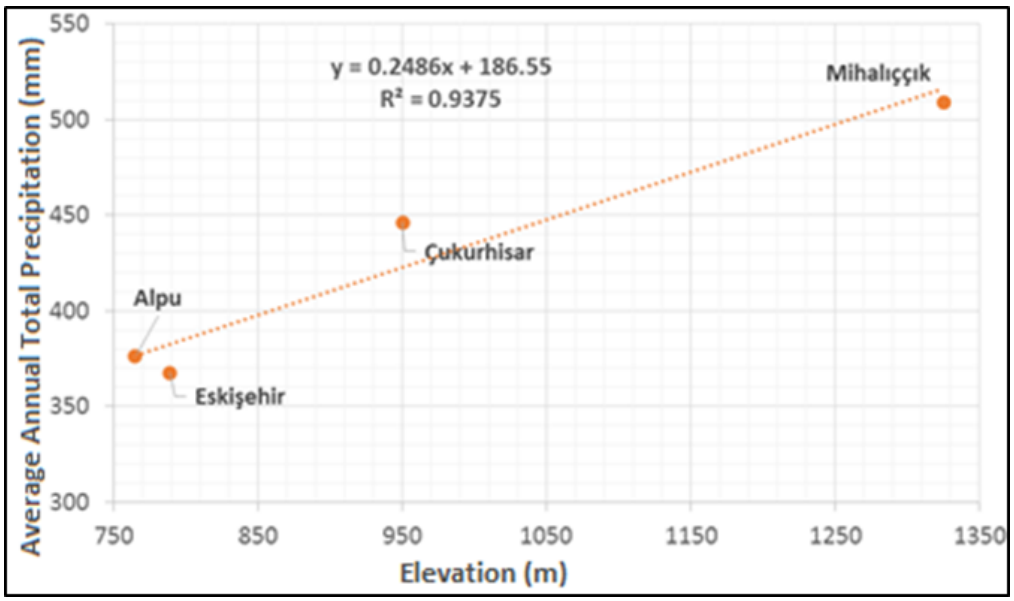

Figure 3.14. Average annual precipitation and elevation relation of the meteorological stations nearby the study area (DSI, 2010)

Area-elevation relationship (hypsometric curve) for the study area is given in Figure 3.15. As can be seen from this figure, 50 % of the total area of the license area is in between 775-885 m elevation range, whereas remaining %50 is in between 885-1050 m. If 885 meter is accepted as the representative elevation (correspond to %50 of the area) of the license area, based on the linear fit equation given in Figure 3.14, the average annual total precipitation corresponding to this elevation is 407 mm. This precipitation value is very close to the average annual total precipitation value (404 mm) obtained after the correction procedure listed in Table 3.10.

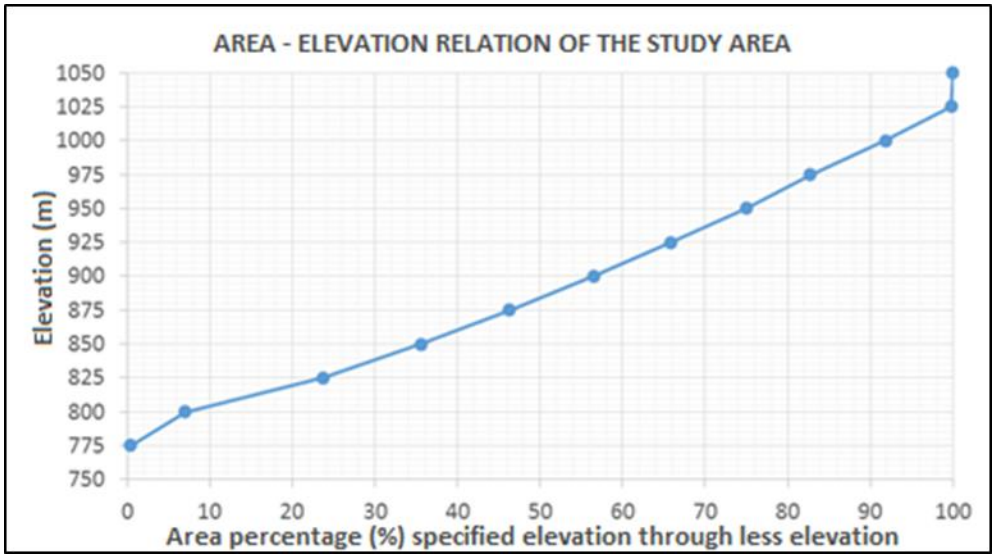

Figure 3.15. Area-elevation relation of the study area

To determine the mean monthly temperature values that will be used in conceptual water budget, the values in Eskişehir and Alpu meterological stations were compared following the same methodology provided above. Investigation of the scatterplots given in Figure 3.16 indicates that mean monthly temperature values measured in Eskişehir and Alpu stations scattered around and/or follow the 1:1 line with generally high correlation coefficient values (generally higher than 0.9).

As listed in Table 3.11, the highest % BIAS values range between % 9 and % 18 and occur in cold winter months. For this reason, correcting the temperature values using % BIAS statistic will have insignificant effect on the temperature values. In other words, the monthly average temperature values in Eskişehir and Alpu are very similar. Upon consideration of the topography of the study area, the temperature values are expected to change as a function of elevation. Note that, on average, the temperature values change 1 ^{o}C in every 100 meters change in elevation.

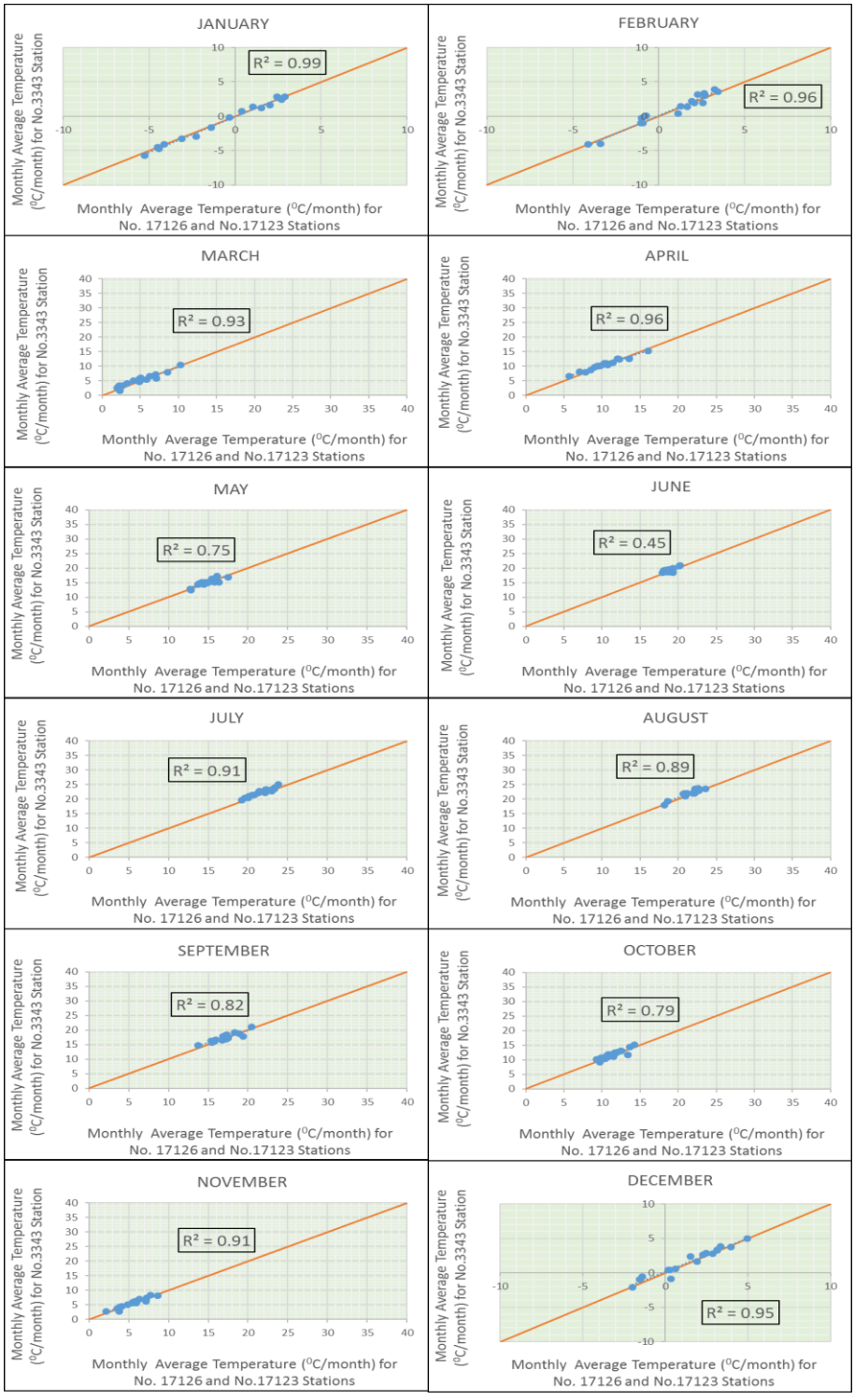

Figure 3.16. Scatterplots of monthly average temperature of Alpu (3343) meteorological station and Eskişehir Reg. Dir. (17126) and Civil Airport (17123) meteorological stations between 1984 and 2002

Table 3.11. Statistical values calculated monthly average temperature data of No.3343, No.17126 and No. 17123 meteorological stations

	Jan.	Feb.	Mar.	Apr.	May	Jun.	July	Aug.	Sept.	Oct.	Nov.	Dec.
R^2	0.99	0.96	0.93	0.96	0.75	0.45	0.91	0.89	0.82	0.79	0.91	0.95
% Error	12.41	17.99	5.63	2.75	1.89	1.69	2.75	2.43	2.43	3.18	2.02	9.18
% |Error|	10.44	19.99	12.39	5.14	3.95	3.03	2.93	2.63	4.03	5.86	7.78	17.39

Considering that the elevation of Eskişehir city center is 785 m and that of study area is 885 m (see Figure 3.15), the monthly average temperature values in the study area is expected to be 1 ^{o}C less compared to the Eskişehir city center. Table 3.12 lists the representative temperature values for Eskişehir city center and the study area. The temperature values that are corrected to represent the study area has been used in the conceptual water budget calculation.

Table 3.12. Estimated monthly average temperature values (^{0}C) for the study area by using measured monthly temperature data (1929-2014) at the center of Eskişehir

	Jan.	Feb.	Mar.	Apr.	May	Jun.	July	Aug.	Sept.	Oct.	Nov.	Dec.
Eskişehir City Center (785 m)	-0.1	1.3	4.9	10.3	15.1	18.9	21.6	21.5	17.2	11.9	6.5	2.0
Study Area (885 m)	-1.1	0.3	3.9	9.3	14.1	17.9	20.6	20.5	16.2	10.9	5.5	1.0

According to the Thornthwaite method, uncorrected monthly potential evaporation (UPET; mm/month) is calculated by:

$$UPET_m = 16x\left(\frac{10t_m}{I}\right)^a \tag{3.3}$$

where,

m : month index;

t : mean monthly temperature (^{o}C);

I : annual heat index;

a : coefficient that depend on heat index and calculated as:

$$a = (675x10^{-9})I^3 - (771x10^{-7})I^2 + (179x10^{-4})I + 0.492 \quad (3.4)$$

where,

I : the sum of monthly heat indexes,

i can be calculated by a formula:

$$i = \left(\frac{t}{5}\right)^{1.514} \quad (3.5)$$

Surface runoff values were estimated using the "Curve Number (CN)" method developed by US Soil Conversion Service (SCS, 1964). In CN method the surface runoff values are calculated on the basis of: (a) direct runoff (or excess rainfall), Pe, is less than or equal to total precipitation (P); (b) soil moisture retention occurring after runoff begins (Fa) is less than or equal to the potential soil moisture retention (S). Until precipitation reaches a certain value (Ia, initial abstraction) runoff is not observed, thus, potential runoff is equal to P- Ia. In the CN method, the ratio of two real and two potential values mentioned above, are equal:

$$\frac{F_a}{S} = \frac{P_e}{P - I_a} \quad (3.6)$$

Also, according to the continuity principle:

$$P = P_e + I_a + F_a \tag{3.7}$$

By combining Equations 3.6 and 3.7, and solving for Pe, direct runoff (or excess rainfall) value is acquired:

$$P_e = \frac{(P - I_a)^2}{P - I_a + S} \tag{3.8}$$

Based on the data obtained from small watersheds, the equation Ia=0.2S is empirically determined. Thus, Equation 3.8 can be written as:

$$P_e = \frac{(P - 0.2S)^2}{P + 0.8S} \tag{3.9}$$

Equation 3.9 presents a generalized form of the Curve Number method (Chow et. al. 1988). The standardized "Curve Numbers (CN)" are acquired from curves drawn based on the relationship between P and Pe from data corresponding to many basins. CN is related to potential soil moisture retention by CN=1000/(S+10), or S(in) = (1000)/CN-10. Thus, runoff Curve Numbers (CNs) indicate the runoff potential from a hydrologic soil-cover complex during periods when the soil is not frozen. A higher CN indicates a higher runoff potential. Runoff Curve Numbers (CNs) vary as a function of land use, landcover, and hydrologic soil groups. Hydrologic soil groups are divided into four types:

- Group A: Well drained soils that have low runoff potential and high infiltration rates even when they are thoroughly wetted (such as sand, conglomerate, silt).
- Group B: Soils that have moderate runoff potential and infiltration rates (such as sandy loam).

- Group C: Soils that have high runoff potential and low infiltration rates (such as clay loam).

- Group D: Soils that have very high runoff potential and very low infiltration rates (such as plastic clay).

Landuse/landcover data that is required to estimate the Curve Number values were obtained from the National Soil Database (UTVT). The landuse map and the primary soil groups map obtained from this database are given in Figures 3.17 & 3.18, respectively. The soils in the study area are classified as hydrologic soil group type B, having moderate runoff and infiltration potential. Moreover, gradient and soil depth information in UTVT database has also been incorporated in the calculations. Soil located on steep slopes are classified as Group C. The areal distribution of landuse/landcover and hydrologic soil groups were calculated for each subwatershed located in the license area. Using this information, a weighted Curve Number value for each subwatershed has been calculated (Table 3.13). The calculated Curve Number values range between 65 and 75; the weighted average value for all watersheds is 71. Upon considering the study area shown in Figures 3.17 & 3.18 the weighted average Curve Number value is calculated as 72.

The calculated Curve Number is used to determine the proportion of runoff on the basis of the monthly precipitation data. The long term mean monthly precipitation values for the study area were estimated by using the methodology explained above. The potential evaporation values, on the other hand, were calculated by using the Thornthwaite method explained earlier. The remaining portion of the precipitation is considered as infiltration to groundwater. Hence, components of long term hydrologic water budget are determined conceptually for each month (Table 3.14). In Table 3.14 the rows from 1 to 6 correspond to the potential evaporation calculations using the Thornthwaite method.

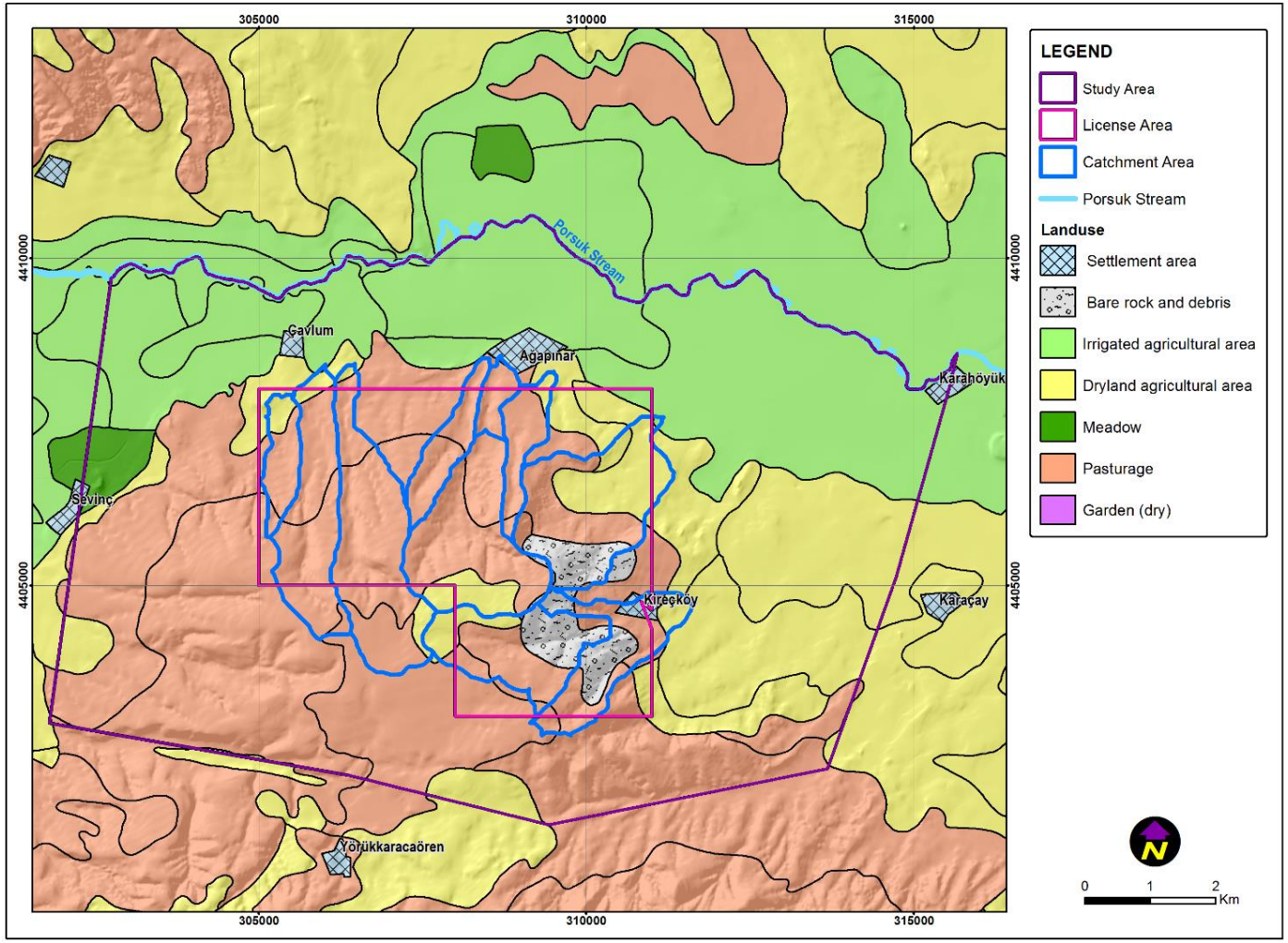

Figure 3.17. Landuse map of the study area

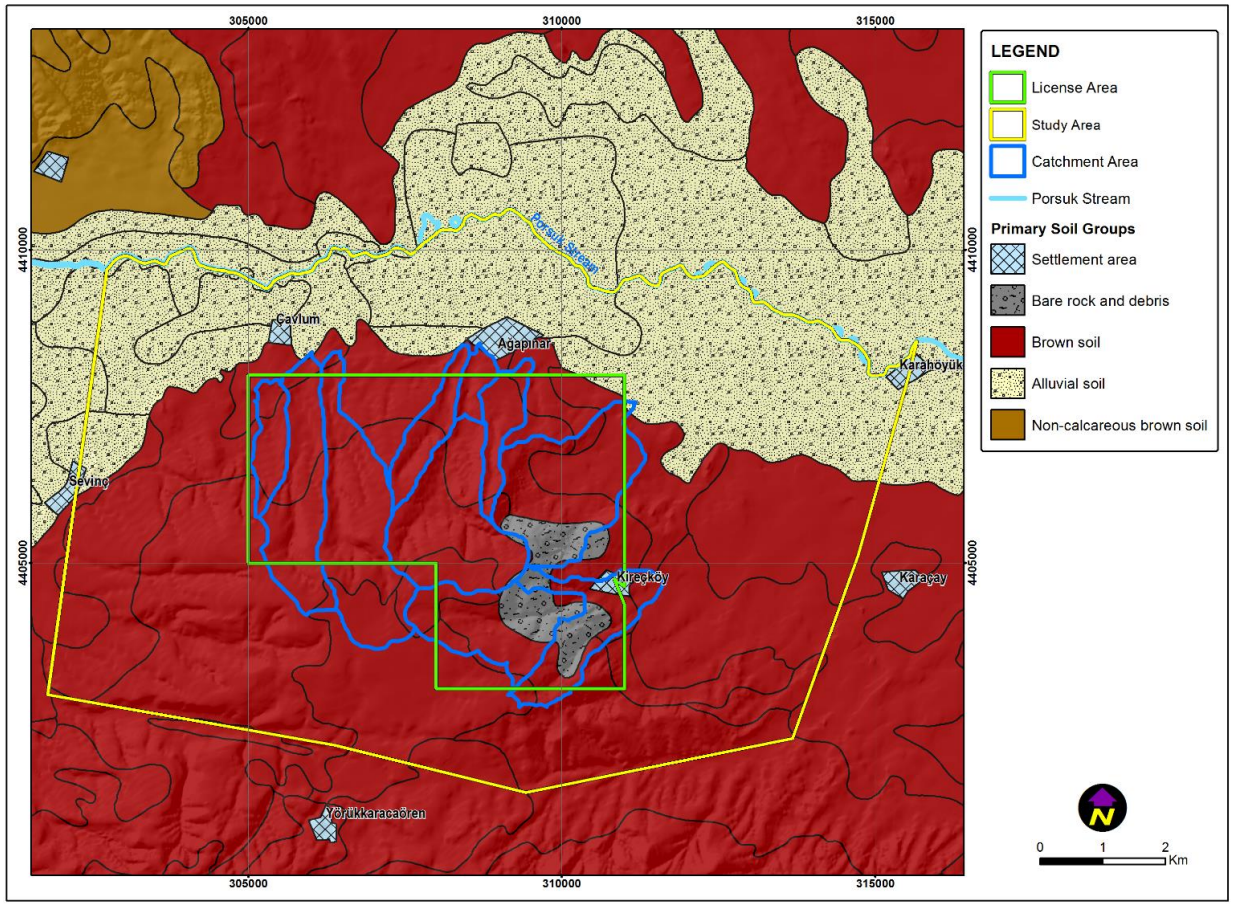

Figure 3.18. Primary soil groups map of the study area

Table 3.13. SCS Curve Number (CN) calculation for subwatersheds

Subwatershed No.	Land Use and Plant Cover	Hydrologic Soil Group	CN	Area (km^2)	Area %	Area x CN/100 %	Subwatershed CN
1	Pasturage	B	61	0.64	70.12	42.77	65
1	Pasturage	C	74	0.08	8.41	6.22	
1	Dryland Agriculture	B	75	0.20	21.46	16.10	
2	Pasturage	B	61	1.03	36.27	22.12	69
2	Pasturage	C	74	1.55	54.68	40.46	
2	Irrigated Agriculture	B	78	0.01	0.21	0.16	
2	Pasturage	B	61	0.09	3.03	1.85	
2	Dryland Agriculture	B	75	0.17	5.81	4.36	
3	Pasturage	B	61	0.49	12.41	7.57	70
3	Pasturage	C	74	2.40	60.84	45.02	
3	Pasturage	B	61	0.84	21.18	12.92	
3	Dryland Agriculture	B	75	0.17	4.43	3.32	
3	Dryland Agriculture	B	75	0.05	1.14	0.86	
4	Pasturage	B	61	0.45	41.66	25.41	69
4	Pasturage	C	74	0.63	58.34	43.17	
5	Pasturage	B	61	0.48	11.45	6.98	70
5	Pasturage	B	61	0.77	18.4	11.22	
5	Pasturage	C	74	2.16	51.93	38.43	
5	Bare Rock	C	85	0.05	1.26	1.07	
5	Dryland Agriculture	B	75	0.70	16.77	12.58	
5	Settlement	B	72	0.01	0.2	0.14	
6	Pasturage	B	61	0.83	81.9	49.96	63
6	Pasturage	C	74	0.06	6.22	4.60	
6	Dryland Agriculture	B	75	0.12	11.89	8.92	
7	Pasturage	B	61	1.32	34.24	20.89	72
7	Irrigated Agriculture	B	78	0.02	0.45	0.35	
7	Pasturage	C	74	0.13	3.42	2.53	
7	Dryland Agriculture	B	75	1.46	38.08	28.56	
7	Dryland Agriculture	B	75	0.16	4.22	3.17	
7	Bare Rock	C	85	0.75	19.59	16.65	
8	Pasturage	B	61	0.09	1.74	1.06	75
8	Pasturage	B	61	0.54	11.05	6.74	
8	Pasturage	C	74	1.06	21.6	15.98	
8	Pasturage	C	74	0.50	10.27	7.60	
8	Pasturage	C	74	0.01	0.12	0.09	
8	Dryland Agriculture	B	75	0.03	0.61	0.46	
8	Bare Rock	C	85	0.77	15.76	13.40	
8	Bare Rock	C	85	0.71	14.46	12.29	
8	Pasturage	B	61	0.24	4.84	2.95	
8	Pasturage	B	61	0.12	2.42	1.48	
8	Dryland Agriculture	B	75	0.50	10.27	7.70	
8	Settlement	B	72	0.15	2.97	2.14	
8	Dryland Agriculture	B	75	0.19	3.88	2.91	

Table 3.14. Long term monthly conceptual water budget results of the study area

Row No.	Parameter	Jan.	Feb.	Mar.	Apr.	May	Jun.	July	Aug.	Sep.	Oct.	Nov.	Dec.	Total	Ratio to Precipitation (%)
1	**Monthly Average Temperature (°C)**	-1.1	0.3	3.9	9.3	14.1	17.9	20.6	20.5	16.2	10.9	5.5	1		
2	**i**	0.00	0.01	0.69	2.56	4.80	6.90	8.53	8.47	5.93	3.25	1.16	0.09	42.38	
3	**a**	1.2	1.2	1.2	1.2	1.2	1.2	1.2	1.2	1.2	1.2	1.2	1.2	13.96	
4	**UPET**	0.00	0.73	14.52	39.92	64.79	85.53	100.72	100.15	76.15	48.02	21.67	2.98	555.19	
5	**PET**	0.00	0.62	14.96	44.32	79.69	106.05	126.90	118.17	79.20	46.10	18.20	2.44	636.66	
6	**r: monthly correction coefficient**	0.85	0.84	1.03	1.11	1.23	1.24	1.26	1.18	1.04	0.96	0.84	0.82		
7	**Precipitation (mm)**	**45.1**	**38.2**	**38.1**	**40.8**	**48.5**	**29.4**	**13.2**	**14.9**	**14.5**	**35.3**	**32.2**	**54.2**	404.4	
8	**Surface Runoff Coefficient**	1	1	1	1	1	1	0	0	0	1	1	1		
9	**Surface Runoff (mm)**	5.17	2.90	2.87	3.70	6.48	0.86	0.00	0.00	0.00	2.11	1.39	8.91		
10	**Infiltration (SZ)**	39.92	35.30	35.23	37.10	42.02	28.54	13.20	14.90	14.50	33.19	30.81	45.29		
11	**SZ- PET**	39.92	34.68	20.27	-7.21	-37.67	-77.51	-113.70	-103.27	-64.70	-12.92	12.61	42.85		
12	**Total (P-PET)**	0.00	0.00	0.00	-7.21	-44.89	-122.40	-236.10	-339.37	-404.07	-416.99	0.00	0.00		
13	**Soil Moisture**	100.00	100.00	100.00	93.04	63.84	29.41	9.43	3.36	1.76	1.55	14.15	57.00		
14	**Soil Moisture Variation**	39.92	3.08	0.00	-6.96	-29.21	-34.43	-19.97	-6.07	-1.60	-0.21	12.61	42.85		
15	**AET**	0.00	0.62	14.96	44.06	71.23	62.97	33.17	20.97	16.10	33.40	18.20	2.44	**318.13**	79%
16	**Excess Precipitation (SZ - AET)**	5.17	34.51	23.14	3.70	6.48	0.86	0.00	0.00	0.00	2.11	1.39	8.91	**86.26**	
17	**Surface Runoff**	5.17	2.90	2.87	3.70	6.48	0.86	0.00	0.00	0.00	2.11	1.39	8.91	**34.39**	9%
18	**Infiltration**	0.00	31.60	20.27	0.00	0.00	0.00	0.00	0.00	0.00	0.00	0.00	0.00	**51.87**	13%
													TOTAL	**404.39**	**100%**

In this table, UPET value (Equation 3.3), is corrected by using the coefficient "r" on the basis of the latitude of the project area (39°), and hence, monthly potential evaporation (PET) values are obtained. The surface runoff is calculated according to Equation (3.9), by using monthly precipitation values (P) and Curve Number (CN=72). The difference between monthly precipitation and runoff is equal to infiltration (SZ). The soil moisture (ST) capacity is assumed to be 100 mm, and for each month, change in soil moisture (delta ST) is computed. Based on these values, actual evapotranspiration (AET), surface runoff and groundwater recharge (infiltration) values were calculated. In addition, soil moisture capacity has been taken as 100 mm in the conceptual model. For this model setup, the groundwater recharge value is calculated as 51.9 mm. The results of the monthly conceptual water budget provided in Table 3.14, indicate that % 78.7 of annual precipitation is lost to the atmosphere as actual evapotranspiration, % 8.5 runs off and, % 12.8 percolates into ground to recharge the groundwater system in the study area (Table 3.15).

The reliability of the annual conceptual water budget provided above could be enhanced through continuous monitoring (for example precipitation and surface runoff), estimation of soil hydraulic properties and development of a numerical hydrogeological model which will be explained in detail in the following chapters.

Table 3.15. Annual conceptual hydrologic budget results of the study area

Hydrologic Component	Amount (mm/year)	Ratio to Annual Precipitation (%)
Precipitation	404.4	100
Evaporation	318.1	78.7
Surface Runoff	34.4	8.5
Recharge	51.9	12.8

3.3.2. Conceptual Hydrogeological Budget

The conceptual hydrogeological budget (Table 3.16) is estimated to examine the recharge and discharge mechanisms within the study area. Furthermore, it will provide a basis to compare the groundwater budget obtained from the numerical groundwater model. In the study area, groundwater recharge takes place through infiltration of precipitation and surface runoff. According to hydrological budget of the study area given in Table 3.16, the amount of 12.8 % of the precipitation (404.4 mm/year) infiltrates into groundwater which is equal to 51.9 mm/year for the 95.6 km^2 surface area. Thus, the annual recharge from the percolation of precipitation was calculated as $4.96x10^6$ m^3 in the study area. Although recharge from the precipitation is the main component of the recharge mechanism, other 17.75 % of the recharge originates from the infiltration of surface runoff. Because the surface runoff that result from the upland areas infiltrate into groundwater at the lowland areas, the groundwater recharge from this component is calculated by determining the area (31 km^2) where the elevation values are higher than the median elevation of the study area, 885 m. According to hydrological budget given in Table 3.15, the amount of 8.5 % of the precipitation (34.4 mm/year) turns into surface runoff from this upland area. As a result, the annual recharge from the surface runoff infiltration was calculated as $1.07x10^6$ m^3. The sum of these two components gives the annual total recharge amount of the study area as $6.03x10^6$ m^3.

Table 3.16. The conceptual groundwater budget of the study area

RECHARGE (m^3/year)		**DISCHARGE (m^3/year)**	
Precipitation	$4.96x10^6$	Springs and captages	$4.73x10^5$
Surface runoff infiltration	$1.07x10^6$	Base flow to Porsuk Stream	$1.20x10^6$
		Pumping from wells	$2.34x10^6$
		Evapotranspiration	$1.91x10^6$
		Subsurface outflow	$1.05x10^5$
TOTAL	**$6.03x10^6$**	**TOTAL**	**$6.03x10^6$**

The total recharge is equal to the total discharge in the conceptual budget. The discharge components of the budget are comprised from spring and captages, baseflow to Porsuk Stream, pumping from wells, evapotranspiration and subsurface outflow.

The discharge rate from the springs and captages was calculated by the help of field measurements and observations. Discharge rates are estimated as 1 L/s and 14 L/s for springs and captages, respectively. Therefore, annual discharge rate from these components was calculated as $4.73x10^6$ m^3.

Baseflow to Porsuk Stream is the another important discharge component of the study area. This stream is recharged from the groundwater and the recharge amount was calculated by using flow rates of the DSI flow gauging stations located in Ağapınar and Süleymaniye villages mentioned in detail in Chapter 3.1.1. The difference between the flow rates of these two stations for the Alpu basin in September which represents the dry season is proportionally reduced by using the ratios of drainage areas. According to DSI (2010), for 2152.5 km^2 total basin area, the baseflow to Porsuk Stream is equal to 0.836 m^3/s or $2.64x10^7$ m^3/year. When this value is proportionally reduced to 95.6 km^2 study area, the baseflow is calculated as $1.2x10^6$ m^3/year.

In the study area, the main discharge component is pumping from the cooperative and private wells. To calculate discharge amount from pumping wells, irrigational requirements from DSI wells and private wells and drinking and domestic water requirements from village wells were taken into the consideration. The five of the DSI wells (44130, 55322, 55323, 55324 and 55325) are used for irrigation of the 189 hectares area by Kireçköy Irrigational Cooperative with a pumping rate of $9.90x10^5$ m^3/year (DSI, 2010). Therefore, this number gives the annual discharge rate for irrigation of the cooperative area from the DSI wells. Additionally, 78 private wells are used for irrigational purposes in the study area. To calculate the discharge from these private wells, firstly irrigated surface areas were calculated by using Google Earth images taken on May 7, 2015. According to these images, 241 hectares area are irrigated by private wells. Then, these calculated areas were rated with required water

amount for the 189 hectares area (DSI, 2010). As a result, $1.26x10^6$ m^3 annual discharge rate was calculated for irrigational requirements of the private wells. Discharge rates from village wells is insignificant compared to other components. However, it is calculated as $9x10^4$ m^3/year by using population of the villages and animal numbers. Then, discharge from pumping wells were estimated as $2.34x10^6$ m^3/year which is the % 38.8 of the total discharge amount.

In conceptual hydrogeological budget, evapotranspiration is an important component for the areas where depth to groundwater level is higher than 1-2 m below ground surface. Especially for valleys and eastern part of the study area, discharge from this component is noted. To calculate this discharge amount, groundwater elevation map (Figure 3.10) was subtracted from the digital elevation model (Figure 2.1) of the study area and the areas where the depth to groundwater level is 1 m and lower were calculated as 6 km^2. According to hydrologic budget given in Table 3.15, the amount of 78.7 % of the precipitation (318.1 mm/year) leaves from the study area as evapotranspiration. By the light of these information, annual discharge from evapotranspiration was calculated as $2.34x10^6$ m^3.

The last discharge component of the conceptual budget is the subsurface outflow from the southwestern part of the study area approximately along 2.9 km length. To calculate discharge amount from this component, Darcy law was used. According to groundwater level map (Figure 3.10), the hydraulic gradient is 0.038 for this area. Therefore, for average 300 m depth and $1x10^{-7}$ m/s hydraulic conductivity, this discharge component was calculated as $1.05x10^5$ m^3/year.

The estimated total recharge and discharge from the groundwater budget, however, is based upon several assumptions and should be verified by comparing it with the numerical model results. It provides an initial starting point and basis for the numerical model results which will be explained in detail in the following chapters.

CHAPTER 4

GROUNDWATER FLOW MODEL

4.1. Model Description

Model is a quantitative framework to simplify the complicated real world system which is not easy to understand under complex hydrogeological conditions. It gives answers about groundwater flow systems, management of groundwater resources and prediction of the effects of certain actions.

Groundwater models can be subdivided into three distinct categories: physical, analog and mathematical models, including analytical and numerical models. Physical models include a laboratory tank filled with porous material (usually sand) and saturated with water to demonstrate flow and transport mechanism. However, since these model can not simulate a multilayer aquifer exposed to various stresses such as precipitation, surface streamflow, leakage from deep underlying strata and changing some of its geometric and hydrogeologic properties, they are useful for educational and demonstrative purposes. Analog models simulate groundwater flow using the analogy between groundwater flow and some other physical processes such as the flow of electrical currents. This type of models is used to simulate a unique aquifer system. When a different aquifer is to be studied, new analog model must be built. Therefore, since these models can not simulate the real complicated system, they were used before the development of computer modeling (Kresic, 2006).

Mathematical models which use a set of differential equations to govern the groundwater flow can be examined under the two different categories: analytical and

numerical. Analytical models solve governing equation of groundwater flow at a given time and the result can be applied to one point or line of points in the analyzed flow field. The feasible application of these models terminates for the complex conditions. On the contrary, numerical models provide solutions for the three-dimensional heterogeneous media with complex boundaries and a complex network of source and sinks. By the help of these models, study area discretized into small pieces called as cell or element and governing flow equation is solved for each of them. The solution of the numerical models is the distribution of hydraulic heads at points that usually located at the center of the cell. Due to their versatility, finite difference and finite element models are the most commonly used numerical models. In this study, numeric finite difference groundwater model which will be discussed in detail in the following section has been used.

4.1.1. Computer Code Selection

In this study, regional groundwater numeric model for the coal exploration area and its surroundings has been developed by using MODFLOW-SURFACT Software (HydroGeoLogic Inc., 1996).

MODFLOW-SURFACT is fully integrated groundwater flow model based on U.S.G.S. modular three-dimensional (3D) groundwater flow modeling code, MODFLOW. This software uses rectangular mesh grids for the block-centered finite difference analysis to solve the groundwater flow equation of both saturated and unsaturated conditions.

MODFLOW-SURFACT is added in the MODFLOW Software to enhance its convergence capability and computational robustness. Without SURFACT Engine, MODFLOW Software converts an unsaturated variable - head cell into a no-flow inactive cell. It causes ambiguous and inaccurate simulation results. To prevent this phenomenon, McDonald et al. (1991) developed rewetting function which uses head

of the neighboring cells to decide whether to reconvert a no-flow cell into a variable-head cell. However, when this function operates, it causes convergence and stability problems because procedure used to rewet dry cells is incompatible with flow and mass conservation principles. Additionally, if the transmissivity of the head-dependent neighboring cell is zero, it causes the calculation of unstable average transmissivity of the model (Goode and Appel, 1992). To encounter all these problems related to dry inactive cells, MODFLOW SURFACT uses pseudo-soil simulation without any data requirement. For this simulation, pseudo-soil function is used. It is a step function combined over the grid cell height. According to this function, degree of saturation (S_w) is calculated as 0 above the water table and it is calculated as 1 under the water table. If the water table is located at the middle of the grid cell, degree of saturation is equal to 0.5. These grid cell heights related saturation values are used to calculate saturated conductivity (K_{rw}) which conducts the vertical flow of the water along the fully dry cells at the unsaturated zone. If unsaturated zone parameters are known, real soil functions can be used to understand travel times and movement of the moisture at this zone. In this study, because of all these benefits of MODFLOW-SURFACT, this software is used with pseudo-soil simulation.

4.1.2. Mathematical Model

Mathematical models have been used to translate physical real earth system into mathematical terms and equations since the late 1800s (Wang & Anderson, 1982). These models comprise set of differential governing equations to describe physical processes and boundaries of a groundwater system.

In this study, governing partial differential equation of the model is derived by Darcy's equation which is used to calculate flow of water in saturated conditions. According to this governing equation, for three-dimensional groundwater flow in variably saturated media is described by Huyakorn et al., (1986) as:

$$\frac{\partial}{\partial x}\left(K_{xx}k_{rw}\frac{\partial h}{\partial x}\right)+\frac{\partial}{\partial y}\left(K_{yy}k_{rw}\frac{\partial h}{\partial y}\right)+\frac{\partial}{\partial z}\left(K_{zz}k_{rw}\frac{\partial h}{\partial z}\right)-W=\phi\frac{\partial S_w}{\partial t}+S_wS_s\frac{\partial h}{\partial t}$$

(4.1)

where,

x, y and z	: Cartesian coordinates (L);
K_{xx}, K_{yy}, and K_{zz}	: principal components of hydraulic conductivity along the x, y and z coordinate axes, respectively (LT^{-1});
k_{rw}	: relative permeability, which is a function of water saturation;
h	: piezometric head, (L);
W	: volumetric flux per unit volume representing sources and/or sinks of water, (T^{-1});
ϕ	: drainable porosity taken to be equal to the specific yield, S_y;
S_w	: degree of saturation of water, which is function of the pressure head;
S_s	: specific storage of the porous material, (L^{-1});
t	: time, (T).

For fully saturated medium, degree of saturation is equal to 1 (S_w = 1). Therefore, Equation 4.1 reduces to:

$$\frac{\partial}{\partial x}\left(K_{xx}\frac{\partial h}{\partial x}\right)+\frac{\partial}{\partial y}\left(K_{yy}\frac{\partial h}{\partial y}\right)+\frac{\partial}{\partial z}\left(K_{zz}\frac{\partial h}{\partial z}\right)-W=S_s\frac{\partial h}{\partial t} \quad (4.2)$$

Equation 4.2 is the basic groundwater flow equation used in the development of MODFLOW (McDonald and Harbaugh, 1988). It is also governing equation for MODFLOW SURFACT below the water table in confined system.

In addition to flow equations, to define the functional relationship at the unsaturated zone, pseudo-soil functions are used. These function can be expressed as:

$$S_w = S_w(\Psi) \quad \text{and} \quad k_{rw} = k_{rw}(S_w) \qquad (4.3) \text{ and } (4.4)$$

where,

Ψ : pressure head defined as $\Psi = h - z$, with z being positive in the vertically downward direction.

4.1.3. Numerical Solution

Spatial discretization of a hypothetical aquifer system with a mesh of blocks, called cells, is shown in Figure 4.1. For this discretization, right-handed Cartesian coordinate system is used. Location of the grid cells are described with respect to rows, columns and layers. For a system consisting of "nrow" rows and "ncol" columns and "nlay" layers,

i: row index, i = 1, 2, 3, … , nrow;
j: column index, j = 1, 2, 3, … , ncol;
k: layer index, k = 1, 2, 3, … , nlay.

To solve the Equation 4.1 with the finite difference approximation, an assumption is made that layers are generally correspond to horizontal geohydrologic units or intervals. Therefore, according to Cartesian coordinates; k index implies changes along the vertical, z; because layers are numbered from top to bottom and so increase in the k index corresponds decrease in the elevation. In the same manner, rows are considered parallel to the x-axis and so, increase in the row index, i, corresponds decrease in y; and finally columns are considered parallel to y-axis and so, increase in the column index, j, corresponds increase in x. However, model application depends

upon only rows and columns fall along consistent orthogonal directions within the layers, not the designation of x, y or z coordinates.

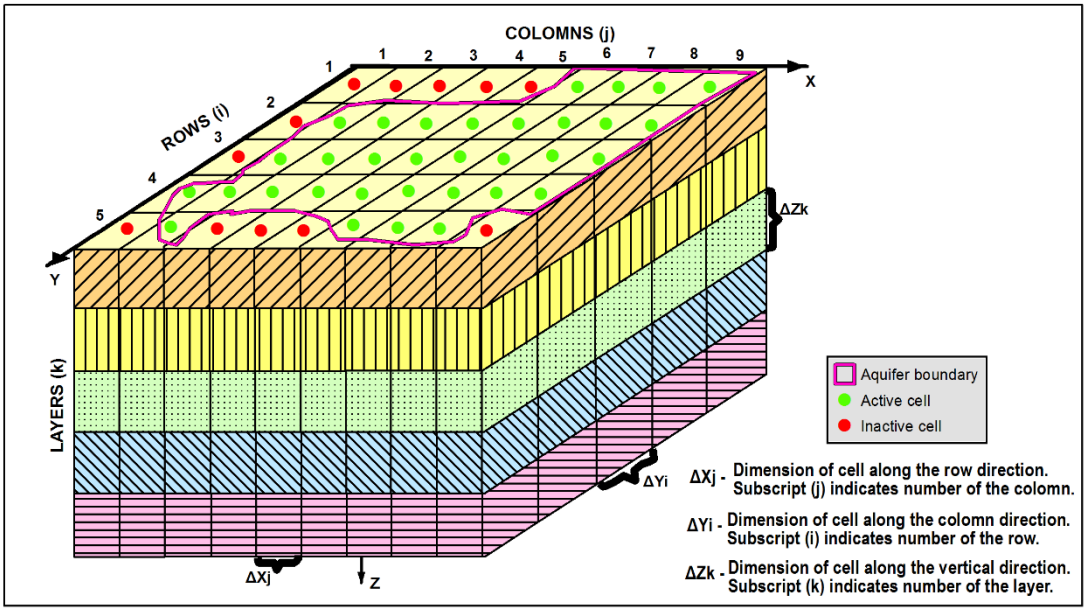

Figure 4.1. Spatial discretization of a hypothetical aquifer system (Modified from McDonald and Harbaugh, 1988).

According to Figure 4.1,

Δr_j: width of cells in the row direction, at a given column, j;

Δc_i: width of cells in the column direction, at a given row, i;

Δv_k: thickness of cells in a given layer, k.

In Figure 4.2 (McDonald and Harbaugh, 1988), a cell i, j, k with six adjacent aquifer cells i-1, j, k; i+1, j, k; i, j+1, k; i, j, k-1 and i, j, k+1 are shown. As an assumption, when flows enter the cell i, j, k, they are considered as positive and the negative sign has been dropped from all terms.

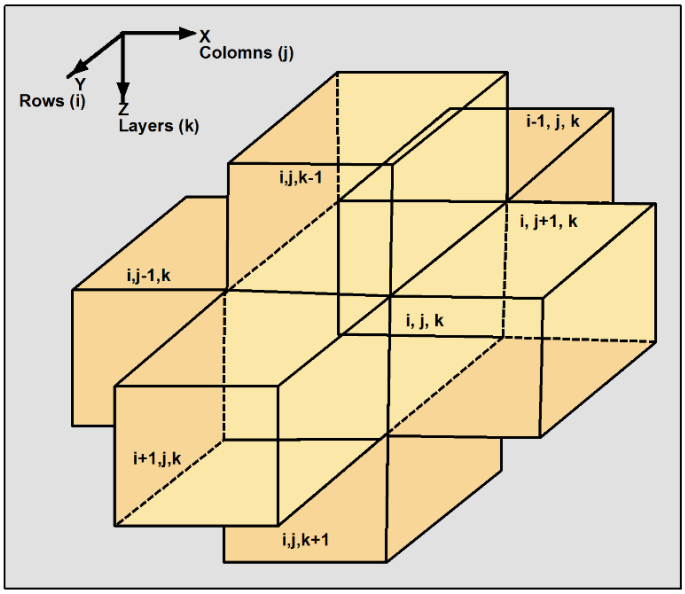

Figure 4.2. Cell i, j, k and indices for the six adjacent cells (Modified from McDonald and Harbaugh, 1988).

According to Darcy Law, flow into cell i, j, k, in the row direction from cell i, j-1, k is written as:

$$q_{i,j-1/2,k} = KR_{i,j-1/2,k}\Delta c_i \Delta v_k \frac{(h_{i,j-1,k} - h_{i,j,k})}{\Delta r_{j-1/2}} \quad (4.5)$$

where,

$h_{i,j,k}$: head at node i, j, k;

$h_{i,j-1,k}$: head at node i, j-1, k;

$q_{i,j-1/2,k}$: volumetric fluid discharge through the face between cells i, j, k and i, j-1, k (L^3/T^{-1});

$KR_{i,j-1/2,k}$: hydraulic conductivity along the row between nodes i, j, k and i, j-1, k (L/T^{-1});

$\Delta c_i \Delta v_k$: area of the cell faces normal to the row direction;

$\Delta r_{j-1/2}$: distance between nodes i, j, k and i, j-1, k (L).

Inflow though the six faces of cell i, j, k (Figure 4.2) in terms of heads, grid dimensions and hydraulic conductivity are simplified by combining grid dimensions and hydraulic conductivity into a single constant, the hydraulic conductance or conductance.

$$\mathrm{CR}_{i,j-\frac{1}{2},k} = KR_{i,j-\frac{1}{2},k} \Delta c_i \Delta v_k / \Delta r_{j-1/2} \tag{4.6}$$

where,

$\mathrm{CR}_{i,j-1/2,k}$: conductance in row i and layer k between nodes i, j-1, k and i, j, k (L^2/T^{-1})

Substituting conductance from Equation 4.5 and 4.6 yields:

$$q_{i,j-1/2,k} = CR_{i,j-1/2,k}\left(h_{i,j-1,k} - h_{i,j,k}\right) \tag{4.7}$$

Using the cell indices shown in Figure 4.2, the final finite-difference form of the Equation 4.1 for cell i, j, k can be expressed as:

$$\mathrm{CR}_{i,j-\frac{1}{2},k}\left(h^m_{i,j-1,k} - h^m_{i,j,k}\right) + \mathrm{CR}_{i,j+\frac{1}{2},k}\left(h^m_{i,j+1,k} - h^m_{i,j,k}\right) + \mathrm{CC}_{i-\frac{1}{2},j,k}\left(h^m_{i-1,j,k} - h^m_{i,j,k}\right) + \mathrm{CC}_{i+\frac{1}{2},j,k}\left(h^m_{i+1,j,k} - h^m_{i,j,k}\right) + \mathrm{CV}_{i,j,k-\frac{1}{2}}\left(h^m_{i,j,k-1} - h^m_{i,j,k}\right) + \mathrm{CV}_{i,j,k+\frac{1}{2}}\left(h^m_{i,j,k+1} - h^m_{i,j,k}\right) + P_{i,j,k}h^m_{i,j,k} + Q_{i,j,k} = SS_{i,j,k}\frac{\left(\Delta r_j \Delta c_i \Delta v_k\right)\left(h^m_{i,j,k} - h^{m-1}_{i,j,k}\right)}{t_m - t_{m-1}} \tag{4.8}$$

where,

$P_{i,j,k}\, h_{i,j,k} + Q_{i,j,k}$	: general known external flow term for cell i, j, k;
SS	: specific storage;
$\Delta r_j \Delta c_i \Delta v_k$	: volume of the cell i, j, k;
t_m	: time at which the flow terms are evaluated;
t_{m-1}	: time which precedes t_m;
h^m	: hydraulic head at each node for time t_m;
h^{m-1}	: initial hydraulic head for time t_{m-1}.

4.2. Conceptual Model of the Study Area

Developing a conceptual model is the first and most important stage of the modeling procedure. It provides benefit to represent surface and groundwater regime in a graphical form prevailing in the study area with simplifying field problem. To develop this model, well understanding of hydrogeology, hydrology and groundwater flow dynamics are necessary.

Conceptual hydrologic and hydrogeological budgets which are the components of the conceptual model are given in Chapter 3.3. In these budgets, key elements of surface water and groundwater flow regime prevailing in the study area are represented in a numerical form. Moreover, although in Chapter 3.2 the hydrogeology of the study area is explained in detail, hydrogeological system should be also defined conceptually. In the study area and its surroundings, Paleozoic and Mesozoic aged rocks are considered as basement units as already mentioned before. Paleozoic metamorphics, Mesozoic ophiolites and Triassic metadetritics are impermeable–semi permeable units and they can bear water only along the fractures resulted from faulting. However, within these basement rocks, Jurassic-Cretaceous limestones may show permeable–semi permeable character. The pumping test results conducted within this unit show that, it

has nearly impermeable character in the study area. Therefore, all these basement rock units can be considered as a single low permeable unit for the model domain and so they form an impervious boundary, where no flow is observed.

Lignite intercalated Miocene aged units (m1 and m2) which overlie the basement rocks are generally represented by claystone, sandstone, conglomerate and bituminous shale. According to pumping test results, these Miocene units have low hydraulic conductivity and display unconfined or semi-confined behavior. However, the presence of sandstones and conglomerates within the sequence cause heterogeneity and hence producing local increase in permeability.

Silicified limestone (m3) which is the upper unit of the Miocene aged Porsuk Formation overlie the m1 and m2 units. This limestone is highly permeable and includes karstic cavities in itself. Therefore, it can be defined as one of the main water bearing unit in the study area. In addition to silicified limestone, from bottom to top Pliocene and Quaternary units are also water bearing units within this domain.

In the study area, groundwater flow is generally from southern upland areas to the north toward the Porsuk Stream and to simulate this flow, model layers comprised from the above mentioned units were defined as confined / unconfined character. It is the layer property of MODFLOW SURFACT to simulate variable saturation conditions.

4.3. Model Domain and Finite Difference Grid

For numerical model design, determination of the model domain and discretization are the starting points. In this study, because the hydrogeological system cannot be divided according to boundary of the license area, a larger domain with a size of 95.6 km^2 surrounding the Eczacıbaşı Industrial Raw Materials Inc. license area was selected (Figure 4.3).

After model domain designation, the other critical step is the finite difference grid design. For this purpose, area of interest was discretized into cells in which hydraulic and hydrogeological properties are assumed as uniform. These discretized cells can be uniform with same dimensions or custom with different sizes. In this study, because there is not more interest in some parts of the model area than others since the mining activities has not been planned yet, uniform grid mesh size is preferred. Then, to determine the size of grid mesh, accuracy of the simulations, computer memory and modeling time criteria are taken into the account. Although the smaller grid mesh size gives more accurate simulation results, it causes more computer memory usage and requires more calculation time. In the light of these information, 50 m x 50 m uniform grid size was chosen for the model domain. These grid size resulted in 38506 active cells in a single layer (Figure 4.3).

In this study, the model has been subdivided into 6 layers according to distribution of the geological units to simulate the different vertical hydrogeological properties as can be seen from the cross sections H-H' and V-V' in Figure 4.3. The top of the uppermost layer is the topographical surface with 760 m-1027 m elevation range within the model domain. The thickness of first layer which is uniformly 50 m was determined according to maximum alluvium and silicified limestone thickness within the study area. The second layer thickness is also determined as 50 m uniformly according to thickness of the Pliocene unit. Miocene aged Porsuk Formation is subdivided as silicified limestone (m3) and clayey m2 and m1 unit within model domain. The silicified limestone unit (m3) which outcrops in the southern portion of the study area is represented by the first model layer in that area. Then other m2 and m1 units are subdivided into four groups located at the uppermost five layers. Fourth model layer corresponds to lignite seams in Miocene aged m2 unit. The top of this layer is drawn by upper lignite seam (A) top elevations whereas the bottom of it is drawn by the lower lignite seam (C) bottom elevations. The elevation distribution of the upper part of the lowermost layer was determined by the elevation ranges of the basement rock units measured during the drilling of the coal exploration boreholes in the study area and this layer is continued through the 50 m elevation above mean sea level.

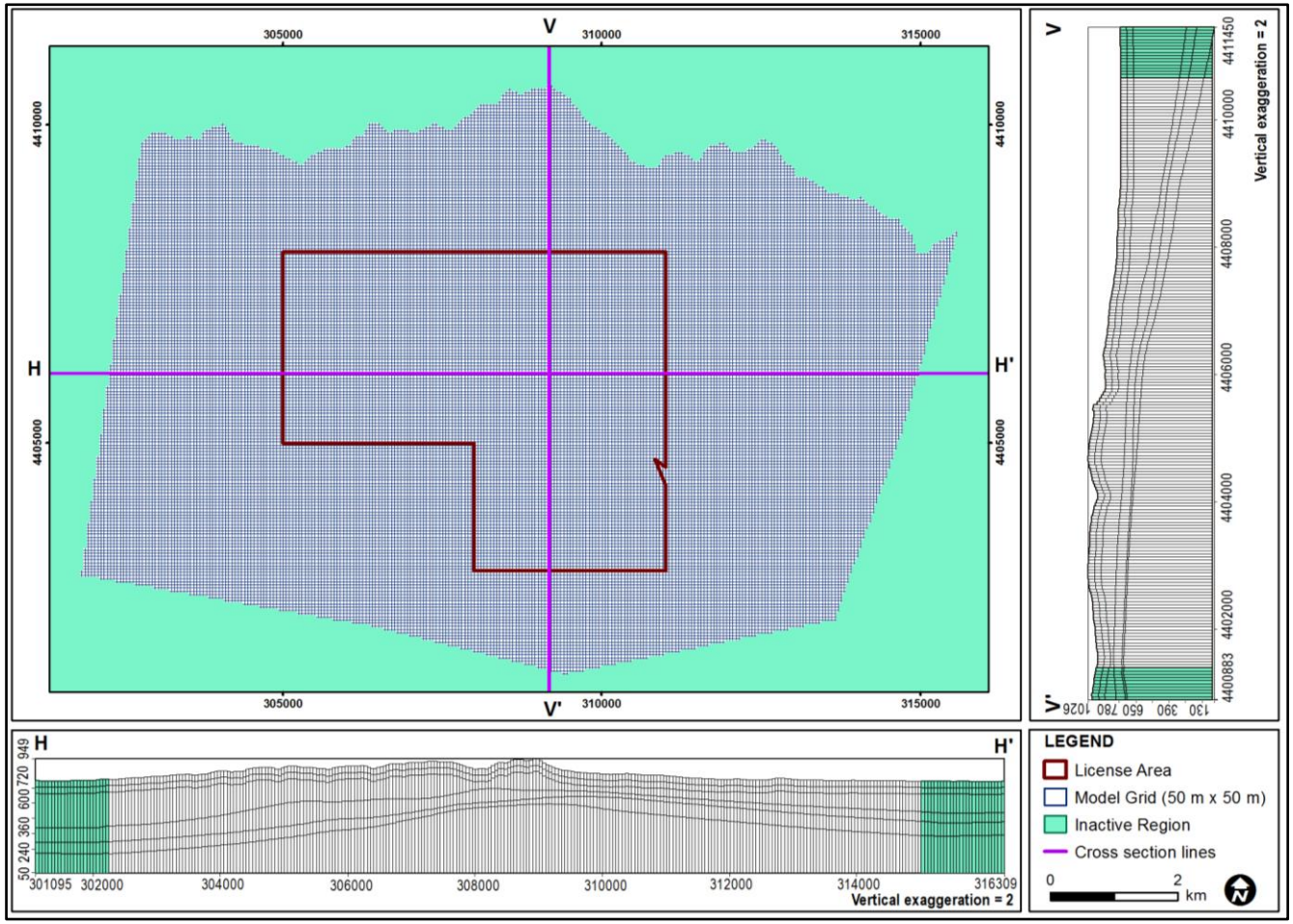

Figure 4.3. Model grids and vertical layout of the model layers

4.4. Boundary Condition

Defining boundary conditions is the key component of the numerical modeling procedure. Since the selection of the right boundary conditions is a critical issue, area of interest should be analyzed carefully in terms of geological, hydrogeological and hydrological aspects. Boundary conditions used in the study area are shown in Figure 4.4.

In the study area, the most important perennial surface water body is the Porsuk Stream which flows along the northern boundary of the model domain. This physical boundary was simulated in the model as river boundary along the northern extent of the domain. The river stage was assigned to approximately 5 m below the ground surface and it decreases from west to east.

Designation of the southern external boundary of the model domain is controlled by watershed boundaries. This external boundary coincides with watershed boundary and act as a groundwater divide. Therefore, it was selected as no flow boundary in the model.

According to groundwater level map of the study area given in Chapter 3.2.2, in the southwestern part of the study area, groundwater elevation contours are parallel to boundary and groundwater flow direction is toward the southwest. Thus, flow of groundwater out from the system in this direction is indicated. Therefore, from southwestern corner of the model domain up to Sevinç village (nearly 2.9 km), general head boundary condition was assigned to the uppermost three layers (nearly 300 m) to simulate head dependent flux boundary conditions along this line. For this boundary, horizontal hydraulic conductivity was assigned as $1x10^{-7}$ m/s as the average horizontal hydraulic conductivity of the silicified limestone and first two layer of m2 unit.

In addition to external boundaries, for springs and captages within the study area, drain boundary condition is selected. This boundary condition simulates flow which is

directed only from the aquifer toward the drain and it stops when the head in the aquifer drops below the elevation of the drain. For captages, 10 m below the topographical surface is taken as drain cell elevation whereas it is 5 m for springs.

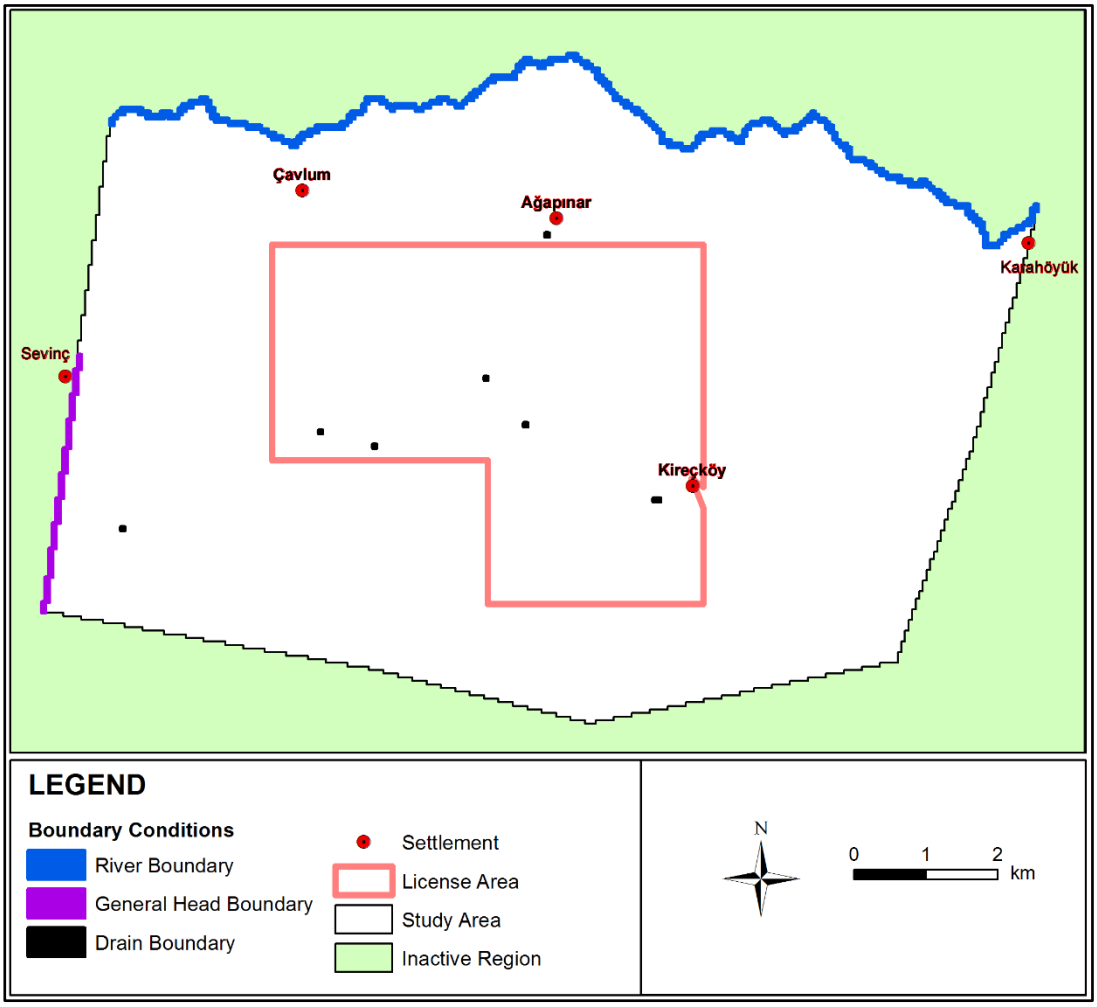

Figure 4.4. Boundary conditions of the model domain

The last and the most problematic boundary conditions to define in the study area are eastern and western boundaries because there is no physical boundary for these directions. Therefore, these boundaries are set farther away from the license area so that the response of the system to various stimuli within the license area will not be

affected significantly by the presence of the boundaries. After these distances were determined, no flow boundary conditions were assigned to them because groundwater level contours (Figure 3.10) nearly cut these boundaries perpendicularly.

CHAPTER 5

CALIBRATION OF THE GROUNDWATER FLOW MODEL

5.1. Model Parameters

Assigning model parameters is the next important step after discretization and specifying model domain and boundary conditions. These parameters are composed of hydrogeological characteristics and discharge-recharge parameters. They are gathered by the evaluation of the geological and hydrogeological properties of the materials in the study area, field observations, in-situ measurements and laboratory analyzes. In the model calibration stage, input model parameters are restated while staying in the limits of the field tested values until the model simulated heads closely match the observed heads.

5.1.1. Hydraulic Conductivity

The hydraulic conductivity (K) is the most critical and sensitive model parameter for the most of the hydrogeological systems (Kresic, 2006). The initial distribution of the K values is identified according to field conducted pumping/recovery and slug tests and lithological properties of the geological units. Then, during calibration they are modified within the ranges of these test results given in Table 3.7. However, only for the clayey Miocene m1 and m2 units which are composed of clay, shale, sandstone and lignite seams, additional lithological analysis is required besides test results. Since these units include lithologies with different hydrogeological properties and show heterogeneous character, clay/sand ratio of the model layers were calculated from 94

coal exploration well logs data to understand hydraulic conductivity distribution of these units. According to results given in Figure 5.1, although it is expected that the permeability of the clay dominated units decrease with depth since increasing overburden pressure causes compaction (Williamson & Grubb, 2001), except first layer, clay/sand ratio decreases through the bottom layers which shows that permeability of the m1-m2 units show an increasing trend with increasing depth. Therefore, lateral hydraulic conductivity values of these units were assigned to the layers in a downwards increasing manner. Although m1-m2 units show permeable character at the first layer (Figure 5.1) in a limited area of the model where they outcrop, it is seen that hydraulic conductivity of this layer must be slightly lower than other clayey layers according to the calibration results.

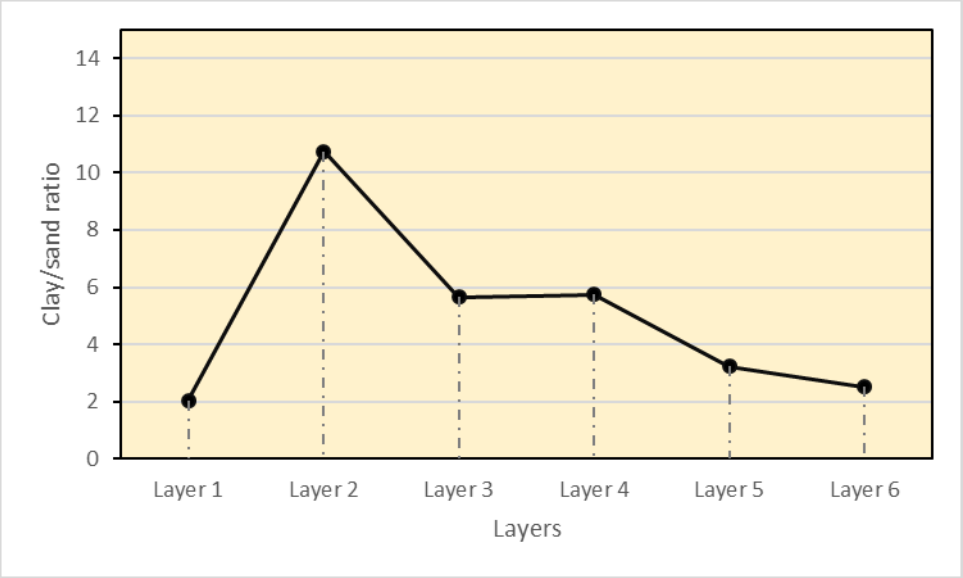

Figure 5.1. Clay/sand ratios for the Miocene m1 and m2 units

The vertical hydraulic conductivity values of the geological units are determined with calibration since there is no in situ measurements for these parameters. According to initial distribution of vertical K values, anisotropy ratio of horizontal (K_h) and vertical (K_v) hydraulic conductivity (K_h/K_v) was set to be 10/1 for all the units. However, during calibration, this ratio was modified as 1 for silicified limestone and 100/1 for basal limestone and m1-m2 unit in the uppermost two layers. Finally, for model domain, a total of 8 different conductivity zones for 6 layers were determined (Figure 5.2).

5.1.2. Groundwater Recharge

In the study area, groundwater recharge is sourced from precipitation and surface runoff infiltration. Most of the precipitation is lost from the system via evapotranspiration. The remaining part turns into surface run off and recharge. As previously mentioned in Chapter 3.2.1, monthly potential evapotranspiration values were calculated by Thornthwaite method using climatological data while surface runoff values are determined by the Curve Number method for model domain. According to results obtained from these methods, annual groundwater recharge from precipitation and surface runoff infiltration were calculated as 51.9 mm/year and 34.4 mm/year, respectively.

Groundwater recharge from precipitation was assigned all over the model area without any restriction. However, since the surface runoff coming from the southern upland region percolates into the groundwater from the plain area around the Porsuk Stream, surface runoff infiltration was simulated for this flat terrain. By using 34.4 mm/year annual surface runoff infiltration, groundwater recharge for flat plain was calculated as 16.5 mm/year and it makes the total recharge as 68.4 mm/year for this area. During calibration, by analyzing model response it can be said that no modification was needed for groundwater recharge values. In Figure 5.3, areal distribution of the groundwater recharge within the model domain is shown.

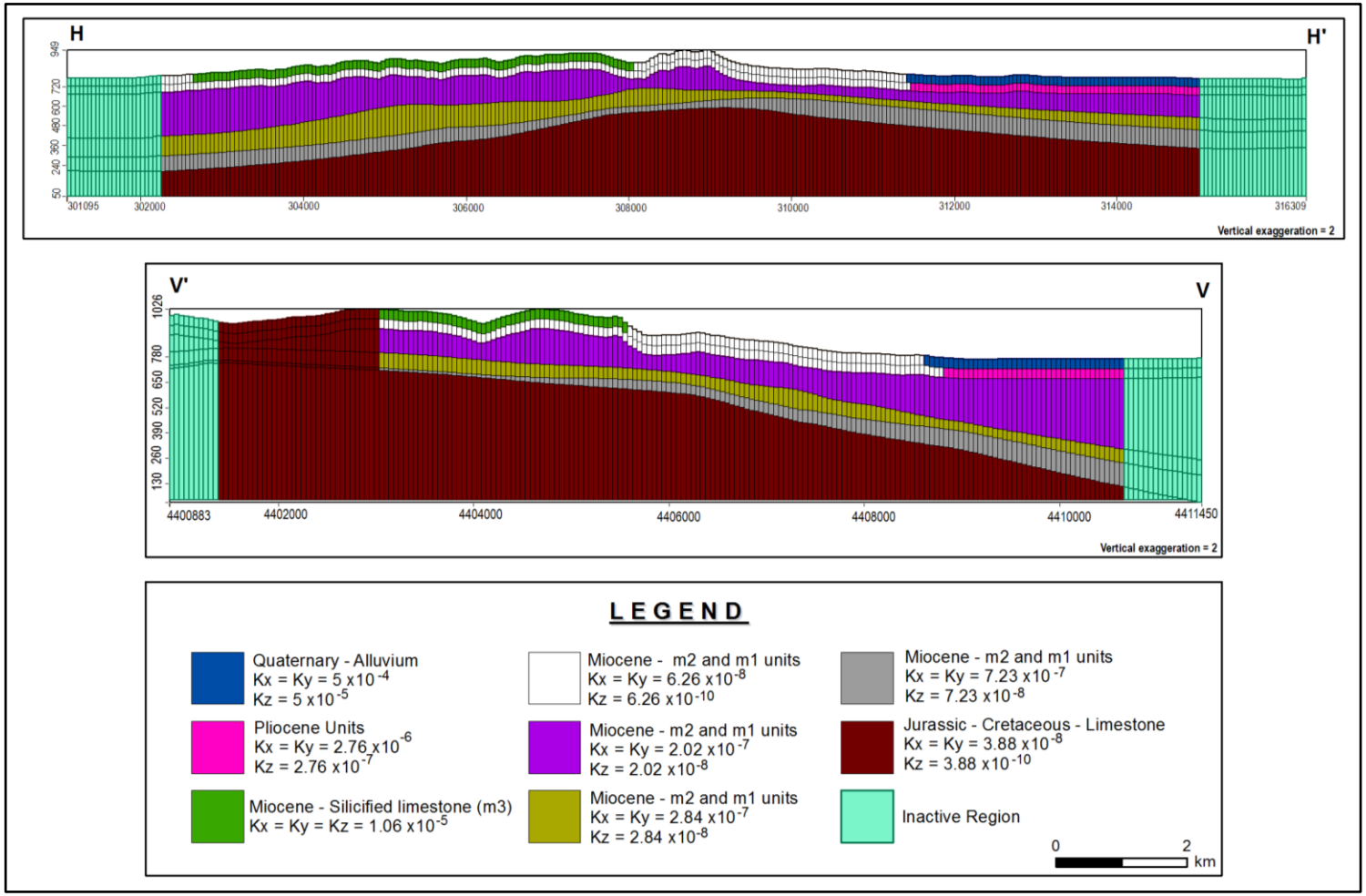

Figure 5.2. Hydraulic conductivity distribution used in the calibrated model

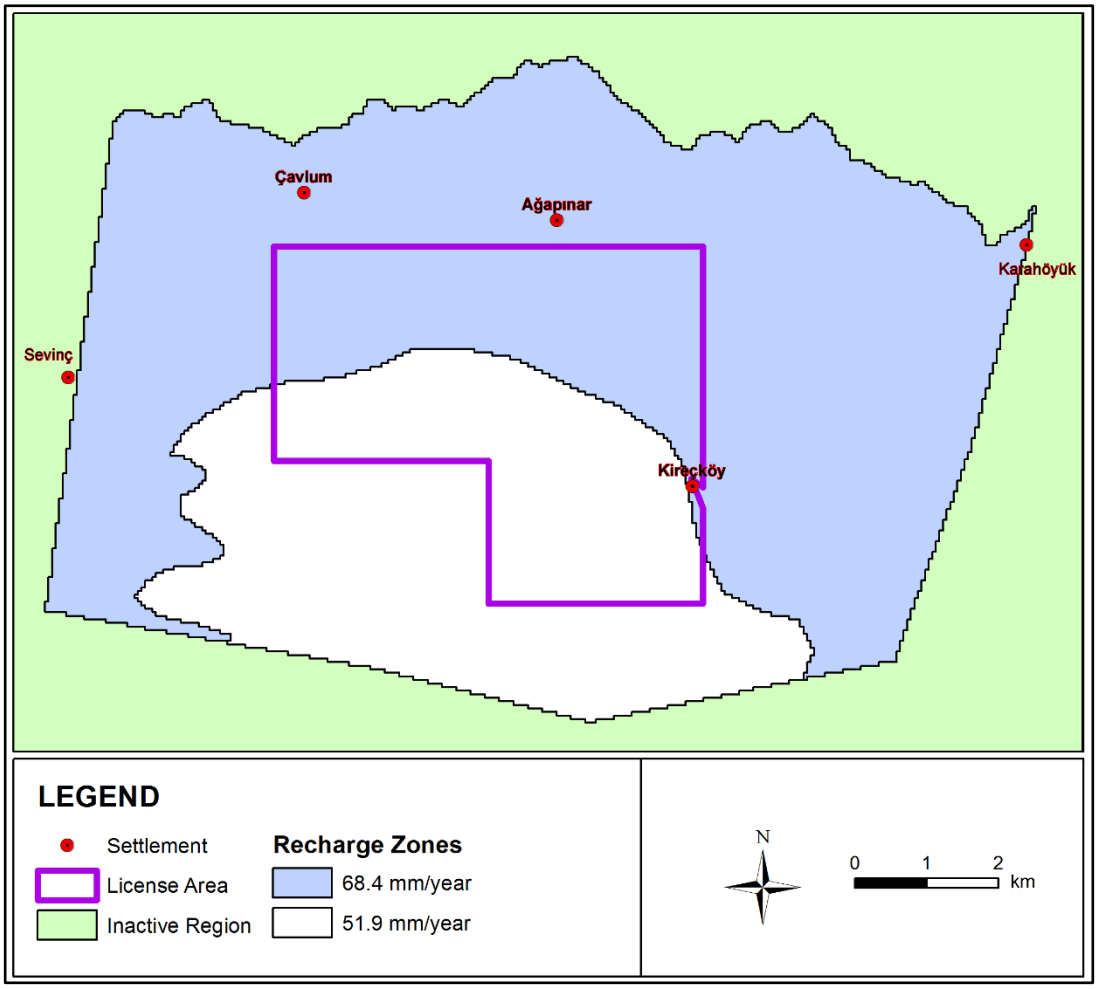

Figure 5.3. Areal recharge distribution used in calibrated model

5.1.3. Groundwater Discharge

In numeric model, some of the groundwater discharge components such as baseflow to Porsuk Stream, discharge from springs/captages and subsurface outflow were simulated as boundary conditions. In addition to these components, groundwater discharge is also originated from evapotranspiration and well discharges. From the previous section, it is known that evapotranspiration is the significant component for groundwater discharge and it was calculated by Thornthwaite method as 318.13 mm/year as mentioned in detailed in Chapter 3.1.1.

This value was assigned to model domain with 1 m extinction depth by using evapotranspiration package. It is determined that there is no need to change evapotranspiration value during the calibration stage.

In addition to natural discharge, groundwater pumpage constitutes the other component for the discharge mechanism. In the study area, groundwater is mainly used to meet the drinking and domestic water needs of the settlements as well as to supply irrigation water requirements. Within the province of study area, Ağapınar, and Kireçköy villages meet part of their drinking and domestic water needs through their pumping wells (Figure 5.4).

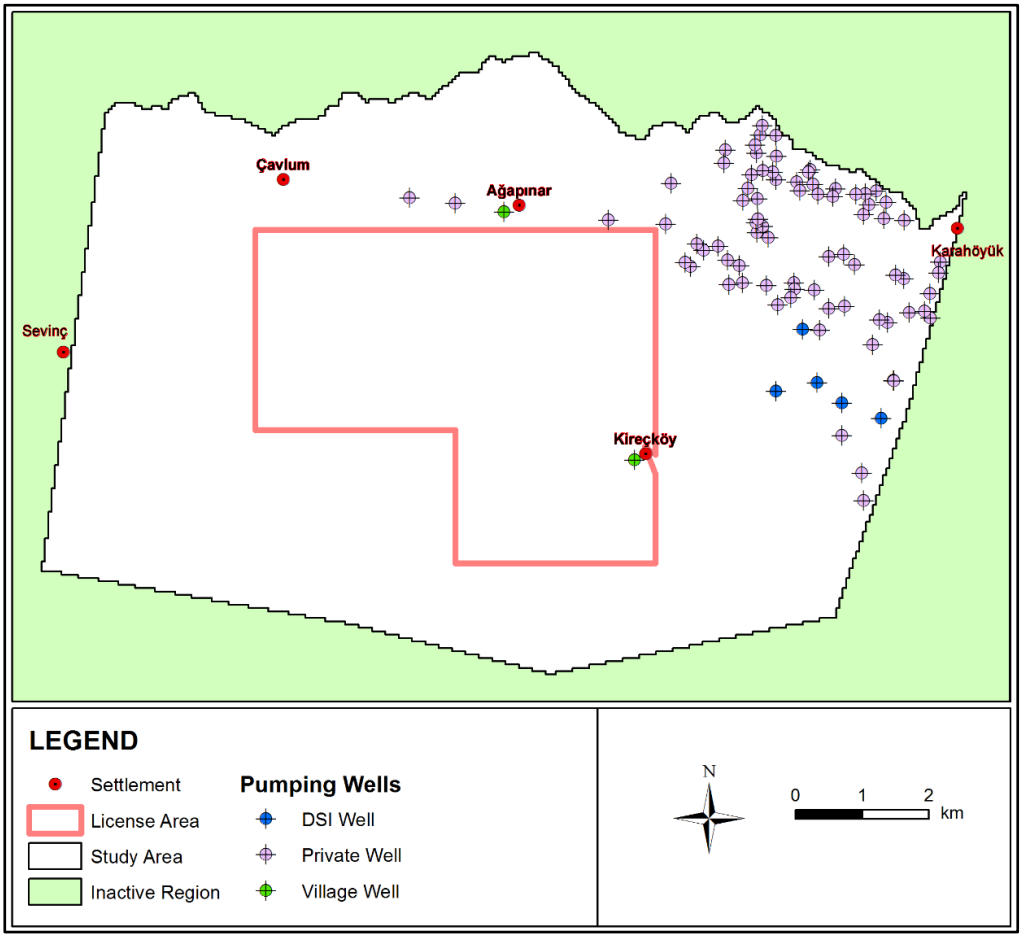

Figure 5.4. Pumping wells within the model domain

For each well, the consumption amount was calculated as 123.3 m^3/day according to conceptual hydrogeological budget given in Chapter 4.2. In addition to this limited consumption amount, most of the groundwater usage is for irrigational purposes in the study area. For this reason, five DSI wells (44130, 55322, 55323, 55324 and 55325) and 78 private wells are used within the domain (Figure 5.4). Because there is no information about the depth and screen intervals of the private wells and they pump water generally from Quaternary alluvium and Pliocene units, they were simulated in model as screened along the top two layers. For each DSI well, 542.5 m^3/day water has been pumped by Kireçköy Irrigational Cooperative to irrigate 189 hectares area. Additionally, 78 private wells irrigate 241 hectares area by 44.3 m^3/day water pumpage amount for each of them. As mentioned before in Chapter 4.2, total amount of pumpage from these wells is equal to $2.34x10^6$ m^3/year.

5.2. Calibration

Model calibration is the adjustment of initial conditions and model parameters to obtain a reasonable match between model results and measured values. During calibration, trial and error method is useful to develop a better feeling for the model by changing model parameters explained in the preceding sections and analyzing their response with making different assumptions.

In this study, model calibration is conducted under steady state conditions. The first step of calibration often ends when there is a good match between calculated and observed groundwater levels. Quantification of the model error with statistical methods is the second step for calibration. Finally, this stage is completed when calculated budget of the system match acceptably with the preset conceptual budget.

5.2.1. RMS (Root Mean Square Error) and Normalized RMS

For comparing model results quantitatively, the Root Mean Square Error (RMS) and Normalized Root Mean Square Error (NRMS) parameters are used.

RMS which is the average of the squared differences between measured and simulated heads can be defined as:

$$RMS = \left[\frac{1}{n}\sum_{i=1}^{n}(h_m - h_s)_i^2\right]^{0.5} \quad (5.1)$$

where,

n : total number of observation points;
h_m : measured hydraulic head;
hs : simulated hydraulic head.

NRMS is the non-dimensional version of the RMS calculated as percentage. The formula of this statistical error parameter can be written as:

$$NRMS(\%) = \frac{RMS}{(h_m)_{max} - (h_m)_{min}} \quad (5.2)$$

where,

$(h_m)_{max}$: maximum value of observed hydraulic head;
$(h_m)_{min}$: minimum value of observed hydraulic head.

When these error parameters are minimized, this stage of the calibration is completed and it is ready for sensitivity analyses.

In the real case, a total of 14 head measurements made in the monitoring wells across the study area were used to calibrate the model (Figure 5.5). At the end of the calibration, a graph of calculated versus observed heads at these observation wells was drawn (Figure 5.6) and RMS / NRMS values were calculated as 7.524 m and 3.971 %, respectively. These error values are within the acceptable limits for a stable model. Additionally, groundwater levels drawn with calibrated model results show consistence with the groundwater level map generated in the conceptual model (Figure 5.7).

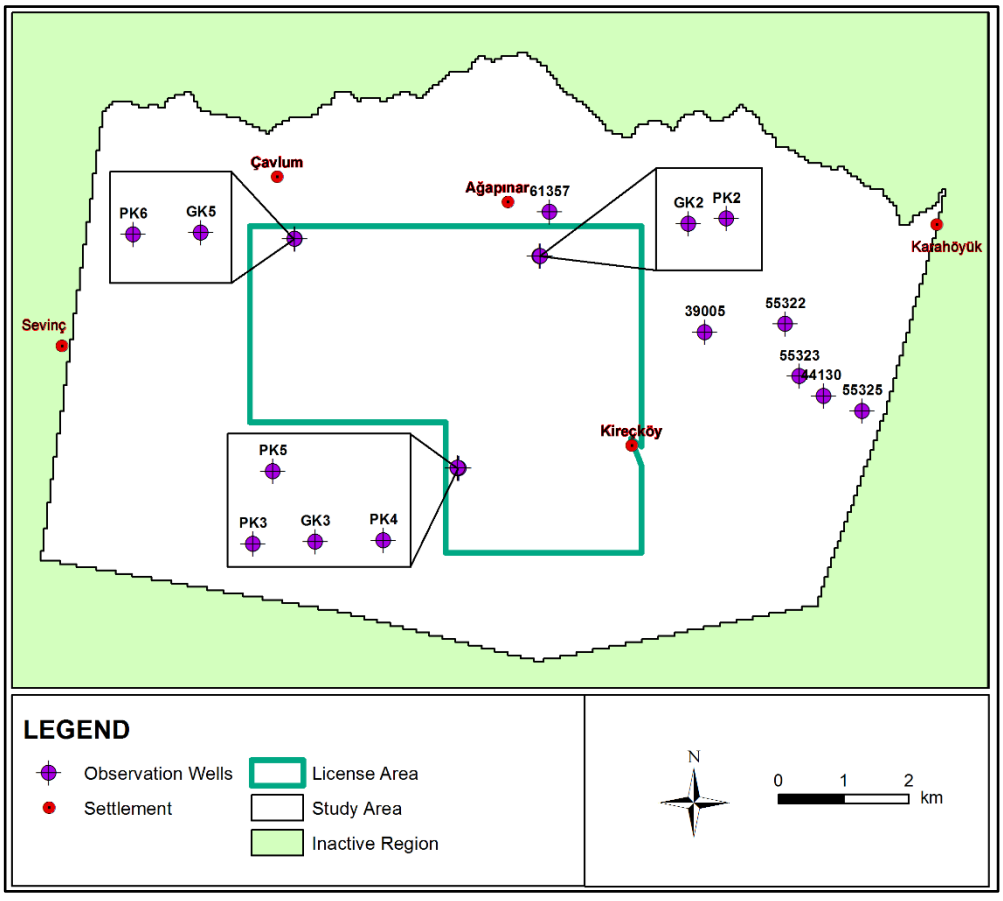

Figure 5.5. Observation wells used for the model calibration

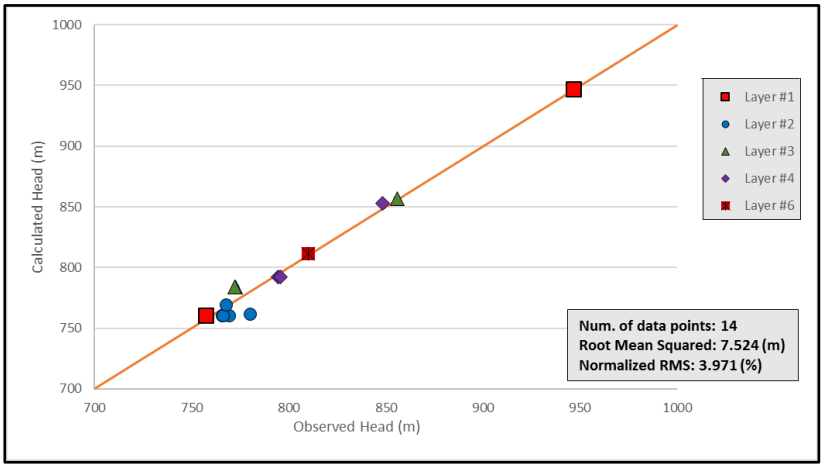

Figure 5.6. Calculated versus observed head values and calibration results of the model

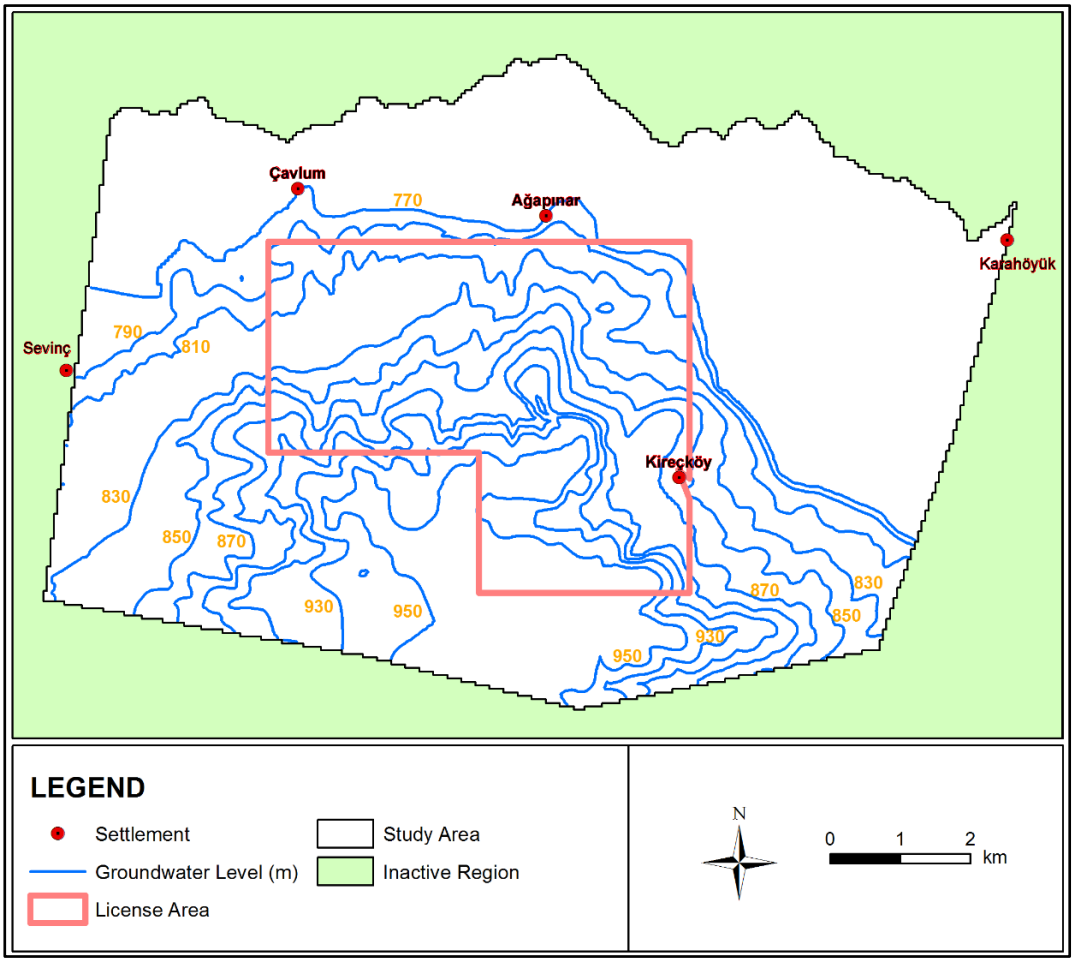

Figure 5.7. Aerial distribution of the calculated groundwater levels

5.2.2. Calculated Groundwater Budget

The final step of the model calibration is comparing calculated groundwater budget with conceptual budget. In MODFLOW SURFACT, this calculation is made by ZoneBudget Engine. Groundwater budget calculated at the end of the calibration for steady state conditions is given in Table 5.1. Hence, the total recharge and discharge are equal to each other.

In calculated model budget, unlike conceptual one, recharge from precipitation and surface runoff were simulated together. Total annual recharge from these components is equal to 6.05×10^6 m^3, which is almost same with conceptual model recharge amount (Table 3.16). The other recharge component which was not stipulated earlier is the river inflow along some reaches of the Porsuk Stream. This recharge component is calculated to be 2.31×10^6 m^3/year. The model, however, simulated a greater amount of outflow (3.42×10^6 m^3/year) to the Porsuk Stream. The difference between this outflow and inflow values gives the net baseflow to Porsuk Stream which is equal to 1.1×10^6 m^3 /year. This result is almost the same with the conceptually calculated baseflow value (Table 3.16).

As can be seen Table 5.1, although most of the discharge components are compatible with the conceptual budget, it can be seen that calculated evapotranspiration loses is 22 % higher than envisaged amount (Table 3.16). This overestimation is probably due to the calculated heads being higher than the ground surface in the steeply sloping valleys that artificially produces more evapotranspiration losses. Another difference between the conceptual budget and the model calculated budget is noted in the discharge rates of springs and captages. The model calculated rates are about two-thirds lower than the conceptually estimated rates. Because it was not possible to measure the discharge rates of the captages in the field, either of both results may be incorrect. Hence, field measurements of the discharge rates of the captages become mandatory to validate this discharge component.

Table 5.1. Groundwater budget for the calibrated model

RECHARGE (m^3/year)		DISCHARGE (m^3/year)	
Recharge from precipitation & Surface runoff infiltration	$6.05x10^6$	**Springs**	$2.82x10^4$
		Captages	$1.40x10^5$
River inflow	$2.31x10^6$	**River outflow**	$3.42x10^6$
		Pumping from wells	$2.34x10^6$
		Evapotranspiration	$2.34x10^6$
		Subsurface outflow	$9.80x10^4$
TOTAL	**$8.36 x10^6$**	**TOTAL**	**$8.36 x10^6$**

5.3. Sensitivity Analyses

Sensitivity analysis has been carried out on key parameters of the model to understand the response of model results. By analyzing relative effect of these parameters, fundamental understanding of the simulated system is provided. The most sensitive model parameter is the most important model parameter for calibration. For this reason, results of the sensitivity analysis give clue about the future data collection efforts, as well as helping to minimize model error. For this analysis, multiple model simulations are conducted by changing parameter(s) by an arbitrary amount. For the evaluation of the sensitivity analysis, groundwater levels, model budget and statistical error parameters (RMS and NRMS) produced from the results of the analysis are compared with the calibrated model results.

In this study, several simulations were performed to analyze the sensitivity of recharge, evapotranspiration and horizontal and vertical hydraulic conductivity parameters. For adjustment of each parameter, a multiplication factor between 0.1 and 10 was used. During sensitivity analyses of hydraulic conductivity, vertical hydraulic conductivity of basal limestone, silicified limestone and upper two layers of the m1-m2 unit and horizontal hydraulic conductivity of the system units were examined. Calculated RMS and Normalized RMS values and their graphical analyses for each simulation are given in Figure 5.8. In this figure, the RMS and normalized RMS values corresponding to the multiplication factor of 1 are the error statistics obtained from the calibrated model.

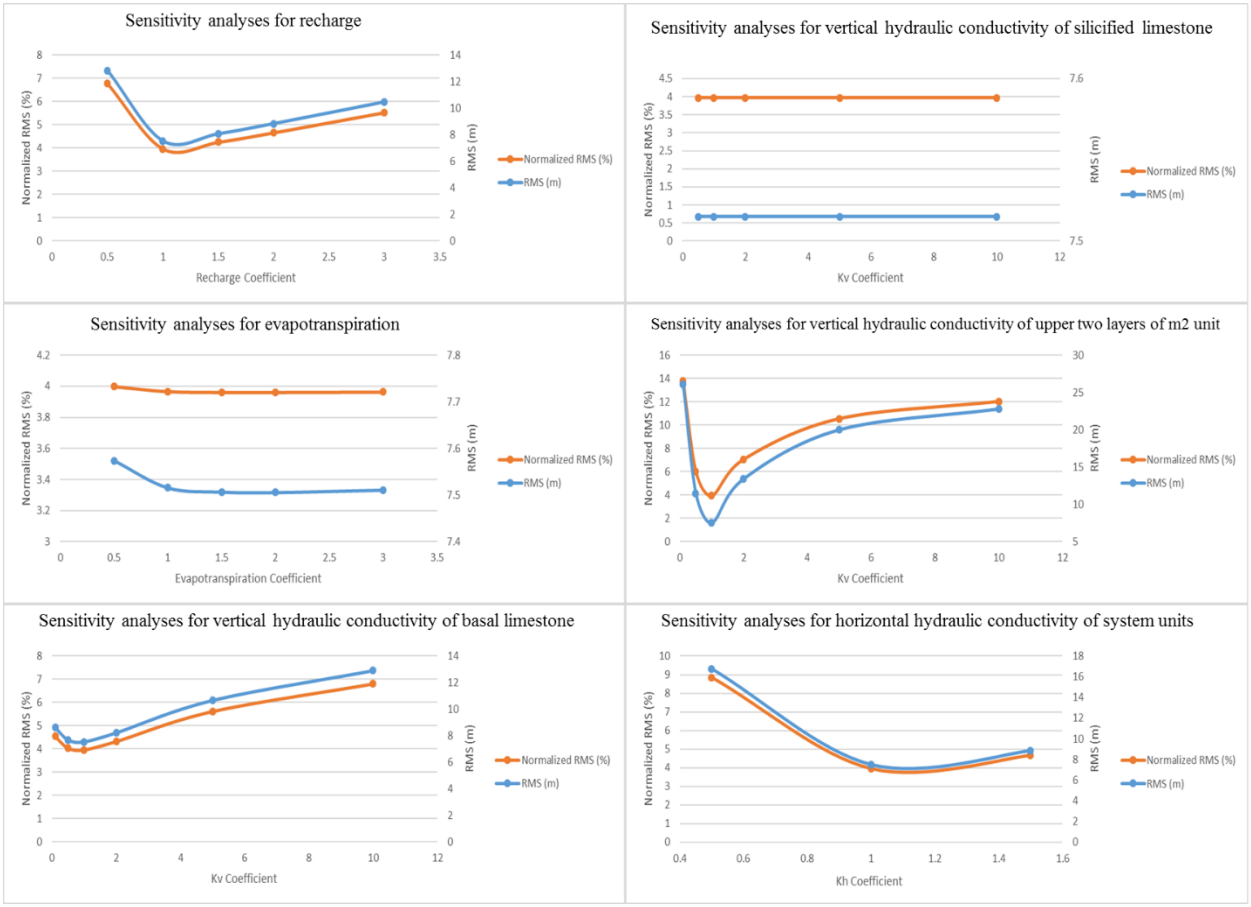

Figure 5.8. Results of sensitivity analyses

According to given graphs in Figure 5.8, model is sensitive to recharge and hydraulic conductivity changes. However, it is not sensitive to evapotranspiration and vertical hydraulic conductivity of silicified limestone.

Finally, it can be stated that the model is sensitive to increase or decrease in the recharge rates and hydraulic conductivity values. The calibrated model produced the minimum RMS and normalized RMS values. Furthermore, an increase or decrease in the vertical hydraulic conductivity of the upper two layers of m1-m2 unit is the most sensitive parameters for the model.

CHAPTER 6

PRELIMINARY DEWATERING SYSTEM SIMULATIONS

6.1. Introduction

After calibration stage is completed successfully, model can be employed to simulate the mine dewatering operations. In this study area, since the lignite seams occur at depths too deep for open cut mining, it is assumed that the deposit will be extracted by a method of underground mining (Palaris, 2016). During underground mining activities, dewatering systems will be required because the deep seated lignite seams lie below the water table, causing water inflow problems. However, since underground mining technique and extracted lignite seams are not determined with certainty at this stage, model responses to the preliminary dewatering activities are tested in this study. The aim of this preliminary study is to determine an initial estimate to the rate of dewatering required and to assess the impact of the predicted amount of water inflow to a typical underground coal panel, not to prepare an appropriate dewatering strategy for the planned underground mine. The calibrated steady state model was taken as a reference to compare the results of this study.

As mentioned in Chapter 2.3, three lignite seams named as A, B, C from top to bottom have been deposited within the Miocene aged sedimentary units. Because no specific design is yet produced for the production of coal from these seams, it is assumed that the underground coal panels are located according to minimum and maximum depths of these lignite seams in the direction perpendicular to the dip directions of them. The dip direction of the upper A lignite seam is to the north and its depth increases toward the northwestern part of the license area. Minimum depth of the A lignite seam is seen

in the southwestern part of the license area. The lignite seam B has a similar distribution to the lignite seam C. For the northwestern part of the license area, their dip direction is to the northwest whereas it is to the north for the southeastern part of the area. These lignite seams reach their maximum depths in the northwestern part of the license area and their shallowest depositions are seen in the southeastern part of this area. For dewatering simulations, 200 m x 2000 m sized panels A-1, B-1, C-1 and A-2, B-2, C-2 were designed at the areas where the maximum and minimum depth of the lignite seams A, B, C are deposited (Figure 6.1).

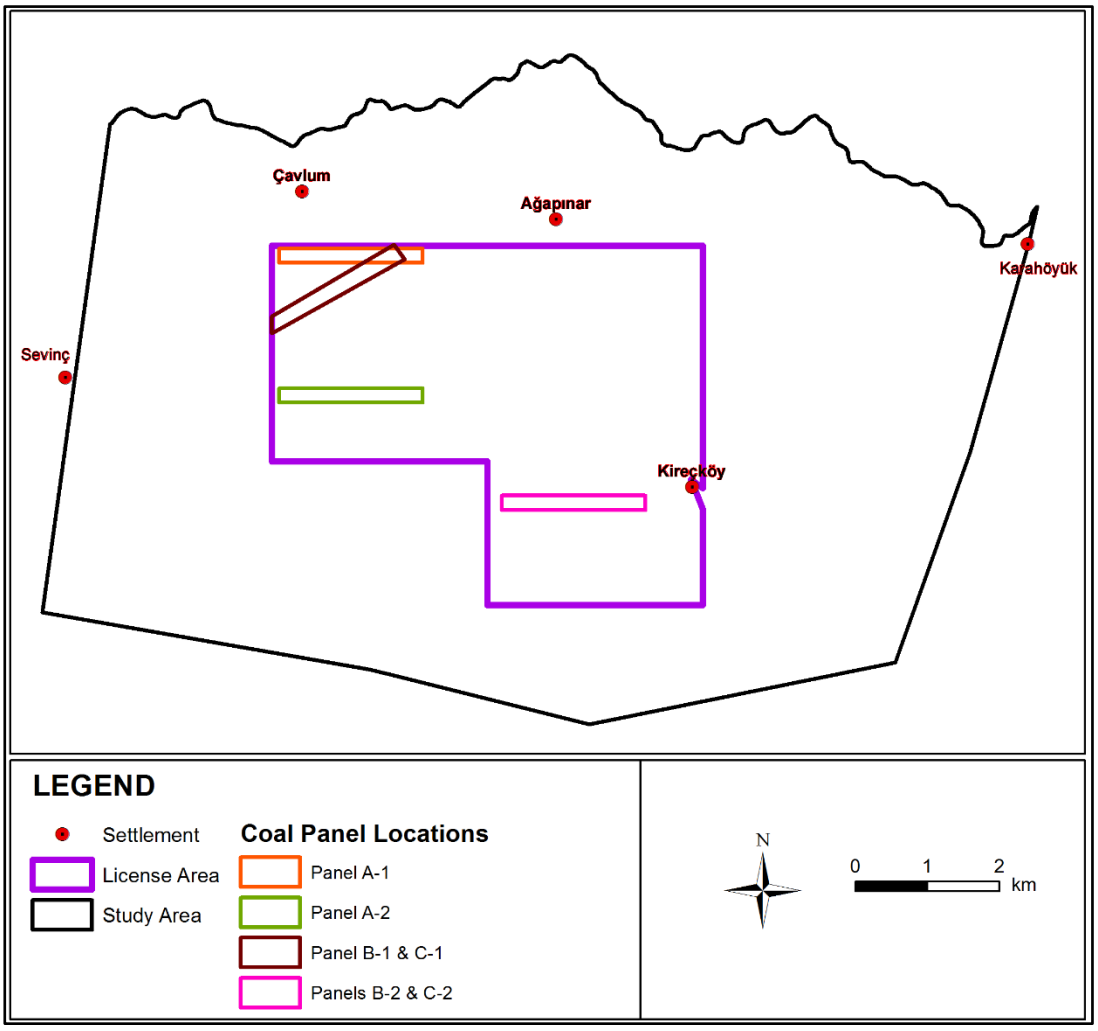

Figure 6.1. Locations of panels used for dewatering simulations

6.2. Prediction of Groundwater Inflow to Underground Coal Panel

Preliminary dewatering simulations are set up under steady state conditions by using drain package of the MODFLOW SURFACT. For these simulations, along the panels seen in Figure 6.1, drain cells were assigned to the bottom altitude of the lignite seams and predicted amount of groundwater inflow to these panels were calculated. The resulting mine inflows give an idea about the pumping requirements for the future studies.

In this study, two different simulations were conducted per each lignite seam. Panel A-1 is located at an area where the maximum depth of the lignite seam A is seen. Groundwater inflow from the drains at this location was calculated as 123.47 L/s, whereas for the panel A-2 it is 52.96 L/s. Lower amount of groundwater inflow is predicted for panel A-2 which is located at a shallow depth in the depositional area of the lignite seam A.

For panels B-1 and B-2, calculated groundwater inflows from the drain cells are 129.92 L/s and 22.45 L/s, respectively. This indicates that during mining activities at the region where the shallower depth of the lignite seam B is seen, lower amount of inflow will be required.

Groundwater inflow amount to Panels C-1 and C-2 were calculated as 133.89 L/s and 23.68 L/s, respectively. As well as the other lignite seams, lower amount of inflow was predicted for the shallower depositional area of the lignite seam C. However, since lignite seam C is deposited below the other two seams, maximum groundwater inflow will be seen during extraction of the deepest part of this seam at panel C-1. Therefore, if this extraction scenario is realized to take place, maximum pumping rates will be required for groundwater inflow from this region.

In Figure 6.2, graphical distribution of the groundwater inflow amounts to the underground coal panels are given. According to this graph, higher amount of

groundwater inflow was calculated from the drains located at the deeper elevations as it was expected. This graph illustrates that the dewatering rates for various panels and lignite seams are expected to lie in the envelope shown in Figure 6.2. Depending upon the coal seam mined and the location of the panel, the groundwater inflow to a typical panel will vary between 23 L/s and 134 L/s. It should be noted that these groundwater inflow amounts will also vary as the panel size changes.

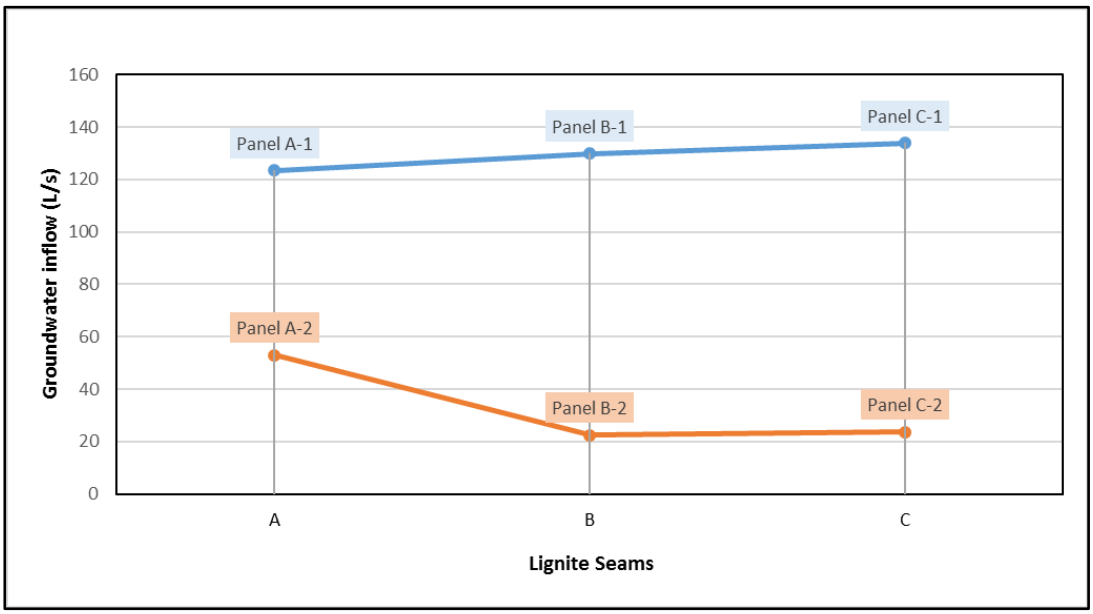

Figure 6.2. Groundwater inflow amounts for the A, B, C lignite seams dewatering simulations

6.3. Groundwater Levels After Preliminary Dewatering Simulations

Mining operations below the groundwater table can induce excessive groundwater inflow to the underground coal panels. Therefore, dry working conditions should be provided by lowering the groundwater heads to the bottom elevations of the lignite seams during these operations. In order to ensure that the heads are lowered to the desired elevations, groundwater heads after dewatering is checked to see if they are at

the bottom of the panels. Consequently, at the end of the dewatering simulations conducted at the underground coal panels given in Figure 6.1, the groundwater levels were drawn for the model layer 4 which coincides the lignite seams bottom elevations in the model domain.

Dewatering simulations at the underground lignite panels A-1, A-2, B-1, B-2, C-1 and C-2 cause the decrease of groundwater levels down to approximately 380-490 m, 610-680 m, 360-450 m, 670-730 m, 340-440 m and 660-720 m as can be seen from Figures 6.3-6.8, respectively. Resulting groundwater levels are sufficient to provide dry working conditions during mining operations of lignite seams in the study area. Maximum drawdown is noted at panel C-1 as 384-454 m (Figure 6.9), whereas it is minimum for panel B-2 as 94-174 m (Figure 6.10). These results are compatible with maximum and minimum calculated groundwater inflows since they are directly proportional.

6.4. Impact Assessment of Preliminary Dewatering Simulations

An impact assessment was performed on the groundwater and surface water resources over an area located within the drawdown cone created by the mine dewatering operations. For this purpose, drying of the springs and captages and reduction of the Porsuk Stream baseflow and decrease in groundwater levels from wells were considered as components of the impact assessment. During this process, position of the simulated drawdown cone with respect to these components and groundwater budget generated based on the dewatering simulations were used.

As mentioned in previous section, the drawdown rates for panels C-1 and B-2 were 384-454 m and 94-174 m at the maximum and minimum quantities given in Figures 6.9 & 6.10, respectively.

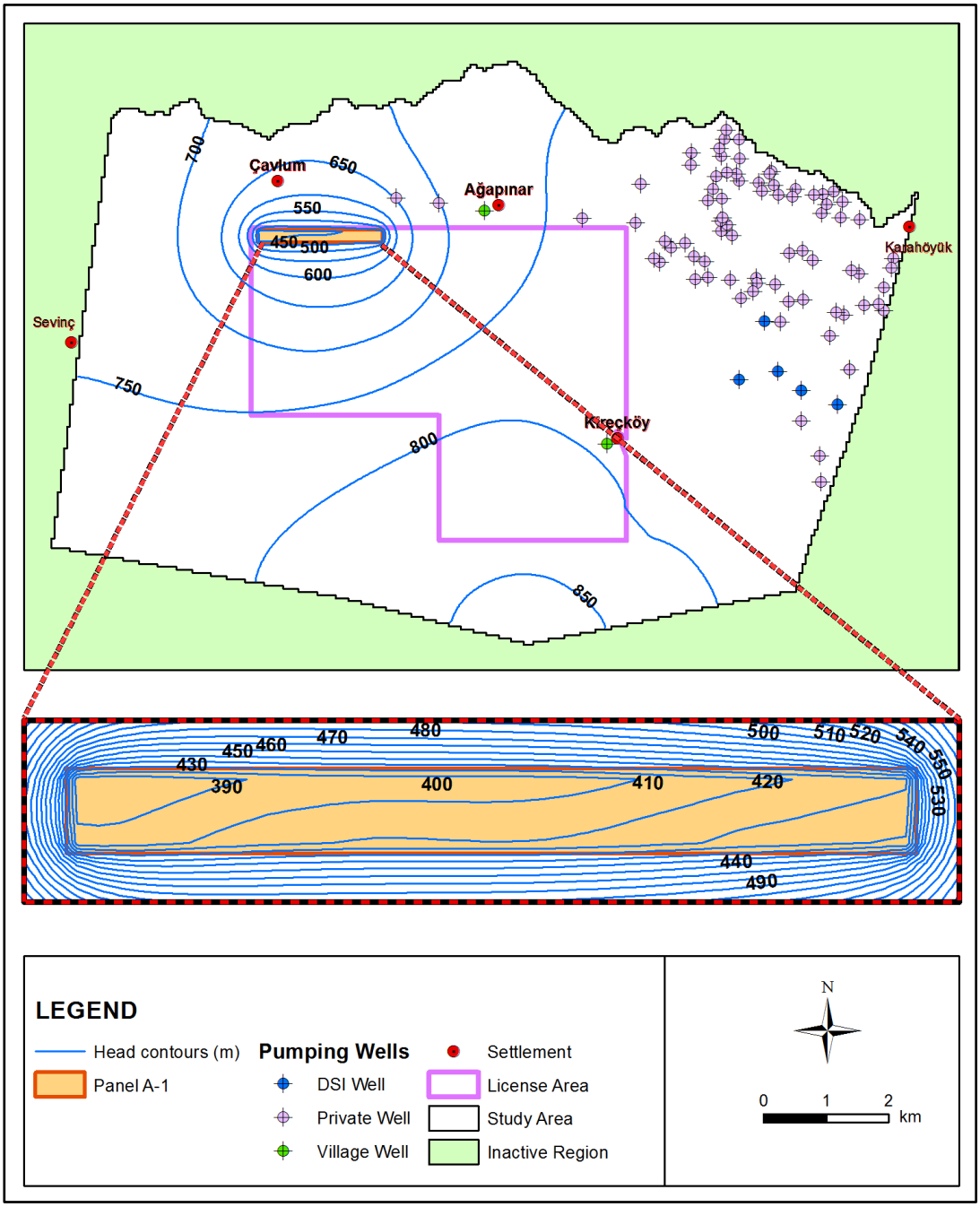

Figure 6.3. Head contours after dewatering simulations at panel A-1

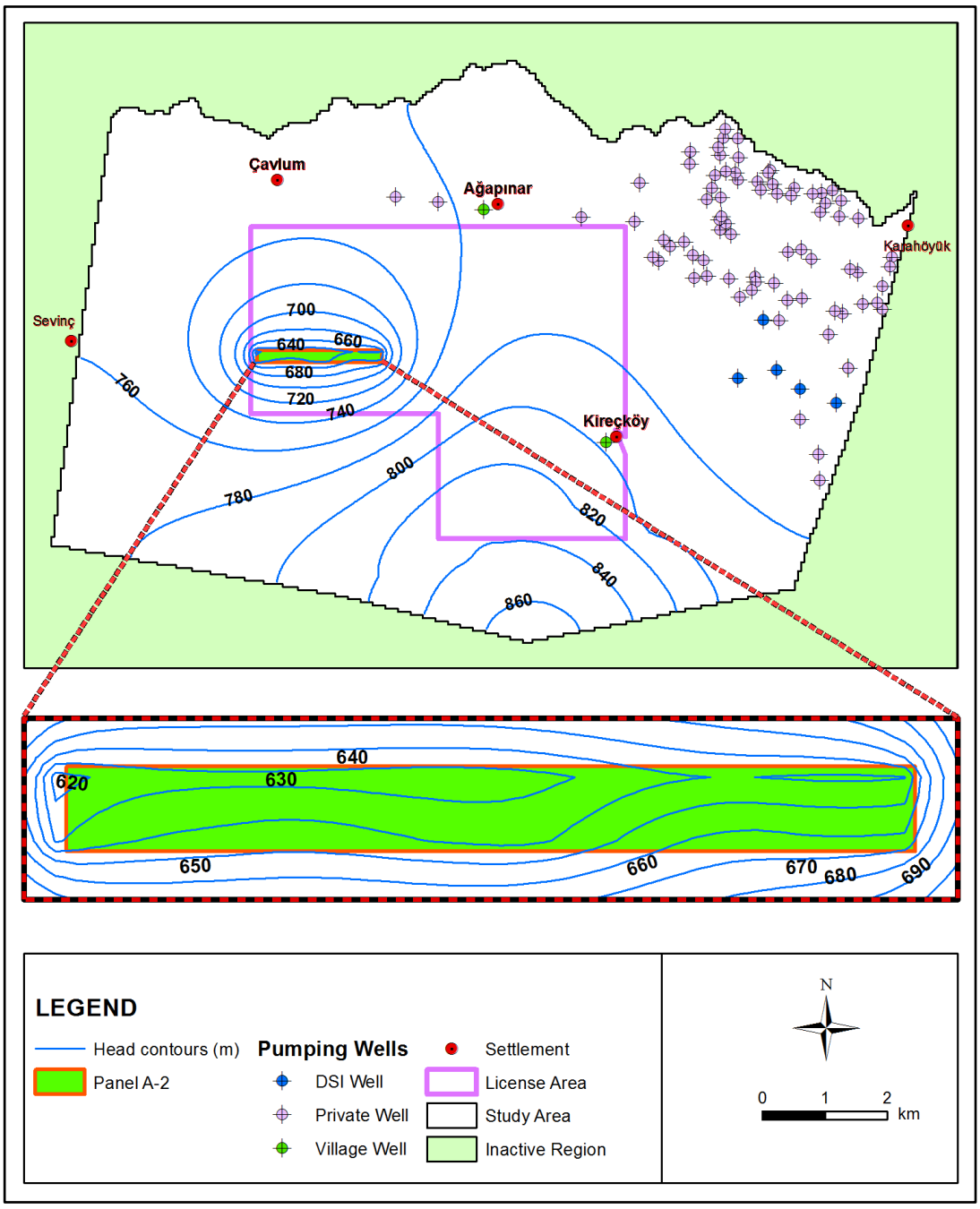

Figure 6.4. Head contours after dewatering simulations at panel A-2

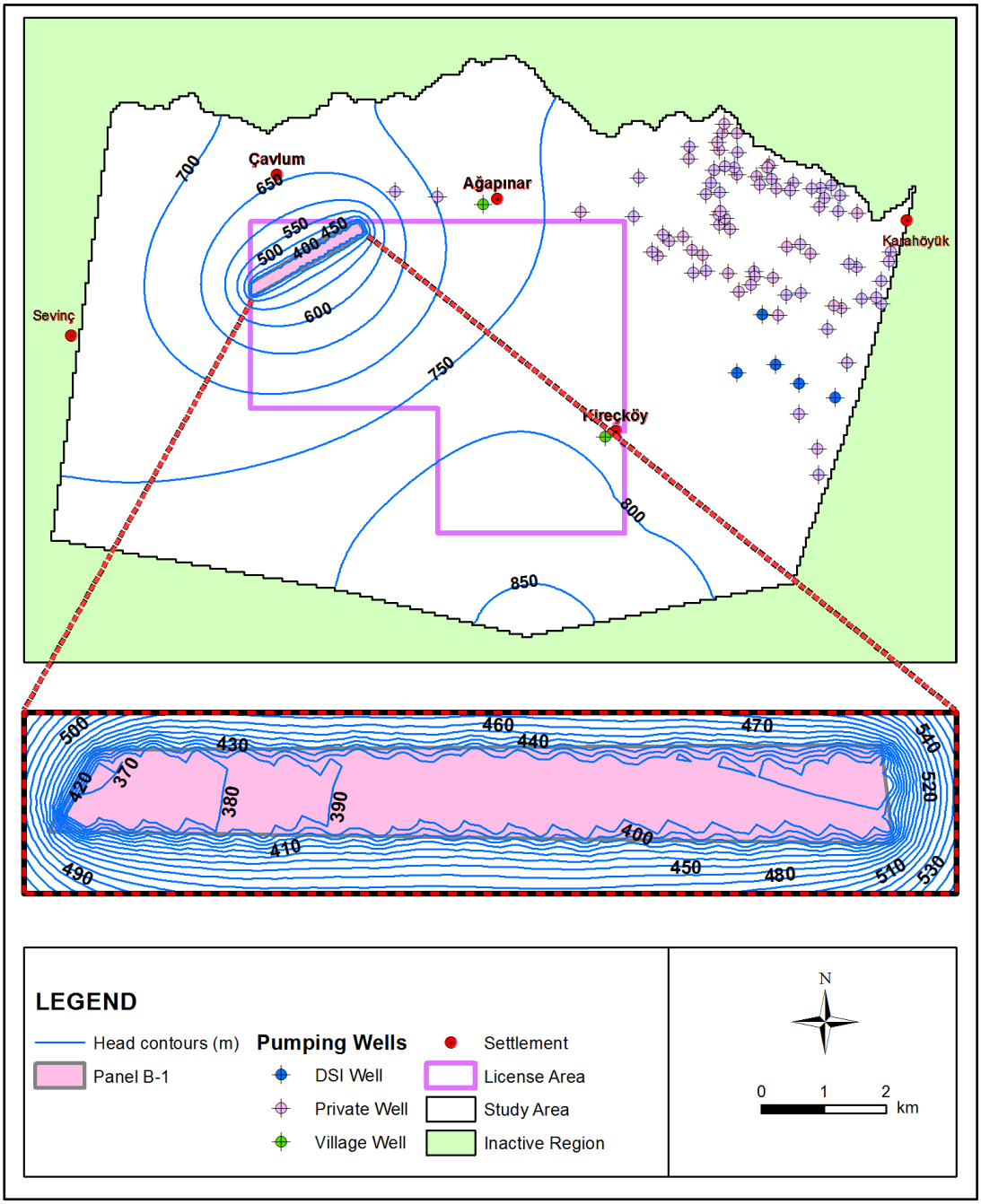

Figure 6.5. Head contours after dewatering simulations at panel B-1

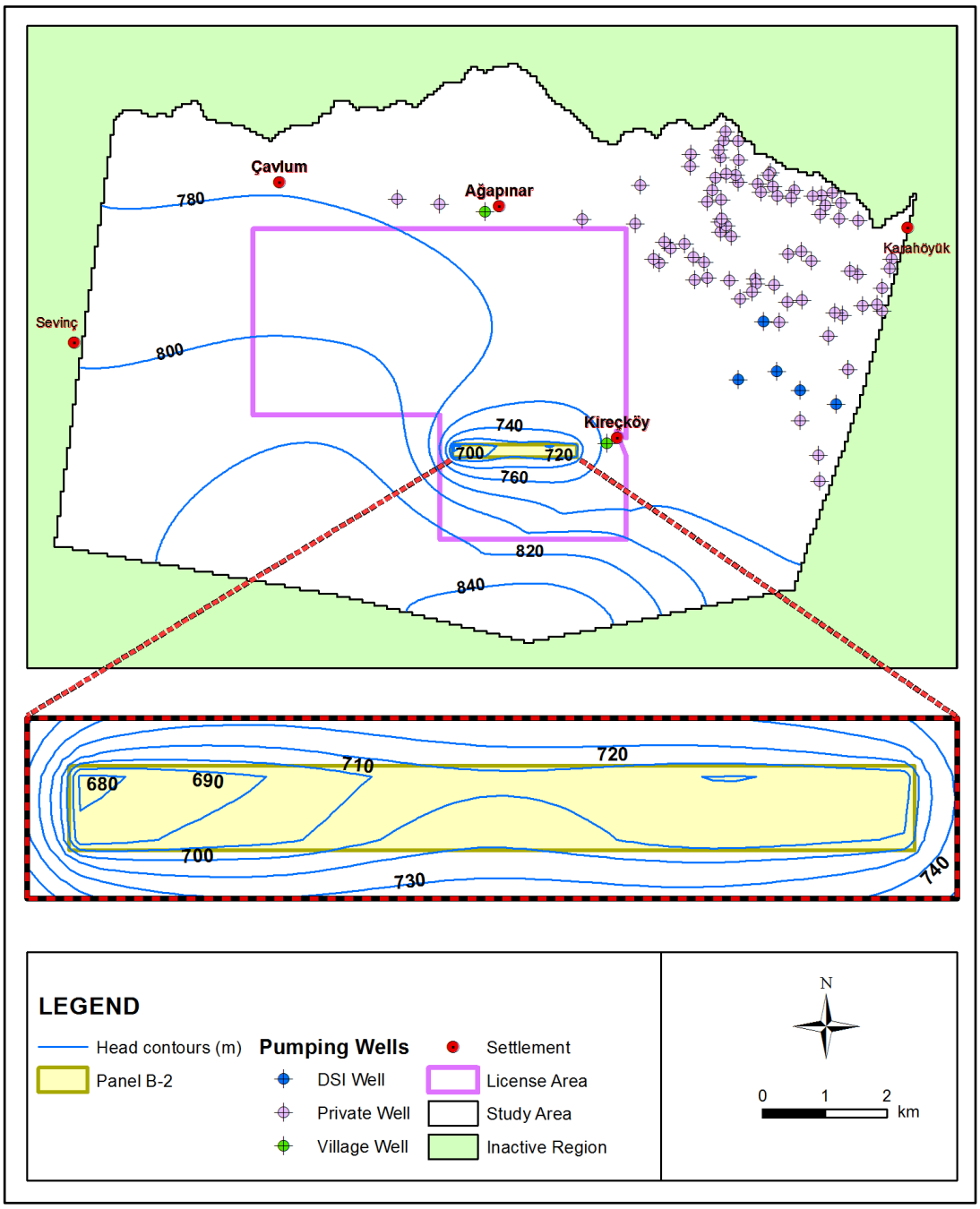

Figure 6.6. Head contours after dewatering simulations at panel B-2

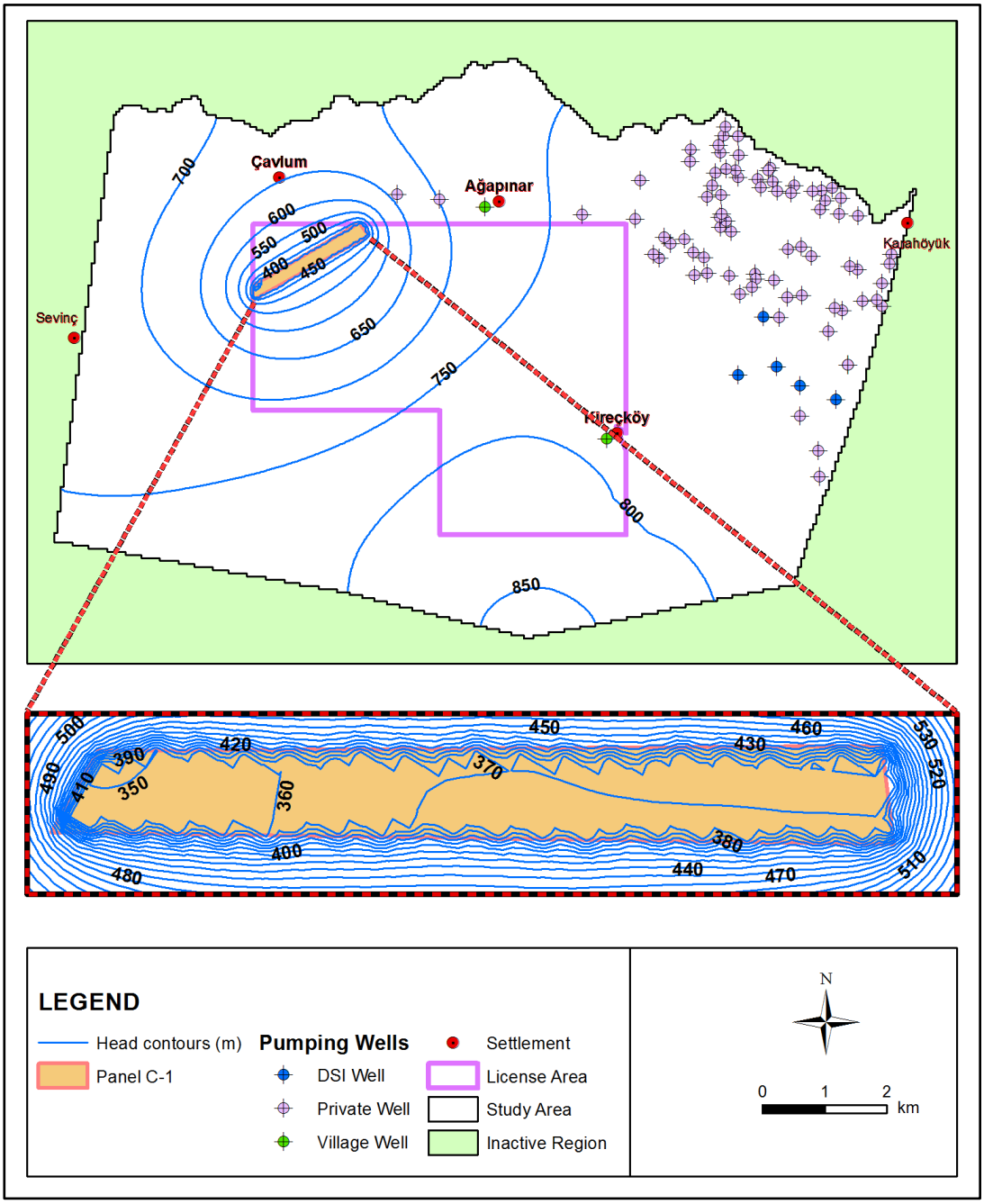

Figure 6.7. Head contours after dewatering simulations at panel C-1

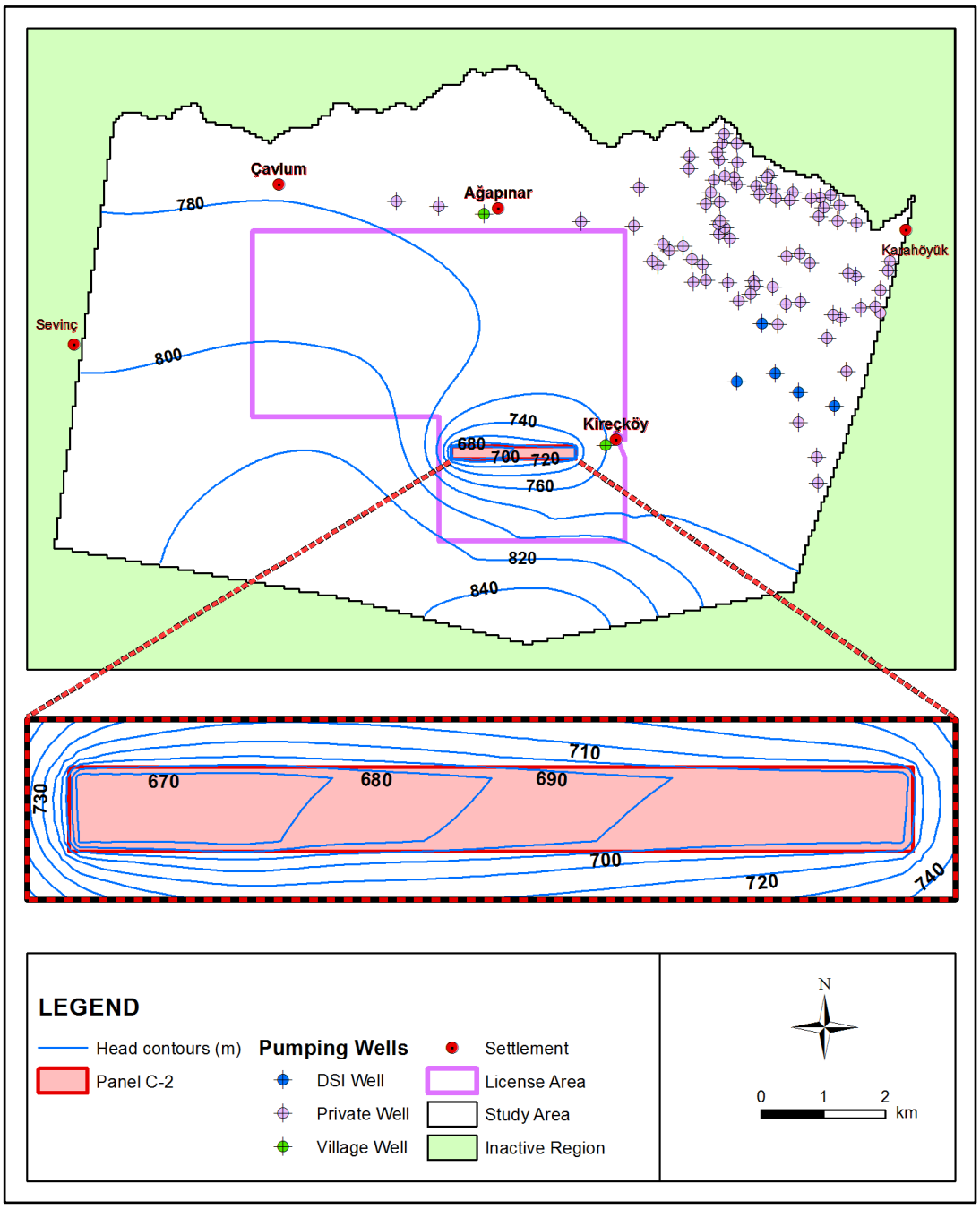

Figure 6.8. Head contours after dewatering simulations at panel C-2

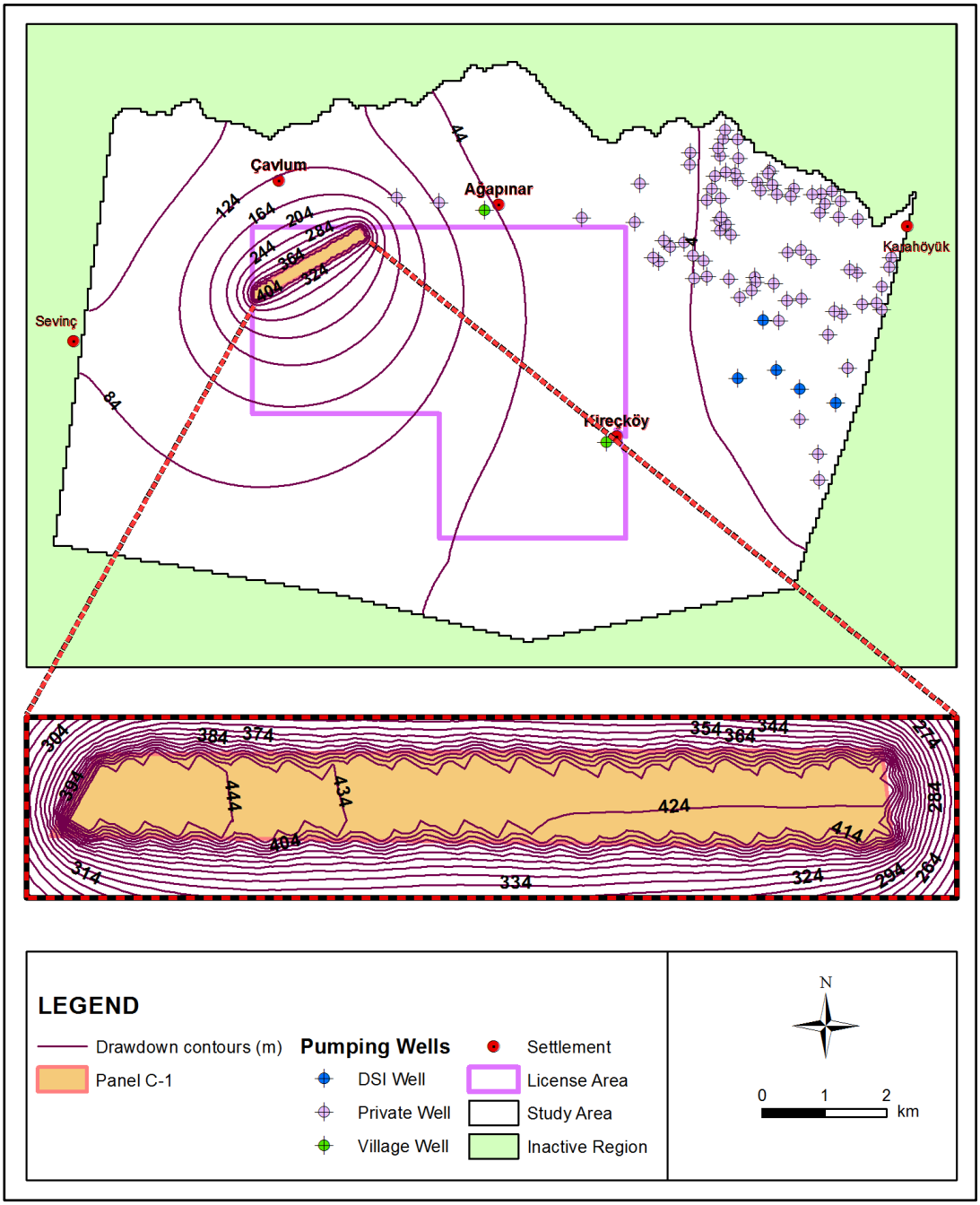

Figure 6.9. Drawdown contours after dewatering simulations at panel C-1

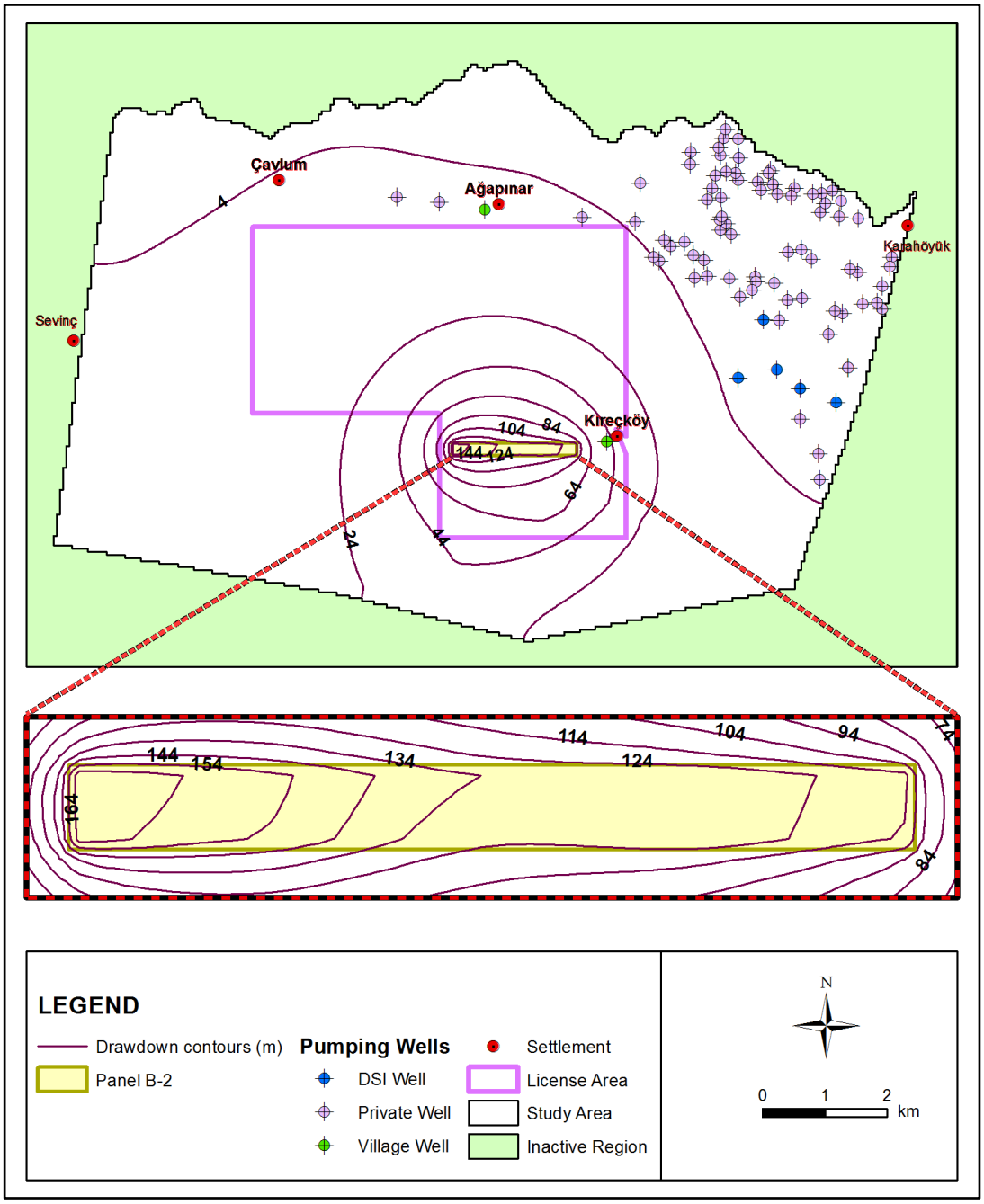

Figure 6.10. Drawdown contours after dewatering simulations at panel B-2

For other panels A-1, A-2, B-1 and C-2, these rates reach 304-414 m, 144-204 m, 334-434 m and 104-194 m at the panel basements as can be seen from Figures 6.11-6.14, respectively. In these figures, drawdown contours were drawn as the multiples of 4 m which is the approximate normalized RMS error value of the calibrated model (Figure 5.6). In view of this error value, it is expected that for the areas where the drawdown values are higher than 4 m, spring, captages and wells are affected by dewatering processes. In this case, as can be seen from the Figures 6.9-6.14, since the most of the pumping wells are located at the northeastern part of the study area, they are not affected from the dewatering simulations. However, groundwater level decreases down to 124 m at the wells around the Ağapınar (Figure 6.9). Although most of the pumping wells are not significantly affected by dewatering simulations, all springs and some captages will be dried after these simulations. New discharge rates from the captages are given in Table 6.1. In addition to these components, changes in the baseflow amounts after dewatering operations are also analyzed. For operations conducted at the deeper depths such as coal panels A-1, B-1 and C-1, no baseflow contribution to the Porsuk Stream is observed, whereas for shallower depths such as coal panels A-2, B-2 and C-2, baseflow decreases at the rates of 84.5 %, 32.7 % and 34.5 %, respectively. In Table 6.1, besides discharge rates from captages, recalculated river inflow and river outflow rates and obtained net baseflow amounts from these production panels are given.

6.5. Impact Assessment of Northwestern No Flow Boundary Condition on Preliminary Dewatering Simulations

In the study area, since the lignite seams become deeper through northwest, the dewatering impacts will not be significant for the eastern no flow boundary condition. Hence, this could be seen with the minimum (a few meters) amount of drawdown in the eastern boundary. Therefore, impact of northwestern boundary is analyzed.

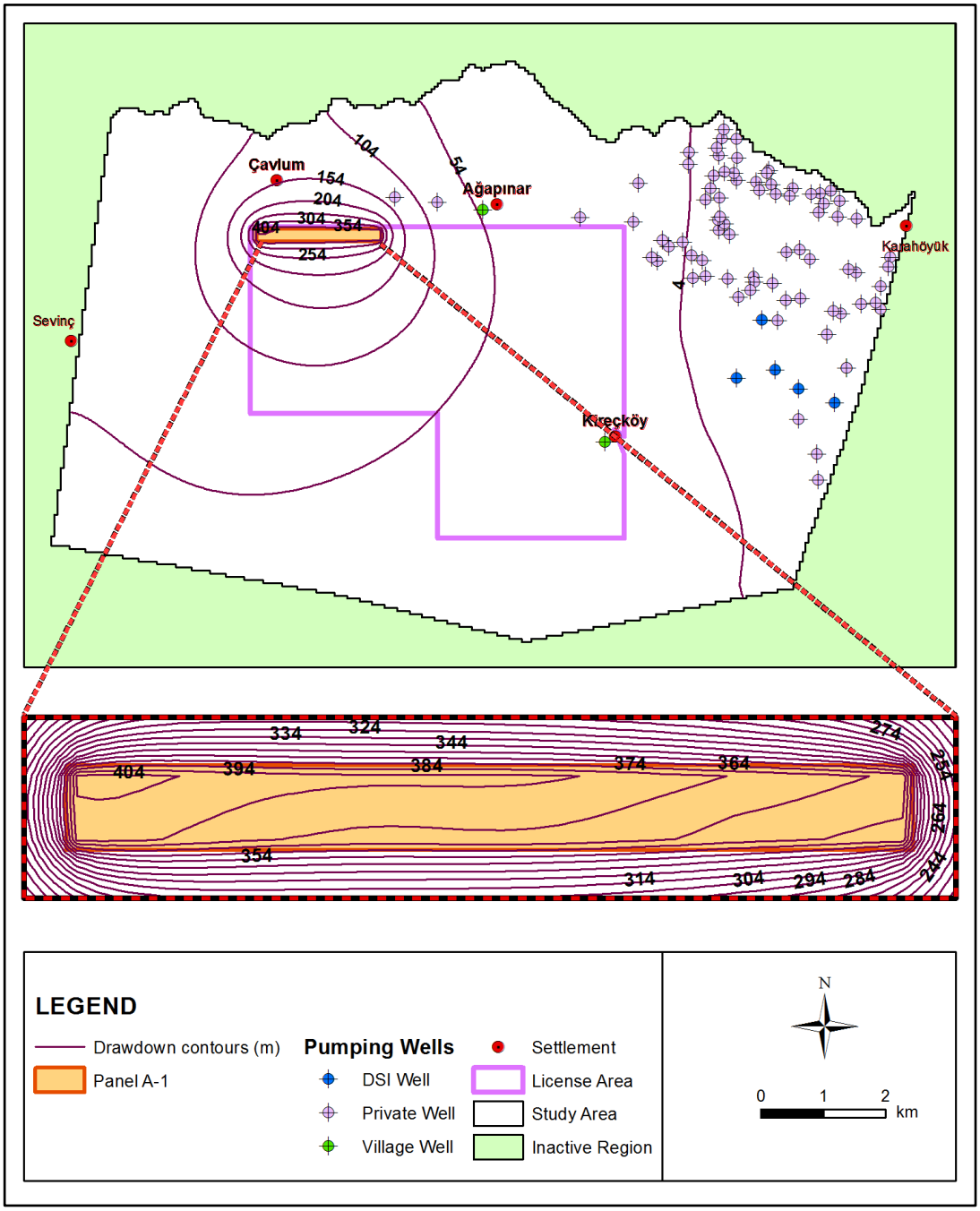

Figure 6.11. Drawdown contours after dewatering simulations at panel A-1

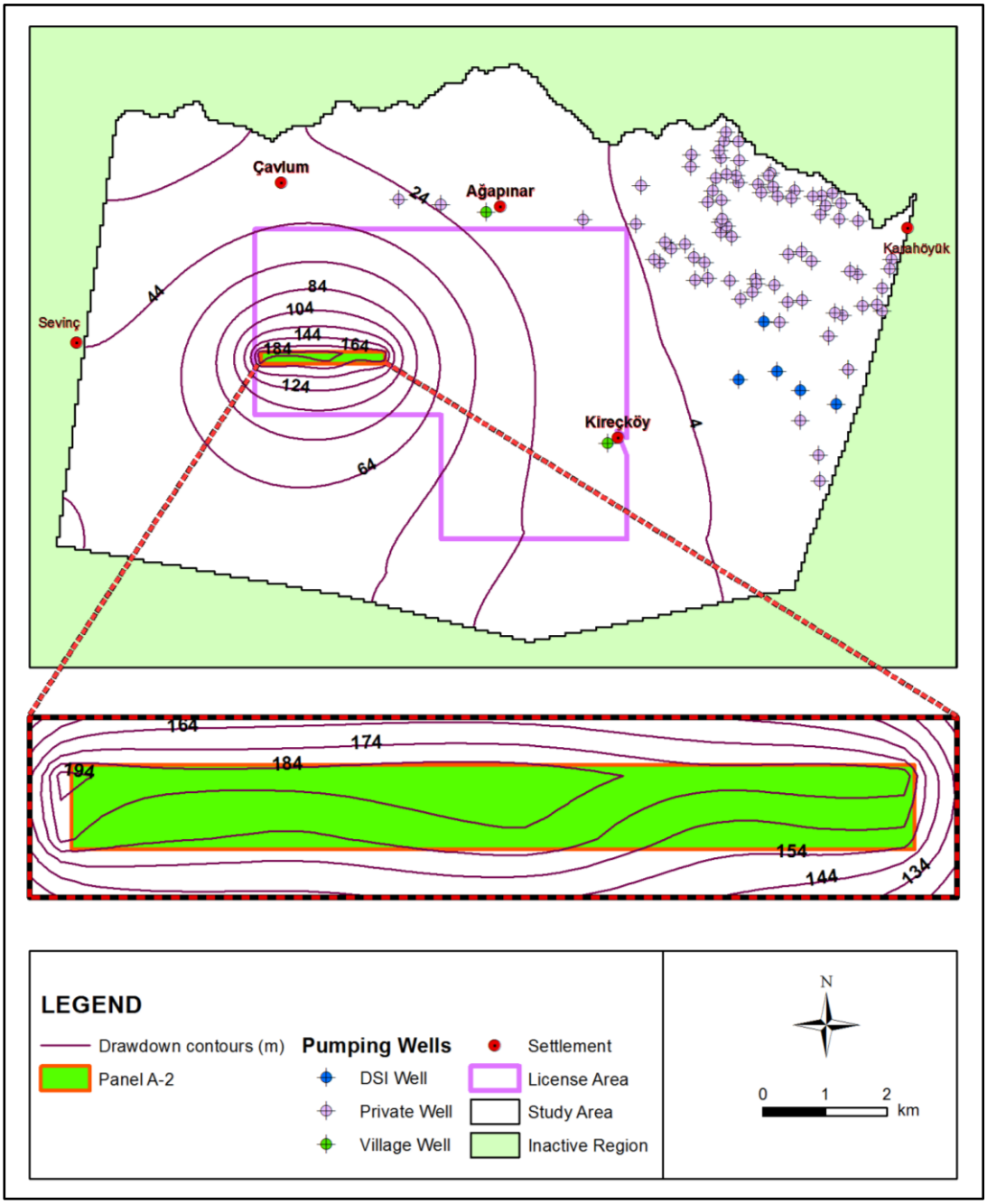

Figure 6.12. Drawdown contours after dewatering simulations at panel A-2

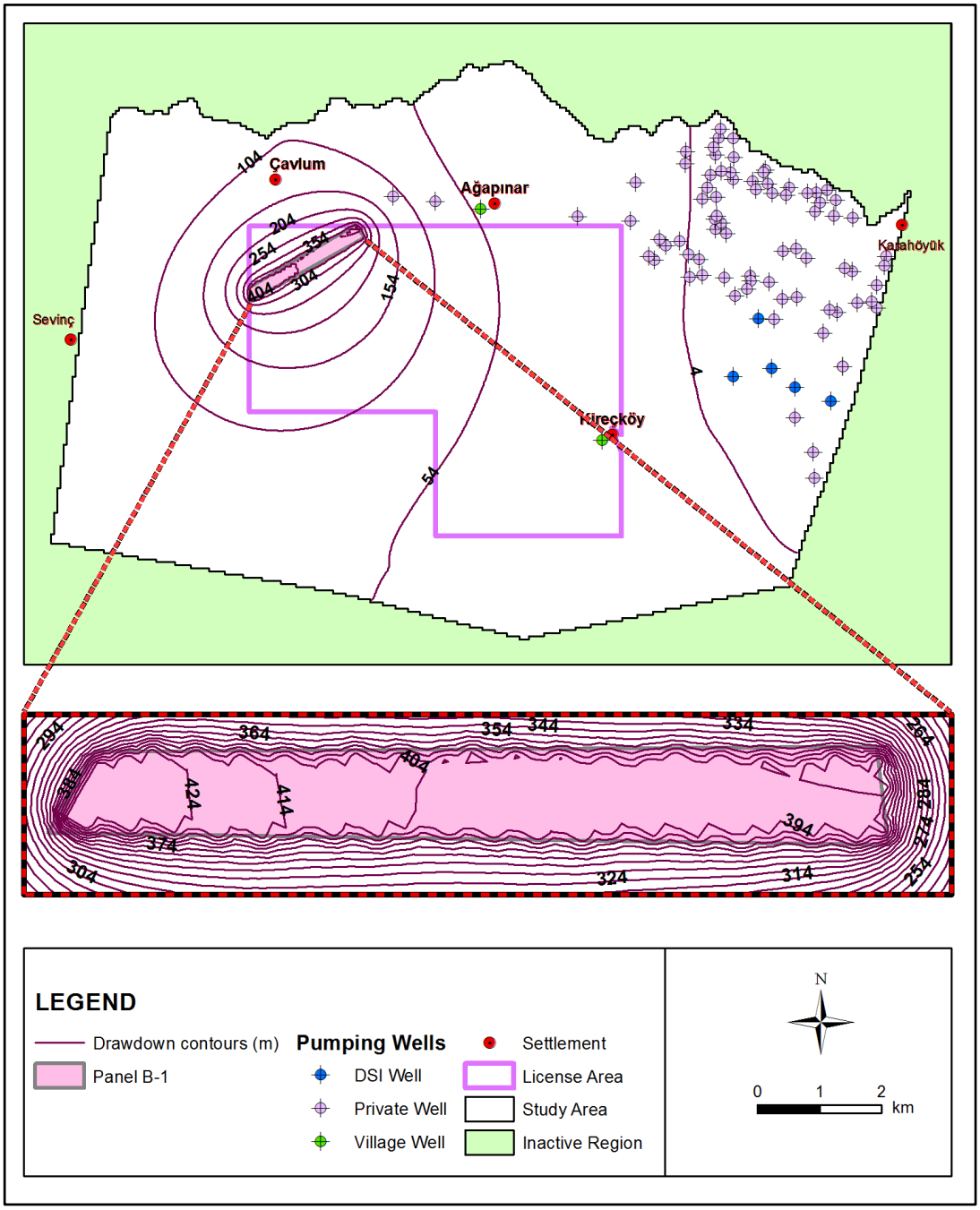

Figure 6.13. Drawdown contours after dewatering simulations at panel B-1

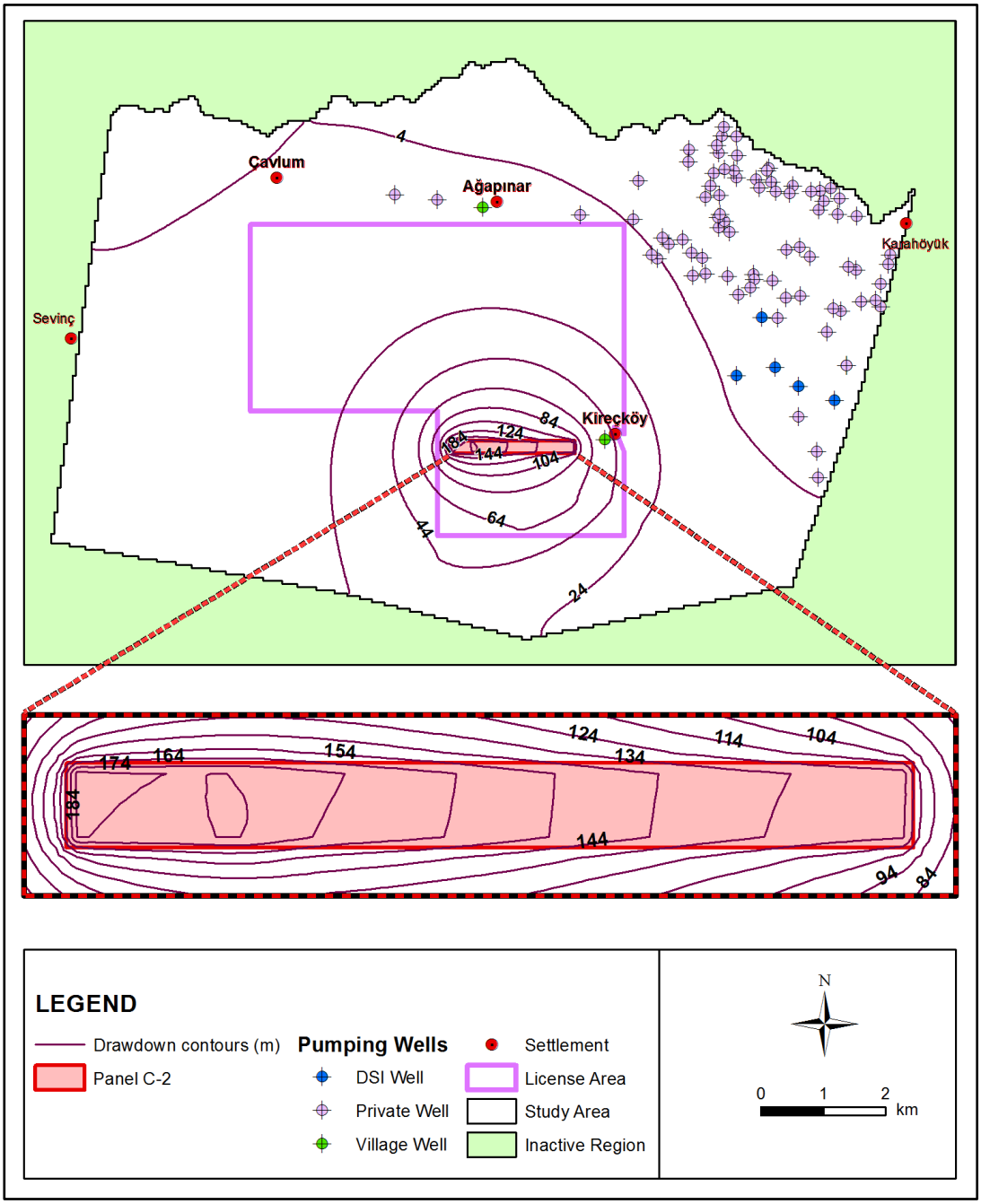

Figure 6.14. Drawdown contours after dewatering simulations at panel C-2

Table 6.1. Calculated groundwater budget components after dewatering simulations

		Underground coal panels					
		A-1	A-2	B-1	B-2	C-1	C-2
Discharge from captages	(m^3/year)	$4.72x10^4$	$4.53x10^4$	$1.14x10^4$	$1.10x10^5$	$7.68x10^3$	$1.09x10^5$
River inflow		$4.06x10^6$	$2.71x10^6$	$4.05x10^6$	$2.47x10^6$	$4.12x10^6$	$2.48x10^6$
River outflow		$2.20x10^6$	$2.88x10^6$	$2.24x10^6$	$3.21x10^6$	$2.21x10^6$	$3.20x10^6$
Baseflow		-	$1.70x10^5$	-	$7.40x10^5$	-	$7.20x10^5$

In the model domain, the northwestern part of the study area is represented by no flow boundary condition which simulates zero flux along the east-west direction. Consequently, this no-flow boundary prevents the simulation of groundwater inflow, if any, from the northwestern part of the study area during dewatering simulations. As a result, this boundary condition may cause underestimation of predicted groundwater inflows to the panels and overestimation of drawdowns within the panels. Therefore, additional dewatering simulations are conducted to analyze the impact of this boundary condition by replacing it with a general head boundary condition. The general head boundary condition which permits the groundwater outflow/inflow to/from the external area according to a given reference head value was assigned to the first three layers of the model along the northwestern no flow boundary (Figure 6.15). Then, the model response to this renewed boundary was examined by analyzing drawdown maps and recalculated groundwater budget components. However, since there is insufficient information to calculate the conductance of this boundary, simulations are repeated with three different horizontal hydraulic conductivity (K_x) values equal to $8.39x10^{-5}$ m/s, $1x10^{-5}$ m/s and $1x10^{-6}$ m/s, along this boundary to test the response of the model to these values.

For the first case, horizontal hydraulic conductivity of the cells along the general head boundary was calculated by using the horizontal hydraulic conductivities of Quaternary alluvium, Pliocene unit and silicified limestone.

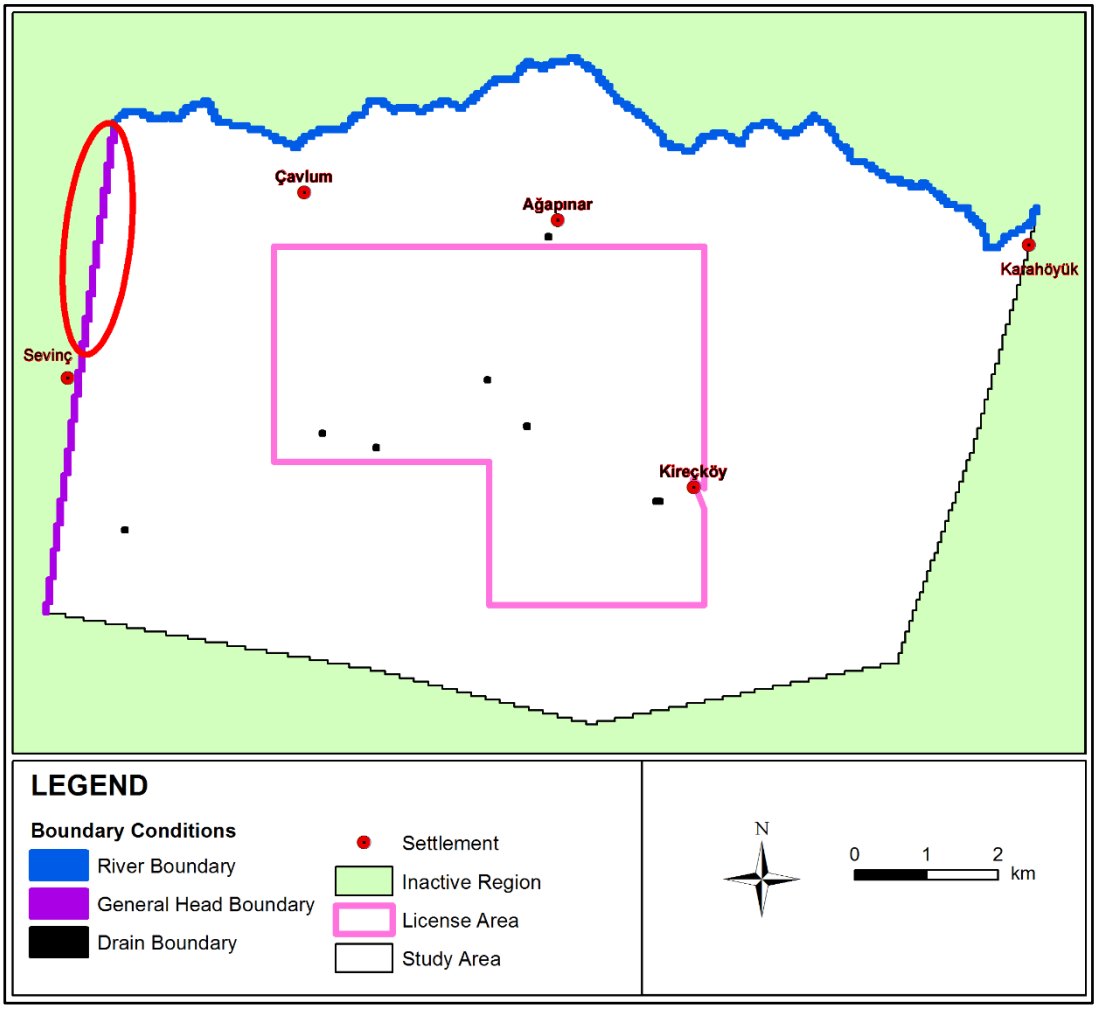

Figure 6.15. Renewed general head boundary condition

For this calculation, the following function is used:

$$(K_x)_{i,j} = \sum_{k=1}^{m} \frac{K_{i,j,k} z_{i,j,k}}{Z_{i,j}} \quad (6.1)$$

where,

K_x : Horizontal hydraulic conductivity through layered aquifer;

K : Hydraulic conductivity of each layer;

z : Thickness of each layer;

Z : Total thickness of the layers.

By the help of Equation 6.1, the horizontal hydraulic conductivity of the cells along the general head boundary shown in Figure 6.15 is calculated to be 8.39×10^{-5} m/s. For the second and third cases, this value is decreased to 1×10^{-5} m/s and 1×10^{-6} m/s to see the reaction of the model for the lower conductance amounts.

After the simulations are conducted with the assumed horizontal hydraulic conductivity values, it is seen that the groundwater inflow rates increased slightly (Table 6.2). While the maximum increase is seen at Panel C-1 as 1.69 L/s for the highest K_x, no change was observed for Panels B-2 and C-2 for the lowest K_x values. As the light of these information, it can be concluded that dewatering simulations are not sensitive to the northwestern no-flow boundary condition of the model.

Besides groundwater inflow rates, the model response was also examined by comparing groundwater budget components (Table 6.3). Because the model is not sensitive to the type of northwestern boundary condition and its conductance values, these components also do not change significantly.

Table 6.2. Calculated groundwater inflow rates after dewatering simulations with general head boundary condition

	Groundwater inflow (L/s)		
	CASE-1 ($K_x=8.39 \times 10^{-5}$ m/s)	CASE-2 ($K_x=1 \times 10^{-5}$ m/s)	CASE-3 ($K_x=1 \times 10^{-6}$ m/s)
Panel A-1	124.46	124.07	123.61
Panel B-1	131.50	130.90	130.14
Panel C-1	135.58	134.94	134.13
Panel A-2	53.36	53.22	53.01
Panel B-2	22.41	22.42	22.44
Panel C-2	23.64	23.65	23.67

Table 6.3. Calculated groundwater budget components after dewatering simulations with general head boundary condition

			Underground coal panels					
			A-1	A-2	B-1	B-2	C-1	C-2
CASE-1 (K_x=8.39x10^{-5} m/s)	Discharge from captages	(m^3/year)	5.17x10^4	4.69x10^4	1.75x10^4	1.08x10^5	1.43x10^4	1.07x10^5
	River inflow		3.33x10^6	2.45x10^6	3.26x10^6	2.31x10^6	3.31x10^6	2.32x10^6
	River outflow		2.41x10^6	3.34x10^6	2.45x10^6	3.60x10^6	2.41x10^6	3.59x10^6
	Baseflow		-	8.90x10^5	-	1.29x10^6	-	1.27x10^6
CASE-2 (K_x=1x10^{-5} m/s)	Discharge from captages	(m^3/year)	4.94x10^4	4.55x10^4	1.46x10^4	1.08x10^5	1.12x10^4	1.07x10^5
	River inflow		3.79x10^6	2.64x10^6	3.75x10^6	2.44x10^6	3.82x10^6	2.45x10^6
	River outflow		2.22x10^6	2.97x10^6	2.25x10^6	3.26x10^6	2.23x10^6	3.25x10^6
	Baseflow		-	3.30x10^5	-	8.20x10^5	-	8.00x10^5
CASE-3 (K_x=1x10^{-6} m/s)	Discharge from captages	(m^3/year)	4.79x10^4	4.55x10^4	1.22x10^4	1.10x10^5	8.59x10^3	1.08x10^5
	River inflow		4.01x10^6	2.70x10^6	3.99x10^6	2.47x10^6	4.06x10^6	2.48x10^6
	River outflow		2.21x10^6	2.89x10^6	2.24x10^6	3.21x10^6	2.22x10^6	3.20x10^6
	Baseflow		-	1.9x10^5	-	7.4x10^5	-	7.2x10^5

CHAPTER 7

SUMMARY, CONCLUSIONS AND RECOMMENDATIONS

7.1. Summary

The purpose of this study was to understand the groundwater flow system and its response to preliminary dewatering for the coal exploration license area of the Eczacıbaşı Industrial Raw Materials Inc. in Eskişehir by using numerical groundwater modeling approach. Within this scope, primarily, available data was compiled from the field investigations and previous studies to characterize the hydrogeological system. Then, MODFLOW SURFACT was chosen as computer code to simulate both saturated/unsaturated conditions in the study area. After computer code selection, conceptual model development including: determination of water bearing units, calculation of hydrological and hydrogeological budget was conducted.

The most important water bearing units within the study area and its vicinity are composed of Quaternary alluvium and Pliocene limestones, sandstone and conglomerates. Moreover, silicified limestone and sandstones and conglomerates within the lignite intercalated Porsuk Formation are also water bearing units. In addition to these, impervious and semi-pervious basement rocks can carry groundwater along fractures that result from faulting.

Conceptual hydrological and hydrogeological budgets were developed for the study area to compute the ratio of the hydrologic cycle components (precipitation, surface runoff, infiltration and evapotranspiration) to total precipitation and to investigate

recharge-discharge components of the groundwater system, respectively. These conceptual budget results were verified by model simulations.

The 95.6 km^2 study area encompassing the Eczacıbaşı Industrial Raw Materials Inc. license area was divided into six layers and discretized by uniform grid mesh with 50 m x 50 m grid size. After specifying the boundary conditions and initial input parameters. The model was calibrated under steady-state conditions by conducting several simulations in which the assigned parameters were adjusted within the field observed ranges until the model calculated heads closely match the field observed heads. Finally, the sensitivity of the model to some critical input parameters was tested by conducting a sensitivity analyses.

This study also outlines the preliminary dewatering system simulations and their impacts on the hydrogeological system. The calibrated model was used by assigning drain cells to the bottom elevations of the coal production panels which were determined according to minimum and maximum depths of the lignite seams to calculate the predicted groundwater inflows into the excavated area. Groundwater level decreases, drawdown amounts and groundwater budget components were evaluated for different lignite seams at different depths to analyze the impacts of dewatering. Finally, the northwestern no flow boundary condition on the dewatering simulations were tested by replacing it with a general head boundary condition with different conductivities to understand whether this boundary causes underestimation of groundwater inflow and overestimation of drawdown amounts or not.

7.2. Conclusions

Based on the results obtained from this study, following conclusions can be made:

- Calibrated groundwater model provides a good representation of hydrogeological conditions of the study area and has allowed for the development of a preliminary dewatering plan.

- The conceptual groundwater budget was verified by comparing it with the calculated groundwater budget obtained from the calibrated model. Although approximately same rates were calculated for all recharge and discharge components, calculated budget indicates an underestimation of discharge from springs and captages and overestimation of evapotranspiration.

- The results of preliminary dewatering simulations show that during the extraction of lower lignite seam (A) from the deepest depositional area, groundwater inflow rates reach maximum value of 133.89 L/s while it is minimum (22.45 L/s) for middle lignite seam (B) at shallower depositional area. These simulations show that for the lignite seams at the lower elevations, higher pumping rates for dewatering will be necessary during mining activities in the future.

- As a result of dewatering activities the baseflow to Porsuk Stream will decrease and all springs and some captages will be dried. For coal panels A-1, B-1 and C-1, it is predicted that no baseflow will be observed, whereas for coal panels A-2, B-2 and C-2, baseflow will decrease 84.5 %, 32.7 % and 34.5 %, respectively. The discharge rates from the captages will decrease with an average rate of 60.7 %.

- The no-flow boundary condition assigned to the nortwestern part of the model domain has an insignificant effect on the calculated dewatering rates, groundwater levels and budget components.

7.3. Recommendations

Based on the results of this study, following recommendations can be made:

- Since the groundwater model must be dynamic, the uncertainties should be removed and the reliability of predictions should be improved by re-calibrating the model as new data is collected.

- The groundwater model is highly sensitive to hydraulic conductivity of the geological units. Therefore, additional pumping-recovery tests can be conducted to test hydraulic parameters of these units, especially the most sensitive uppermost layers of m1-m2 unit and basal limestone.

- River stage should be surveyed along the Porsuk Stream to increase the accuracy of the model.

- After mining method is finalized, dewatering simulations should be repeated by running the model under transient conditions using the proposed mine plans and schedules. Finally, the impact assessment of detailed dewatering design should be investigated.

REFERENCES

Ardejani FD, Singh RN, Baafi E, Porter I (2003) A finite element model to: 1. Predict groundwater inflow to surface mining excavations. Mine Water Environ 22(1):31–38.

Chow V.T., Maidment, D.R., Mays, L.W., 1988, Applied Hydrology, McGraw Hill Publishing, p. 572.

Doherty, J., 2001. Improved Calculations for Dewatered Cells in MODFLOW. Ground Water 39 (6), 863–869.

DSI, 1977. Hydrogeological investigation report for Eskişehir – Alpu basin, General Directorate of State Hydraulic Works, p.39.

DSI, 2010. Hydrogeological investigation report for Eskişehir – Alpu basin, General Directorate of State Hydraulic Works, p.54.

Goode, D. J., and C. A. Appel. 1192. Finite-difference Interblock transmissivity for Unconfined Aquifers and for Aquifers with Smoothly Varying Transmissivity. U.S. Geological Survey Water-Resources Investigations Report 92-4214.

Gözler, Z., Cevher, F., Ergül, E., Asutay, J.H., 1997. Geology of the middle and southern part of the Sakarya Region. General Directorate of Mineral Research and Exploration, Technical Report, No: 9973, Ankara.

Huyakorn, P.S., Springer, E.P., Guvanasen, V., and Wadsorth, T.D., 1986. A threedimensional finite element model for simulating water flow in variably saturated porous media. Water Resour. Res., 22(12): 1790-1808.

HydroGeoLogic Inc., 1996. MODHMS / MODFLOW-SURFACT, A Comprehensive MODFLOW-Based Hydrologic Modeling System, Reston, VA.

Kresic, N., 2006. Hydrogeology and Groundwater Modeling, Second Edition. CRC Press / Taylor & Francis, Boca Raton, FL, p. 806.

McDonald, M.G. and Harbaugh, A.W., 1988. A modular three-dimensional finite difference groundwater flow model: U.S. Geological Survey Techniques of Water-Resources Investigations Book 6, chapter A1.

McDonald, M. G., A. W. Harbaugh, B. R. Orr, and D. J. Ackerman. 1991. A Method of Converting No-flow Cells to Variable Head Cells for the U.S. Geological Survey Modular Finite-difference Ground-water Flow Model. U.S. Geological Survey Open File Report 91-536.

Mailloux, M., Boisvert, V., Millette, D. & Poulin, M. 2009. Potential effects evaluation of dewatering an underground mine on surface water and groundwater located in a rural area. Montreal, Canada. http://www.dhigroup.com/ upload/ publications/ dhiwasy/Mailloux_2009.pdf

Palaris, 2016. JORC Resource Report Alpu Project, Eczacıbaşı Industrial Raw Materials Inc, p.94.

Senguler, I., 2013. Geology and stratigraphy of Eskişehir-Alpu coal basin. Nat. Res. Econ. Bull. 16, 89-93.

Siyako, F., Coşar, N., Çokyaman S., Coşar, Z., 1991. Terriary Geology of the Bozüyük-İnönü Eskişehir-Beylikova-Sakarya regions and their coal potential. General Directorate of Mineral Research and Exploration. Technical Report, No: 9281, Ankara.

Soil Conservation Service (SCS), 1964, SCS National Engineering Handbook, Section 4: Hydrology, Updated 1972, U.S. Department of Agriculture, Washington D.C.

Toprak, S., Sutcu, E. C., Senguler, I., 2015. A fault controlled, newly discovered Eskişehir Alpu coal basin in Turkey, its petrographical properties and depositional environment. International Journal of Coal Geology, (138), 127–144. http://dx.doi.org/10.1016/j.coal.2014.12.013

Wang, H.F., and Anderson, M.P., 1982. Introduction to Groundwater Modeling: Finite Difference and Finite Element Methods. W. H. Freeman and Company, USA, p.237

Williamson, A.K., Grubb, H.F., 2001, Ground-water flow in the Gulf Cost aquifer systems, south-central United States. U.S. Geological Survey Professional Paper 1415-B. Virginia, USA.

Yazıcıgil, H., Çamur, M.Z., Yılmaz, K. K., Çatak, M.O. & Kılıç, H., (2016). Hydrogeological investigation and characterization of the Esan-Alpu coal mine exploration site. Project No. 2014-03-09-2-00-29. Middle East Technical University, Ankara.